5-1-1996

The Colorimetric characterization of CRT-based digital film recorders

Helen Hae-Kyung Shin

The Colorimetric Characterization of CRT-Based Digital Film Recorders

by

Helen Hae-Kyung Shin

A thesis submitted in partial fulfillment
of the requirements for the degree of
Master of Science in the Center for
Imaging Science in the College of Science
of the Rochester Institute of Technology.

May 1996

Signature of the Author _____
Helen Hae-Kyung Shin

Accepted by Dana G. Marsh June 18, 1996
Coordinator, M.S. Degree Program

Rochester Institute of Technology
Rochester, New York

CERTIFICATE OF APPROVAL

M.S. DEGREE THESIS

The M.S. Degree Thesis of Helen H. Shin
has been examined and approved by the thesis
committee as satisfactory for the thesis requirement
for the Master of Science degree

Dr. Roy S. Berns, Thesis Advisor

Dr. Mark D. Fairchild

Dr. Jonathan S. Arney

5/30/96
Date

THESIS RELEASE PERMISSION FORM

Rochester Institute of Technology
Center for Imaging Science

Title of Thesis : **The Colorimetric Characterization of CRT-Based Digital Film Recorders**

I, Helen H. Shin, hereby grant permission to the Wallace Memorial Library of R.I.T. to reproduce my thesis in whole or in part. Any reproduction will not be for commercial use or profit.

Signature _____

Date 6/18/96

The Colorimetric Characterization of CRT-Based Digital Film Recorders

by

Helen Hae-Kyung Shin

A thesis submitted in partial fulfillment
of the requirements for the degree of
Master of Science in the Center for
Imaging Science in the College of Science
of the Rochester Institute of Technology.

ABSTRACT

Digital film recorders play a key role bridging digital imagery and photographic media. The purpose of this research was to characterize the relationship between digital drive signals controlling the exposure of positive 35mm film and the spectral transmittance of the processed film. First, the Beer-Bouger law was verified relating dye concentration and spectral transmittance. Second, an empirical nonlinear relationship was found between status A densities and dye concentration to facilitate the conversion from integral to analytical density alleviating the need for spectral transmittance measurements. Third, the relationship was found between digital drive signals and integral density. This complex relationship modeled the well-known inter-image effects of transparency films: A combination of principal component analysis and cubic spline interpolation was used.

ACKNOWLEDGMENTS

I would like to express my gratitude to all of those who made this thesis possible.

Dr. Roy Berns for his firm guidance, encouragement, and patience.

Dr. Mark Fairchild for his expert advice.

Dr. Jonathan Arney and other faculty members at the center for Imaging Science for their help and guidance.

Center for Imaging Science at R.I.T. for the monetary support allowing me the opportunity to study Imaging Science including Color Science.

My parents for their endless support and encouragement.

Christian Shin for his endless encouragement and love as well as computer support.

Thank you all very much.

Table of Contents

Table of Contents vi

List of Figures viiii

List of Tables xiiii

1 Introduction 1

1-1 Problem Statement and Objectives 1

1-2 The Technology of the Film Recorder 4

1-3 Background 8

1-4 Thesis Overview 9

2 Experimental and Measurements 12

2-1 Spectral Transmittance Measurements 12

2-2 Density Measurements 16

2.2.1 Spatial Variability Correction for Density Measurements 17

2-3 Calibration of the Film Recorder 19

2.3.1 Calset Searching 19

2.3.2 Tone Reproduction Settings 20

2-4 Measurement Variability 24

2.4.1 Variability of Film 25

2.4.2 Film Recorder Variability 25

2.4.3 Other Variability 31

3 Film Model 35

3-1 Background 35

3.1.1 Beer-Bouger Law 35

3-2 Determination of Dye Absorption Curves 38
3-3 Determination of Dye Amounts 41
4 Conversion Between Integral Density and Analytical Density 47
4-1 Background of Density Measurements 47
4.1.1 Integral Density 47
4.1.2 Analytical Density 50
4-2 Linear Regression Model between the Measured Density and the Analytical Density 51
5 Interimage Effects Model 64
5-1 Background of Interimage Effects 64
5-2 Interimage Effects Model 66
5-2-1 Interimage Effects Model by Principal Component Analysis 71
6 Forward Film Recorder Model 86
7 Conclusions 101
7-1 Future Research 103
References 105
Bibliography 107
Appendix A. The digital values of a 90-image target for the eigenvector analysis 111
Appendix B. Digital count data for interimage effects 114
Appendix C. Vector Analysis Results for Interimage Effects by Principal Component Analysis 116
Appendix D. Scalar Analysis Results Using Least Square Fit Based on Equation 5-2 118
Appendix E. Data points for Spline Interpolation in Interimage Effects Model 127

Appendix F. The data set for the concentrations and the ΔE^*_{ab} values of 252 samples from the interimage effects model.....128

Appendix G. Computer Codes for Thesis.....134

List of Figures

Figure 1-1 Sequential film recording process..... 1

Figure 1-2 Schematic Film Recorder Path..... 5

Figure 1-3 Spectral radiance of the Solitaire 8xp's CRT..... 6

Figure 1-4 Solitaire 8xp's filter spectral transmittances..... 7

Figure 1-5 The product of filter spectral transmittance and CRT spectral radiance..... 8

Figure 2-1 Plot for density mean values as a function of wavelength using The Color Sphere (six measurements) and the Color Scan (four measurements)..... 13

Figure 2-2 Plot for standard deviation of grey density values using The Color Sphere and the Color Scan..... 14

Figure 2-3 Plot for density mean values for cyan, magenta, and yellow as a function of wavelength using The Color Sphere (six measurements) and the Color Scan (four measurements)..... 15

Figure 2-4 Plot for standard deviation values of cyan, magenta, and yellow density using The Color Sphere and the Color Scan..... 15

Figure 2-5 A sample slide for the spatial variability.....17

Figure 2-6-1 Average density values for Dmin sample..... 18

Figure 2-6-2 Standard Deviation Values for Dmin sample..... 18

Figure 2-7 First iteration for setting tone reproduction using Colorfit software..... 22

Figure 2-8 Second iteration for setting tone reproduction using Colorfit software 22

Figure 2-9 Third iteration for setting tone reproduction using Colorfit software..... 23

List of Figures (continued)

Figure 2-10 ΔE^*_{ab} changes compared with the first day of measurement as a function of time for cyan, magenta, yellow and grey slides..... 26

Figure 2-11 Chroma changes compared with the first day of measurement as a function of time for cyan, magenta, yellow and grey slides.....27

Figure 2-12 Chroma changes compared with the first day of measurement as a function of time and heat.....28

Figure 2-13 Average and 2ó Std. Dev. of 7 exposure densities within one roll of film 29

Figure 2-14 Average and Std. Dev. of film densities in 9 different positions within one roll of film as a function of exposures..... 30

Figure 2-15 Average and Std. Dev. of 7 exposures of Dmin sample as a function of 9 different positions within one slide..... 32

Figure 2-16 Average density values of 7 exposures from three different days.....33

Figure 3-1 Model for the passage of light in transparent medium..... 36

Figure 3-2 C, M, and Y eigenvectors from equamax rotation..... 39

Figure 3-3 Eigenvectors from C, M, Y ramps..... 40

Figure 3-4 Final eigenvectors from both equimax rotation and C, M, Y ramps..... 41

Figure 3-5 ΔE^*_{ab} histogram for tristimulus matching algorithm for illuminant D50.. 46

Figure 4-1 C, M, and Y dyes, and the composite neutral dye spectral density distributions as a function of wavelength..... 48

Figure 4-2 Spectral densitometer responses for status A densitometry..... 49

Figure 4-3 Concentration vs. measured density for grey samples..... 52

List of Figures (continued)

Figure 4-4 Concentration vs. measured density for 60 color samples..... 53

Figure 4-5 Residual plots for 3x3 transformation for predicted concentrations..... 55

Figure 4-6-1 ΔE^*ab histogram for the predicted concentration from a 3x3 transformation and the concentration from Tristimulus matching algorithm under illuminant A..... 57

Figure 4-6-2 ΔE^*ab histogram for the predicted concentration from 3x3 transformation and the concentration from Tristimulus matching algorithm under illuminant D50..... 57

Figure 4-7 Residual plots for predicted concentrations after taking out outliers..... 59

Figure 4-8-1 ΔE^*ab for the predicted concentrations from Equation 4-2 and concentrations from Tristimulus matching algorithm under illuminant A...60

Figure 4-8-2 ΔE^*ab for the predicted concentrations from Equation 4-2 and concentrations from Tristimulus matching algorithm under illuminant D50 61

Figure 4-9 Red, green, and blue densities as a function of input digital values..... 62

Figure 4-10 C, M, and Y concentrations as a function of input digital values..... 63

Figure 5-1 One of the samples for the interimage effects model.....66

Figure 5-2 Red, green, and blue densities with uniform green and blue exposure levels as a function of red exposure levels..... 68

Figure 5-3 Red, green, and blue densities with uniform red and blue exposure levels as a function of green exposure levels..... 69

List of Figures (continued)

Figure 5-4 Red, green, and blue densities with uniform red and green exposure level as a function of blue exposure levels..... 70

Figure 5-5 The general structure of color film..... 71

Figure 5-6 Difference between TRC for grey sample and TRC for red channel when blue and green channels have uniform exposure levels..... 73

Figure 5-7 Eigenvectors for red density variability..... 75

Figure 5-8 Eigenvectors for green density variability.....76

Figure 5-9 Eigenvectors for blue density variability..... 77

Figure 5-10 Eigenvector comparison for red, green, and blue main gamma variability 78

Figure 5-11 Least squares fit coefficients for interimage effects..... 81

Figure 5-12 Squared_R plots for predicted densities using 2 vectors and scalars 82

Figure 5-13 LUT for red, green, and blue mean vectors using cubic spline interpolation method with 9 data points..... 83

Figure 5-14 LUT for red, green, and blue eigenvectors using cubic spline interpolation 84

Figure 5-15 LUT for least-squares fit coefficients for predicted densities..... 85

Figure 6-1 The image Path for Characterization of a Film Recorder..... 87

Figure 6-2 Predicted density vs. measured density using the interimage effects model for grey samples.....91

List of Figures (continued)

Figure 6-3 Predicted density vs. measured density using the interimage effects model as a function of red exposure....92

Figure 6-4 Predicted density vs. measured density using the interimage effects model as a function of green exposure....93

Figure 6-5 Predicted density vs. measured density using the interimage effects model as a function of blue exposure....94

Figure 6-6 ΔE^*_{ab} using the interimage effects model under illuminant A....96

Figure 6-7 Hue plane (a*b*) delta plot under illuminant A....98

Figure 6-8 Lightness vs. Chroma delta plot under illuminant A....99

Figure 6-9 ΔE^*_{94} using interimage effects model under illuminant A....100

Chapter I. Introduction

1.1 Problem Statement and Objectives

The digital film recorder is a hard-copy output device transferring digital images to conventional film. Since the film recorder produces not the final output image but the latent image, the characterization of a film recorder is more complex than other devices such as printers that produce the output color directly. The film recording process includes the chemical film processing step and the projection stage as well as the exposure stage in the film recorder. The sequential image transformation process is shown in Figure 1-1.

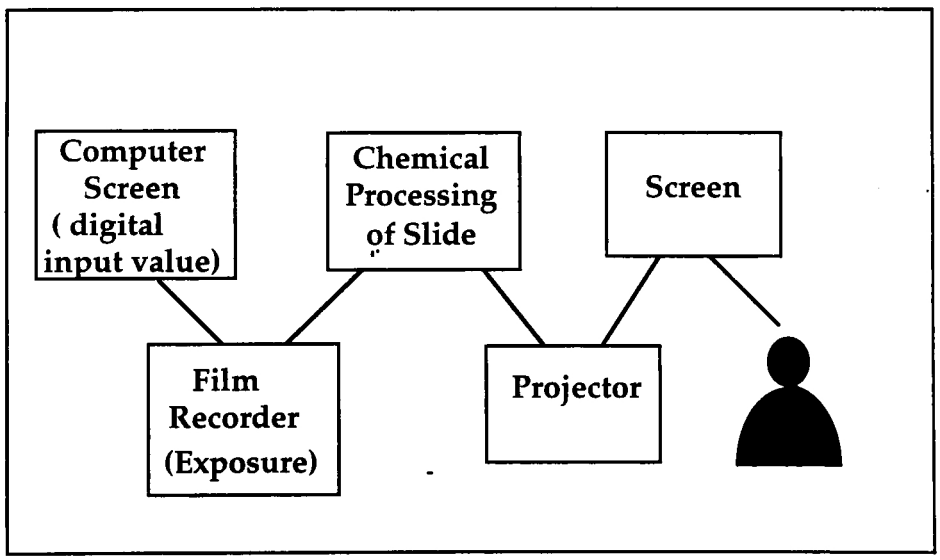

Fig. 1-1 Sequential film recording process.

The first step is either the creation of an image from a host computer or the transformation of an electronic image to a host computer. This typically defines the color of a computer-controlled CRT display from digital data. The second step is the transmission of that image to a film recorder and then finally onto film. This defines the spectral transmittance of the processed film from digital data. The third step is to project the film. This stage defines the color of the projected slide. The fourth step is to take into account the appearance of both CRT and projected images. This thesis mainly focused on the second step.

In order to complete the film recorder model, the relationship between the input color (digital values) and the projected color (tristimulus values) has to be defined. Once the film's spectral transmittance is defined, its tristimulus values are calculated with the spectrum of the light source and the color matching functions by the following equations.

$$X = k\int_{\lambda} L_\lambda T_\lambda \overline{x_\lambda} d\lambda$$
$$Y = k\int_{\lambda} L_\lambda T_\lambda \overline{y_\lambda} d\lambda$$
$$Z = k\int_{\lambda} L_\lambda T_\lambda \overline{z_\lambda} d\lambda$$

where $\mathbf{L}\lambda$ is the spectrum of the light source, $\mathbf{T}\lambda$ is the transmittance of the slide, and $\overline{\mathbf{x}_\lambda}$, $\overline{\mathbf{y}_\lambda}$, and $\overline{\mathbf{z}_\lambda}$ are the CIE color matching functions. Considering the processed film as a transparent medium consisting of dyed gelatin, the relationship between the spectral transmittance and the amount of dyes in the film is described by Beer-Bouger Law.[1]

$$T_\lambda = T_{\lambda,substrate} 10^{-\left(CcD_{\lambda,c} + CmD_{\lambda,m} + CyD_{\lambda,y}\right)}$$

where $T_{\lambda,substrate}$ is the spectral transmittance of the base, C_c, C_m, and C_y are the concentrations, and $D_{\lambda,c}$, $D_{\lambda,m}$, and $D_{\lambda,y}$ are the absorption coefficients of cyan, magenta, and yellow, respectively. The spectral transmittance of the input color is reconstructed by the amount of each dye, and their spectral absorptivities. Finally, in order to achieve the reproducion of input-output color, the model has to be inverted so that the digital data necessary to produce the output color are calculated. The inverse modeling is beyond the scope of this thesis. Since, the main focus of this thesis is the film recorder model before projection, the reconstruction of the spectral transmittance of the processed film is mainly discussed.

In order to model the film exposed by a film recorder driven by the digital values in computer-generated images, the following questions have to be answered:

1. How can we minimize the variability of film recording path including chemical processing step?
2. How can we predict the amount of dye in the film?
3. How can we define the relationship between the measured density and the dye concentration?
4. How can we model the film recorder before the projection stage?

According to the above questions, the following research objectives were defined:

1. Calibrate the film recorder before the colorimetric characterization step to set the film recorder response and minimize the processing variability through the consistant film recording process.
2. Define the absorptivity of each dye and then derive dye concentrations based on the Beer-Bouger Law.
3. Define the relationship between the measured density and the concentration of each dye to use a status A densitometer as a colorimeter. As long as film is characterized properly, the characterization of the film recorder can be performed using status A densitometer.
4. Build the model for the processed slide by one dimensional look-up tables (LUTs) for tone reproduction, and the matrix for inter image effects for the color correction.

1.2 The Technology of the Film Recorder

There are two kinds of film recorders depending on RGB signals. Analog film recorders depend on the RGB analog signals that drive a color monitor. In contrast, digital film recorders use streams of data fed from the computer via a SCSI, parallel, or custom port. Digital color film recorders commonly use a monochrome CRT, RGB filters, and a camera to convert digital data into the film output. The resolution of the film recorder mainly depends on the ability to produce and address small dots on a CRT screen since this is actually photographed. The high-end film recorders have 16K dots across the wide dimension of a 35mm slide permitting projection of a 35mm slide to a large screen while preserving high resolution. The film is then exposed to each primary color

using a black and white display with sequentially interposed red, green, and blue optical filters in the light path between the display and the lens. It is important to have the faceplate of the CRT and the color filters, which are rotated in front of the camera lens, optically correct. The camera lens must also be in focus and geometrically correct. The schematic film recorder path is shown in Figure 1-2.

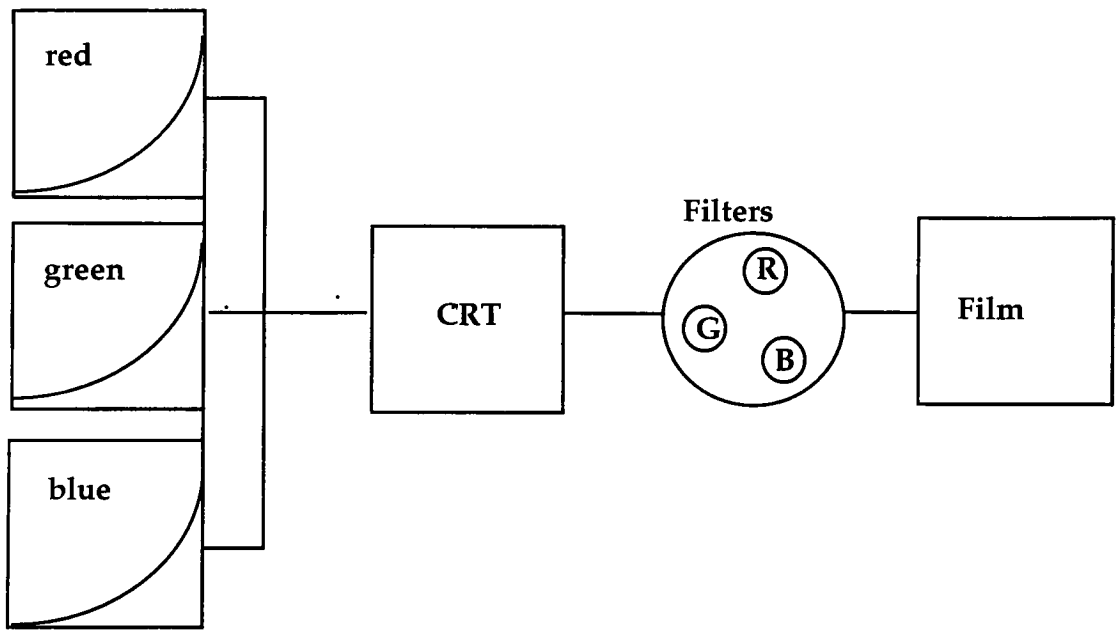

Fig. 1-2 Schematic film recorder path.

In this thesis, a Solitaire8xp was provided by Management Graphics Inc. The Solitaire8xp is a CRT based digital film recorder. The Solitare8xp interfaces to the host computer via the General Purpose Interface Bus (GPIB). The digital images were created using Photoshop 2.5.1 on a Macintosh. The Macintosh display system uses 8 bits per color video LUTs, while the film recorder uses 12 bits per

color LUTs. The Solitaire8xp has alternate choices for color LUTs depending on film types. In this research, Kodak Ektachrome 100 Plus Professional film was used. Each LUT controls the nonlinearity of the film recorder. The data go through these LUTs and are used to drive the light intensity of a CRT from within the film recorder. The CRT's spectral radiance of the Solitaire is shown in Figure 1-3.

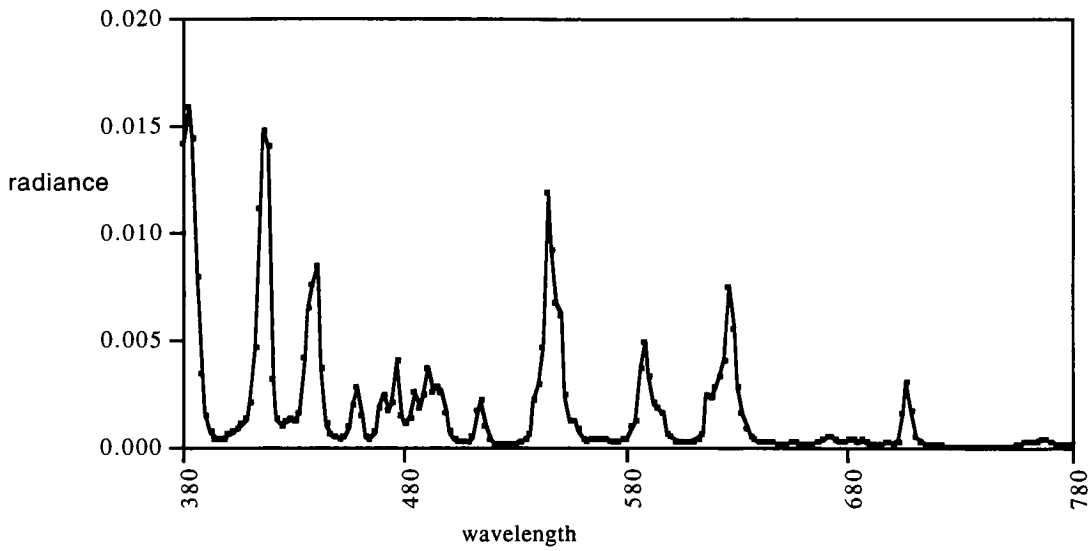

Fig. 1-3 Spectral radiance of the Solitaire 8xp's CRT.

The resolution of a CRT can be described in several ways.[2] The resolution of a CRT is normally described as X by Y, where X is the maximum number of horizontal lines displayed and Y is the number of vertical lines displayed. The resolution of a CRT is also described by its dot pitch. The dot pitch indicates how closely the dots or lines are placed together on the face of the CRT. For

example, if a film recorder produces a spot size of 0.04 mm on a 7-inch CRT, the film recorder is capable of displaying approximately 4500 lines. The Solitaire8xp can address 2K, 4K, and 8K resolutions. In this research, the resolution of the Solitaire8xp was set to 4K. The high resolution of the film recorder was achieved by a small spot size on the CRT.[3] One way to shrink dots on a CRT is to reduce their intensity. However, this may reduce the sharpness of the image. Also, smaller dots are darker which require longer exposure times. This may produce adverse effects due to reciprocity failure. After the data were transformed through the LUTs, each set of color data was photographed using an optically correct camera lens through the appropriate filters. The color filters must accurately match the color characteristics of the selected film. The spectral transmittances of the three colored filters used in the 8xp film recorder are shown in Figure 1-4, and the products of the three filter transmittances and CRT spectral

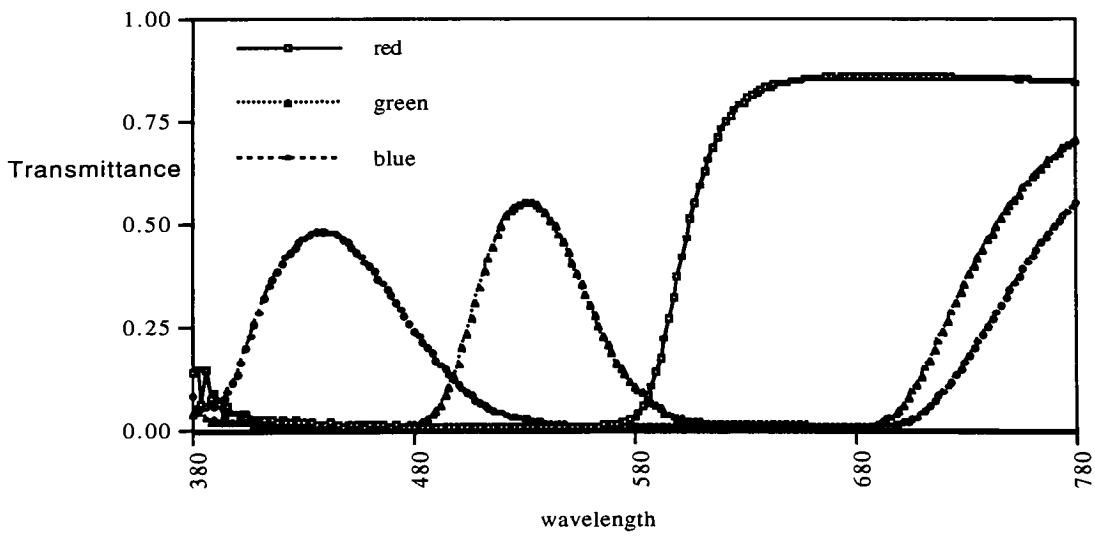

Fig. 1-4 Solitaire 8xp's filter spectral transmittances.

radiance are shown in Figure 1-5. Figure 1-5 represents the sysytem radiances. According to the color information being imaged, the filter positions are moved by the filter wheel. For example if red color information is being imaged, the red filter is set to the active position, thus exposing the red sensitive layer of the film. This reduces the amount of cyan dye, while minimally affecting the yellow and magenta dyes. The film is then processed and the slide is projected with a dark surround.

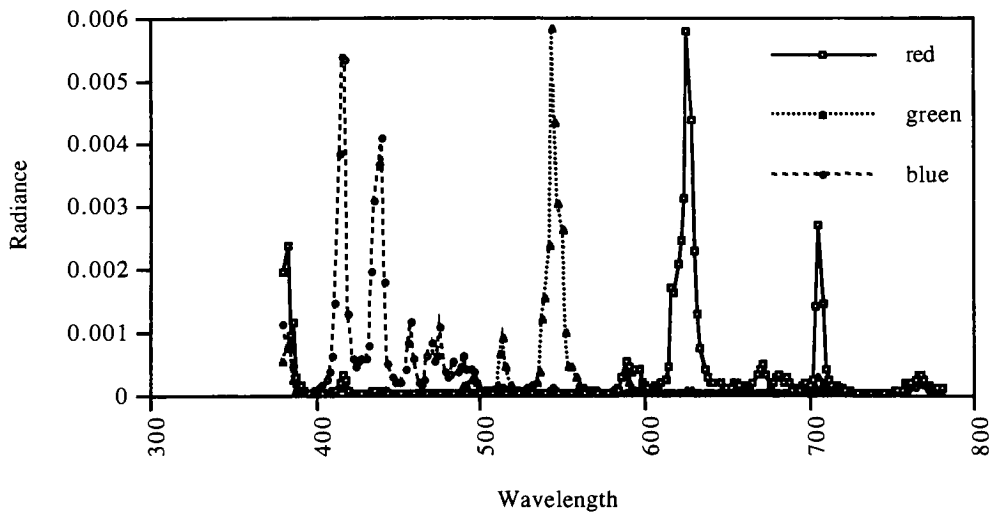

Fig. 1-5 The product of filter spectral transmittance and CRT spectral radiance (system output)

1.3 Background

Unlike other desktop devices such as a scanner and a printer, very little work has been done for the characterization of the film recorder. The formulation of the model-based characterization technique for the film recorder was described

by Wallis.[4] Even though he formulated the color image path for the film recorder, no attempt was made for the application of the model. The basic technique for recording of gray-scale images from computer-generated images was described by Keyes and Rogers.[5] The methodology for creating LUT between the digital count values in gray images and the negative film density was discussed. The LUT was generated using cubic spline interpolation with nine data points. Rosenbaum[6] described the film compensation tables for color transparency film. The LUTs were generated by three tone reproduction curves (TRCs) for red, green, and blue. The LUTs used 16 grid points and then interpolated by a cubic spline function. However, the change in one color's exposure levels have effects on the density of other colors. This crosstalk between layers can be corrected by modeling the interimage effects. Since the LUTs were generated seperately in Rosenbaum's analyses, this method did not include the modeling of interimage effects. It is known that interimage effects are designed into film to improve color reproduction greatly. Berns[1] described an analytical forward model based on Beer-Bouger law. Tone reproduction and interimage effects models were accomplished based on thirty six samples. The model performance was the average ΔE_{ab} of 6.56 with the standard deviation of 3.9. Except for the report by Berns, no colorimetric performance has been reported in the literature.

1.4 Thesis Overview

Chapter 2 covers the experimental phase of the thesis. First, the measurement of the spectral transmittance of the film is described. The spectral transmittance measurement of the film was used for the determination of the dye

absorptivities of the film. In order to select the appropriate instrument for the measurement, two spectrophotometers were selected and evaluated. Second, the density measurement of the film is mentioned. After the film was characterized properly, the characterization of the film recorder was done using a status A densitometer. Third, the procedure for the calibration of film recorder is described. This step set the film recorder response before the characterization step. The calibration step consists of the white balance (Calsets) and tone reproduction settings. Finally, the variability of the film and the film recorder is described.

Chapter 3 presents the film model. The absorptivities of cyan, magenta, and yellow dye and dye concentrations of the film were determined prior to the characterization of the film recorder. First, the background of the film model is explained. Second, the determination of the dye absorptivities is described. Since the single-dye coatings of film were not available in this thesis, each dye's absorptivity was estimated statistically using principal component analysis. Third, the amount of dyes was determined using Allen's tristimulus matching algorithm.

Chapter 4 describes the relationship between integral density and analytical density. For color reproduction purposes, the analytical density of color film must be calculated from the integral density. First, the background of the density measurement is overviewed. Second, the relationship between the integral density and the analytical density is presented using a regression analysis.

In chapter 5, the interimage effects matrix is described. Since the dyes in color film upon exposure are not independent, the interimage effects has to be

taken into account to improve color reproduction fidelity. The interimage effects were analyzed using 252 density measurements.

Chapter 6 covers the forward model between the digital values and dye concentrations. First, a non-linear film tone reproduction curve was modeled using cubic spline interpolation. Second, the interimage effects matrix was applied to achieve color correction. The color correction LUTs between input digital values and the measured density of the processed film were generated. To reconstruct the spectral transmittance, the predicted density was converted to the dye concentrations using the three-by-three matrix listed in chapter 4. The model accuracy was calculated using illuminant D50, the color matching functions for the CIE 1931 standard colorimetric observer (2 degree), and the reconstucted spectral transmittance of the processed film.

Chapter II. Experimental and Measurements

2.1 Spectral Transmittance Measurements

Two spectrophotometers were selected and evaluated. First, a The Color Sphere spectrophotometer (TCS) manufactured by BYK-Gardner was used to measure the spectral transmittance of the processed slide. The TCS uses a filtered tungsten-halogen lamp, a concave holographic grating spectrograph, and a silicon photodiode detector array. The spectral range of the TCS is from 380 nm to 720 nm in intervals of 10nm. The transmittance cell holder block was mounted to measure slide samples. The aperture for the cell holder was 28 mm. Since the mounted slide size was smaller than this aperture, its aperture was adjusted to 20 mm using black paper. Calibration was done with the mask in place. Each recorded transmittance distribution was an average of three measurements. The average standard deviation for a grey sample was 0.003, and the maximum standard deviation was 0.009. Some transmittance values from the TCS had negative values at wavelengths less than 390 nm. If the transmittance value is negative, it is impossible to convert it to a density value. This was the main disadvantage of TCS.

Secondly, the Milton Roy ColorScan was used to measure the spectral transmittance of film. The ColorScan uses a filtered 90-watt quartz tungsten-halogen lamp, a concave holographic grating monochromator, and a PMT detector. The spectral range of the ColorScan is from 380 nm to 720 nm in intervals of 10 nm. The aperture diameter was set to 20 mm. Each recorded

transmittance distribution was an average of three measurements. Since the measurement port is close to the lamp, the slide is affected by heat during the measurment

Figures 2-1 and 2-2 show the average and standard deviation of spectral density values for the grey samples using both the TCS and the ColorScan spectrophotometers. Standard deviation of spectral density for the grey in the TCS was larger than that of the ColorScan at wavelengths less than 550 nm. However, the data in the TCS were from six measurements during two months while the data in the ColorScan were from four measurements during ten days.

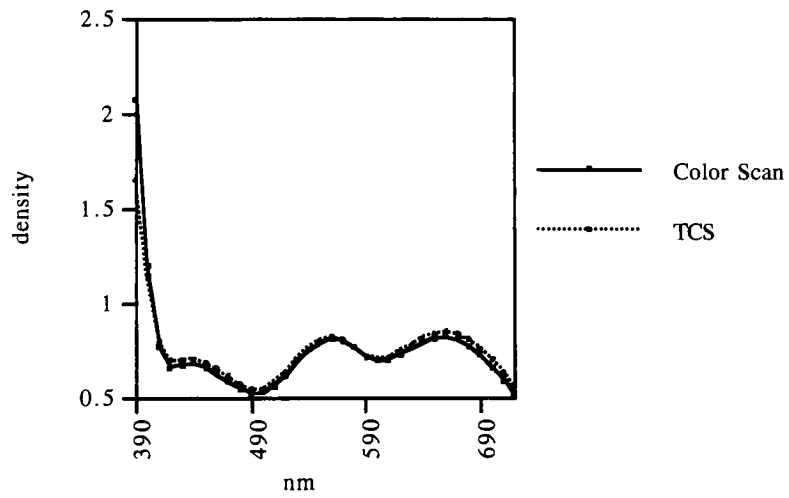

Fig. 2-1 Plot for mean density values as a function of wavelength using The Color Sphere (six measurements) and the ColorScan (four measurements).

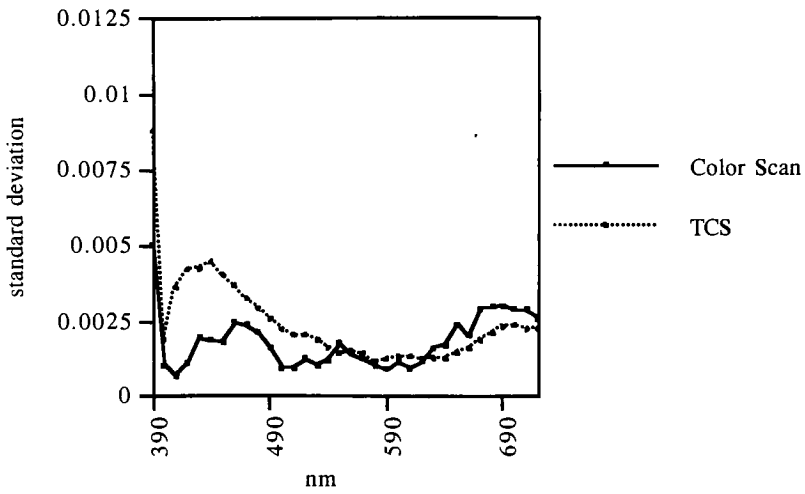

Fig. 2-2 Plot for standard deviation of grey density values using The Color Sphere and the ColorScan.

Figures 2-3 and 2-4 show the average and standard deviation of the spectral density for cyan, magenta and yellow samples using the two spectrophotometers. The spectral density curves for yellow using the TCS in the range of 450nm to 470 nm indicated some possible measurement error which might lead to subsequent modeling errors.

In this thesis, the spectral density was measured by the TCS to prevent possible a thermochromic effect on the slides. Because there was more variation and negative values at wavelengths less than 400 nm, the spectral transmittance values were measured from 400 nm to 700 nm.

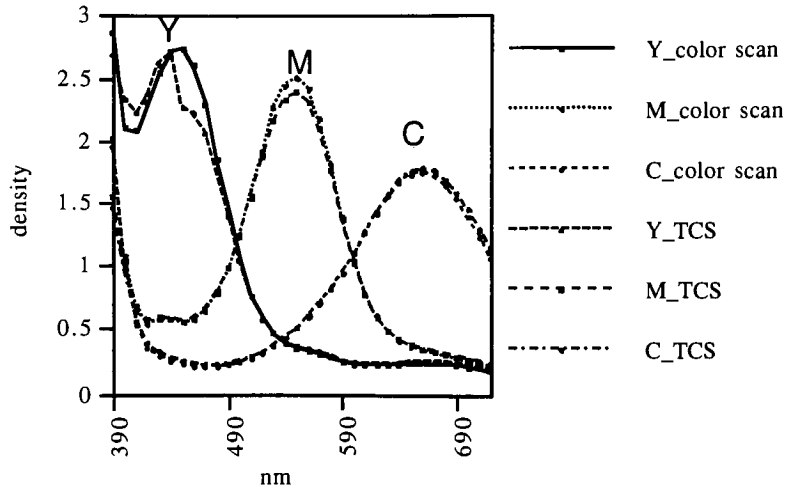

Fig. 2-3 Plot for density mean values for cyan, magenta, and yellow as a function of wavelength using The Color Sphere (six measurements) and the ColorScan (four measurements).

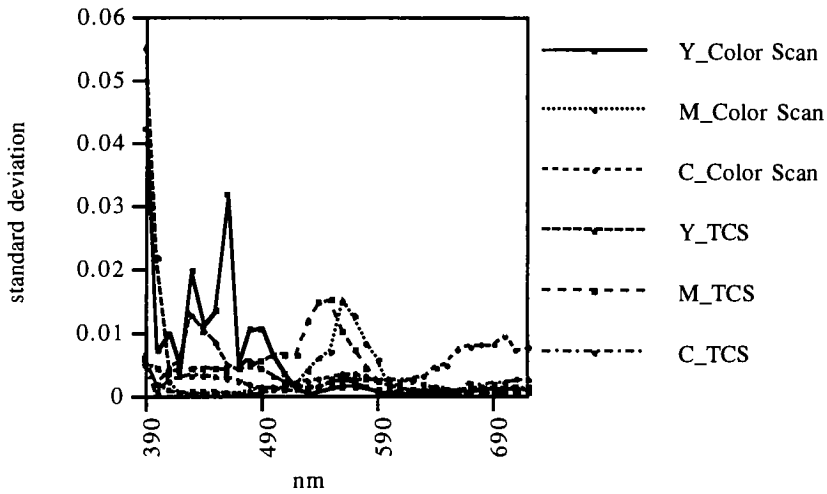

Fig. 2-4 Plot for standard deviation values of cyan, magenta, and yellow density using The Color Sphere and the ColorScan.

2.2 Density Measurements

Transparent film is characterized using the spectral density from the spectrophotometer. If the relationship between the measured densities (integral density) and the dye concentrations (analytical density) is well defined, a densitometer can be used to estimate concentration through Beer-Bouger law. The density values were measured using the Macbeth TR 1224 densitometer. Direct data transfer was available since the Macbeth TR1224 densitometer was connected to the Macintosh. A serial interface was used to transmit density data from all four filter channels to the computer. Connection to the computer was provided by a cable equipped with a telephone-type connector on one end and a DB-25S female connector on the other end. Data output formats for the printer interface are listed in Table 2-1.

Table 2-1. Data output formats for printer interface of the densitometer.

Output Format	Printer Interface
Data Type	ASCII
Baud Rate	300
Start Bit	1
Data Bits	7
Parity	OFF
Stop Bits	1
Bits per Character	9

There are some advantages to using a densitometer. First of all, the price of a densitometer is much lower than that of a spectrophotometer. Secondly, a large portion of variability in the whole color photographic process originates from the processing step in color reproduction. Smaller samples can be placed on one slide because the densitometer has a smaller aperture. Therefore, more information can be obtained from one roll of film. With more samples undergoing the same chemical reaction simultaneously, the processing variability is reduced. Thirdly, a densitometer is common to the film industry. However, the spatial variability within one slide has to be compensated. Densitometer can also be used for the film recoreder calibration (set up).

2.2.1 Spatial Variability Correction for Density Measurement

In order to explain the spatial variability of a slide, the densities of white samples (dr=dg=db=255) were measured in nine different positions. The nine positions are shown in Figure 2-5.

position 1	2	3
4	5	6
7	8	9

Fig. 2-5 A sample slide for the spatial variability.

The spatial variabilities of the Dmin samples depend on the positions. The spatial variability data show that the positions 1,4, and 7 have higher densities than rest of the positions. The average values and standard deviation values are listed in Figures 2-6-1 and 2-6-2.

DR=0.33 DG=0.34 DB=0.31	DR=0.32 DG=0.32 DB=0.30	DR=0.32 DG=0.33 DB=0.30
DR=0.33 DG=0.34 DB=0.31	DR=0.31 DG=0.33 DB=0.30	DR=0.32 DG=0.32 DB=0.30
DR=0.34 DG=0.35 DB=0.31	DR=0.33 DG=0.34 DB=0.30	DR=0.32 DG=0.33 DB=0.30

Fig. 2-6-1 Average density values of seven exposures for Dmin sample.

DR=0.014 DG=0.013 DB=0.014	DR=0.01 DG=0.015 DB=0.008	DR=0.01 DG=0.01 DB=0.008
DR=0.010 DG=0.012 DB=0.012	DR=0.010 DG=0.010 DB=0.010	DR=0.012 DG=0.013 DB=0.010
DR=0.012 DG=0.010 DB=0.010	DR=0.012 DG=0.012 DB=0.012	DR=0.014 DG=0.010 DB=0.011

Fig. 2-6-2 Standard Deviation Values of seven exposures for Dmin sample.

The cause of spatial variability might be the result of an unequal intensity of CRT electron beam, geometric error between CRT and lens, non uniformity of the CRT screen, etc. Each sample was normalized by the mean value of Dmin samples according to the position of each samples in order to compensate for the spatial variability.

2.3 Calibration of the Film Recorder

The dynamic range of film density through a film recorder relies on the relationship between each channel's exposure intensity and film responsivity. It is necessary to have constant dynamic range of film density from exposure to exposure to achieve colorimetric reproduction of film. The dynamic range of film exposed by the film recorder in this research was around 0.25 (Dmin) to 3.00 (Dmax). The tone reproduction curve was obtained within this density range. The film recorder was calibrated by gain and offset adjustments: 1) Calsets (offset adjustment) searching, and 2) tone reproduction (gain adjustment) searching. Calsets determined the maximum output intensity of the CRT before the CRT gun amplifier stage. In this research, the calibration software, Colorfit, was used to find the optimum calsets and the tone reproduction curves for the film recorder. This software was written by Management Graphics Inc.(MGI).

2.3.1 Calset Searching (white balance)

A Calset determines the maximum exposure for red, green, and blue channels and controls the exposure range of the film recorder. On the basis of this exposure range, the tone reproduction curve can be determined. These steps

enable a film recorder to utilize its entire tonal range. A Calset relies on a specific film type and speed. There is a maximum output limit for each channel to prevent CRT blooming. Calsets above 200 produce intensities that cause excessive flare and halo. It is recommended that maximum Calset settings for each channel are below 170 and within 20 units of each other. Therefore, the number of scan lines was adjusted to be below 170 Calset values. Doubling the number of line scans is equal to reducing the Calset values by 18. Table 2-2 shows several settings to find the optimum Calsets. The Colorfit program exposes 27 samples based on the user-defined Calsets, Dmin, and the number of scan lines. This program iterates until the optimum Calsets are obtained. Based on the Calset settings, the tone reproduction curves were determined. Based on the output values from Colorfit, a regression analysis was performed. The predicted Calsets for each channel from the regression analysis were 193:182:158 (r:g:b) with the number of line scans at 1:1:1 for each channel and minimum densities at 0.25:0.25:0.25. Because red and green Calsets are higher than 170, the number of scan lines was adjusted to 4:2:1 for each channel. This resulted in the Calsets 157:164:158 for each channel. When these Calsets were applied to the TRC in linear density steps, the grey steps showed a color shift. In this research, the default Calsets (182:168:158 with line scan 1:1:1) were used.

2.3.2 Tone Reproduction Settings

After the Calset setting was determined, the gray balanced TRC was optimized in an iterative fashion. The Colorfit program used 16 grey steps to determine tone reproduction curves. There are three choices for the TRC:

Table 2-2. Calset searching results from the Colorfit program.

Input			Output	
scan lines (r:g:b)	Dmin	Calsets (r:g:b)	Predicted Calsets (r:g:b)	Dmin (r:g:b)
1:1:1	0.2	182:167:147	200:188:161	0.2:0.2:0.2
4:2:1	0.2	182:167:147	175:182:164	0.18:0.16:0.18
1:1:1	0.32	182:167:147	188:178:130	0.24:2.23:0.24
1:1:1	0.2	172:157:137	199:192:167	0.3:0.28:0.29
1:1:1	0.2	192:177:157	211:196:175	0.19:0.19:0.19
1:1:1	0.2	170:160:150	202:184:184	0.27:0.29:0.27
1:1:1	0.2	180:170:160	205:192:155	0.22:0.23:0.23

density, gamma, and L*(CIE Lab). If a perceptually uniform grey step is needed, lightness of CIELAB space will be adequate. If linear density steps are desired, density units are adequate for TRC. If the same gamma of the computer monitor is desired, the TRC in gamma will be useful.

First, the TRC was optimized to produce even steps in density. In this program, the processing control strip density values can also be taken into account for processing variability. Based on density values of the control strip, measured density was corrected. Figures 2-7, 2-8 and 2-9 show TRC searching steps.

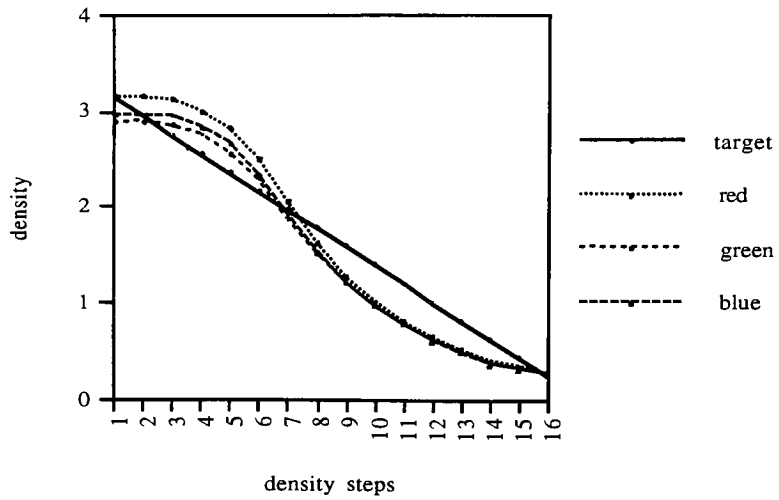

Fig. 2-7 First iteration for setting tone reproduction using Colorfit software.

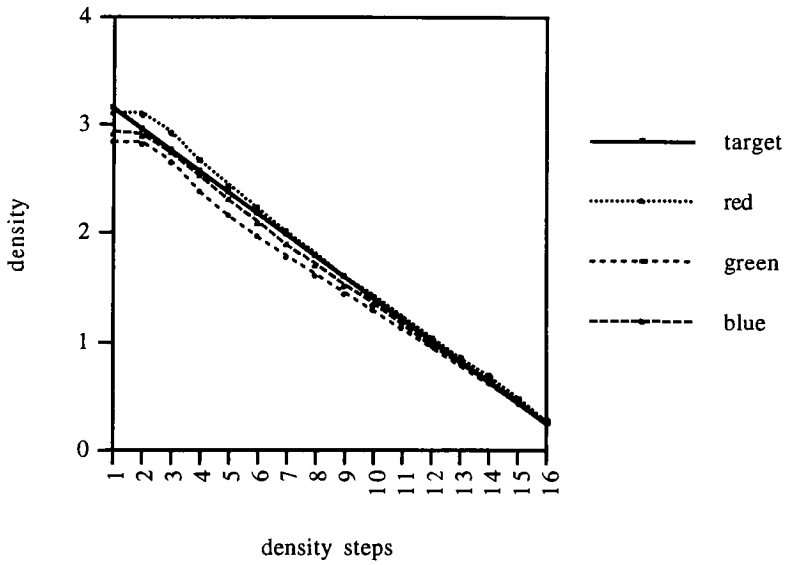

Fig. 2-8 Second iteration for setting tone reproduction using Colorfit software.

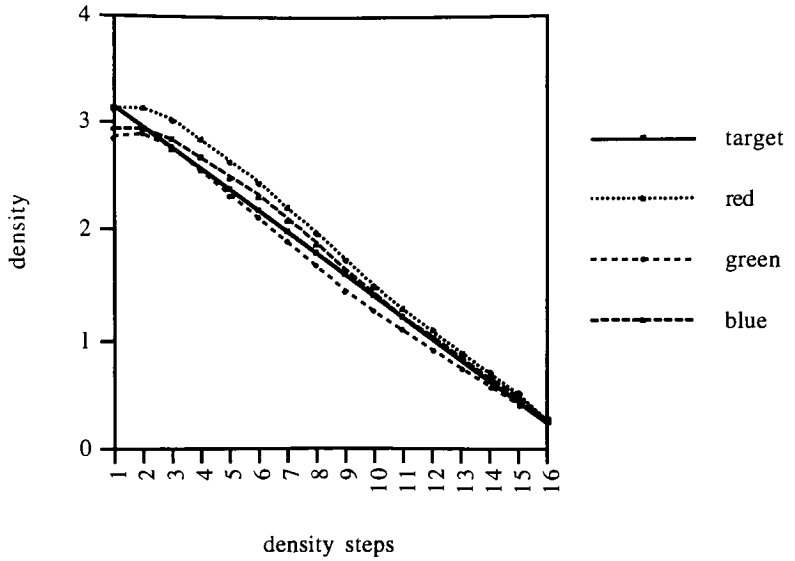

Fig. 2-9 Third iteration for setting tone reproduction using Colorfit software.

Only three iterations yield linear density curves for the given grey samples. The Colorfit program fits the data using a spline interpolation function with 16 density points. Even though TRCs were linear in density after three runs, there was still nonlinearity in the high density regions. This might be a source of modeling error in dark colors. When the film was exposed using this TRC, the neutral did not look grey. TRCs that are linear in density are not graybalanced TRCs.

Secondly, the TRC was generated in gamma that matched the TRC of the computer monitor. The default setting for a Macintosh display is usually a gamma of 1.8. The relative luminance of computer monitor is expressed as

$$Y_{rel} = Y/Y_{max} = \left(dc/dc_{max}\right)^{1.8}$$

where $\mathbf{Y}$ is the absolute luminance for a given digital count, $\mathbf{dc}$ and $\mathbf{Y_{max}}$ is the maximum luminance for a digital count $\mathbf{dc_{max}}$. The image in the computer monitor was viewed under a dim surround, while the film image was projected in a dark surround. The contrast of the image will be different according to viewing conditions. The required increase in gamma is 1.25 for a dim surround and 1.5 for a dark surround.

$$\mathbf{Y_{slide}}^{1/1.5} = \mathbf{Y_{CRT}}^{1/1.25}$$

and,

$$\mathbf{Y_{slide}} = \mathbf{Y_{CRT}}^{1.5/1.25} = \left(\mathbf{dc}/\mathbf{dc_{max}}\right)^{1.8*1.5/1.25} = \left(\mathbf{dc}/\mathbf{dc_{max}}\right)^{2.2}$$

As a result, the TRC for the film recorder was set to a gamma of 2.2. The TRC generated by correcting the gamma yielded a better graybalanced neutral than linearizing the density.

In this research, TRC was generated in gamma of 2.2, and the maximum brightness for each channel was set to 182,168, and 158 for red, green, and blue respectively. The number of scan lines for each channel was set to one.

2.4 Measurement Variability

Even though a digital film recorder is a highly sensitive and accurate means of transferring input RGB values to film output, the film processing steps and the film itself contain a lot of variability from factors such as chemical reaction, humidity, temperature, and so forth. This will eventually affect the accuracy of color reproduction model. However, those factors were beyond the

control of this research. In this thesis, the variability of film was examined using a spectrophotometer. The variability of the measurements were taken into account.

2.4.1 Variability of Film

The variability of the slide after the processing step was examined for two months. These measurements were done using the TCS spectrophotometer. Figure 2-10 shows the ΔE^*_{ab} over a two month period. The first measurement, right after processing, was considered as the standard sample. The ΔE^*_{ab} values were changed from 0.50 to 1.24 two-months later. The samples after 45 days were measured right after the Color Scan measurements. Because the Color Scan heats up the slides, large ΔE^*_{ab} values resulted. When slides were measured 15 days later, the ΔE^*_{ab} values of the slides decreased. The decrease indicated that heat effect did not change the slide permanently if the temperature was not high enough (under 100°C). The plots indicated that the color of the cold slides (before projection) changed over time. Figure 2-11 shows chroma changes over time. The change from normal temperature and humidity over time show that the variability goes in the opposite direction of the heat effect. These also show that the heat effect does not change the slide permanently. After the slide cooled down, the chromic changes showed the same trend as before. However, these changes were minute. The overall chroma plot is shown in Figure 2-12.

2.4.2 Film Recorder Variability

After the Calsets and TRCs were determined, the repeatability of the film recorder was examined by the short-term and the long-term variabilities.

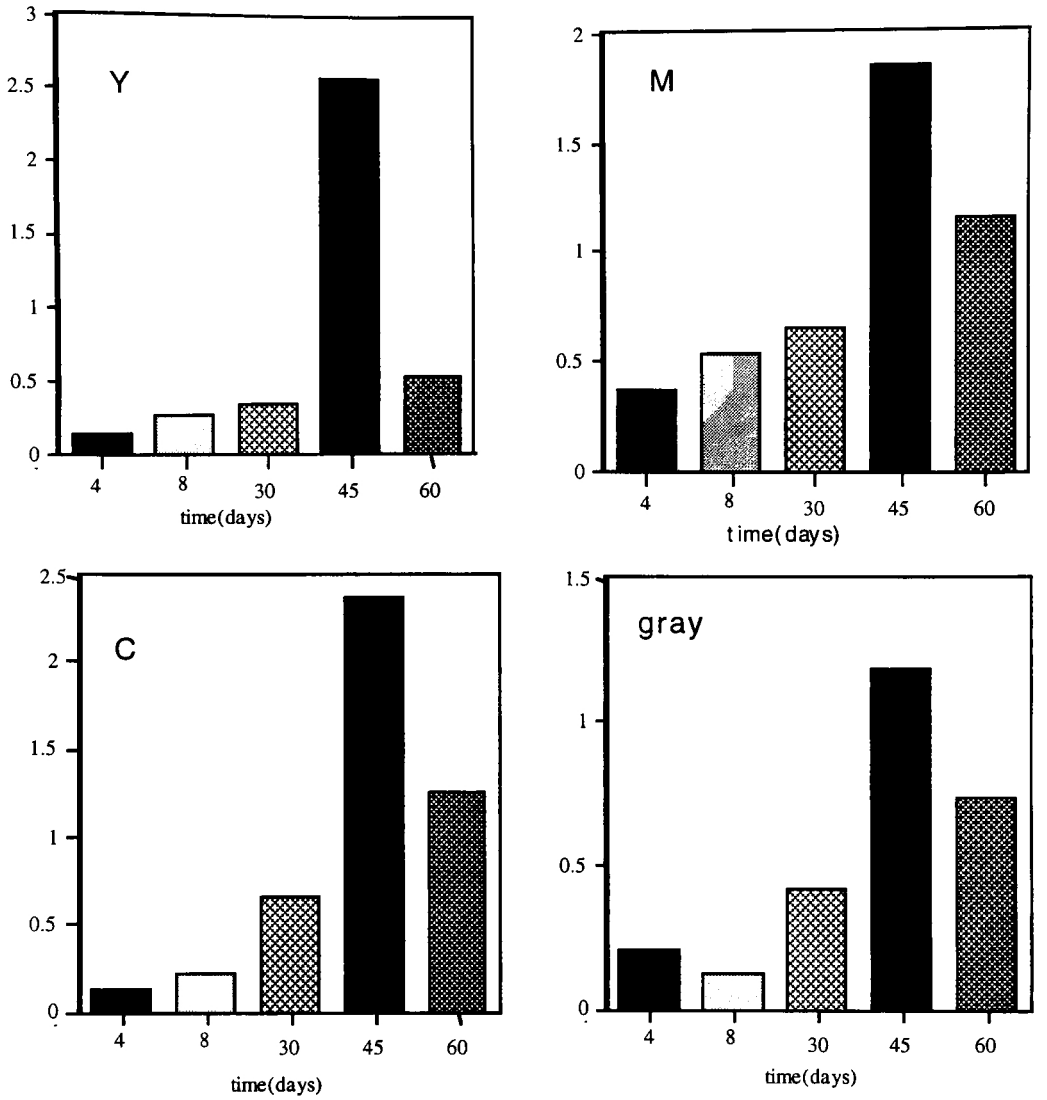

Fig. 2-10 ΔE^*_{ab} changes compared with the first day of measurement as a function of time for cyan, magenta, yellow and grey slides.

First, the short-term variability was examined using five samples. Each sample was repeated seven times within one roll of film. When the red channel changed

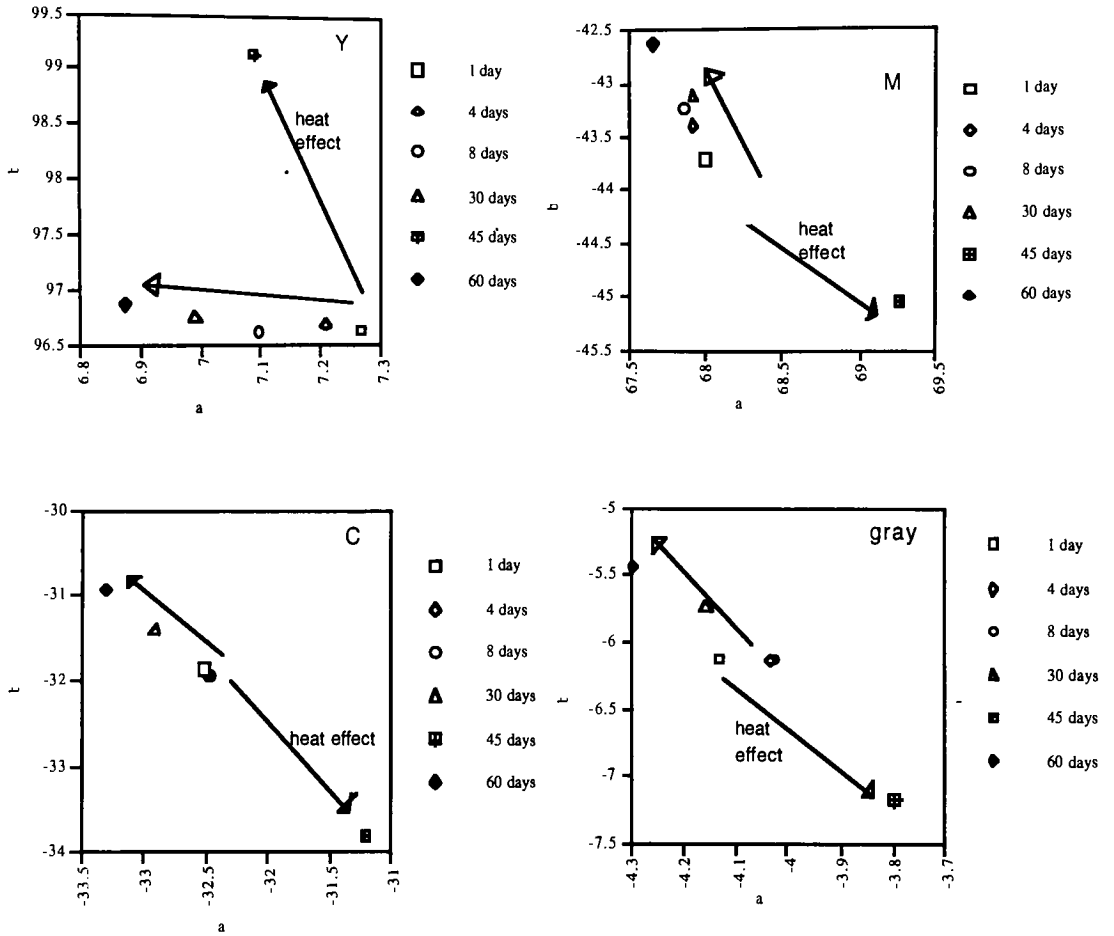

Fig. 2-11 Chroma changes compared with the first day of measurement as a function of time for cyan, magenta, yellow and grey slides.

digital counts from 0 to 255 by increments of 32, green and blue channels remained at 96. It was the same for the blue and green channels. Nine different levels of grey were made since each slide can hold nine different images.
All white samples were also made to explain spatial variability on one slide. Each slide was exposed seven times.

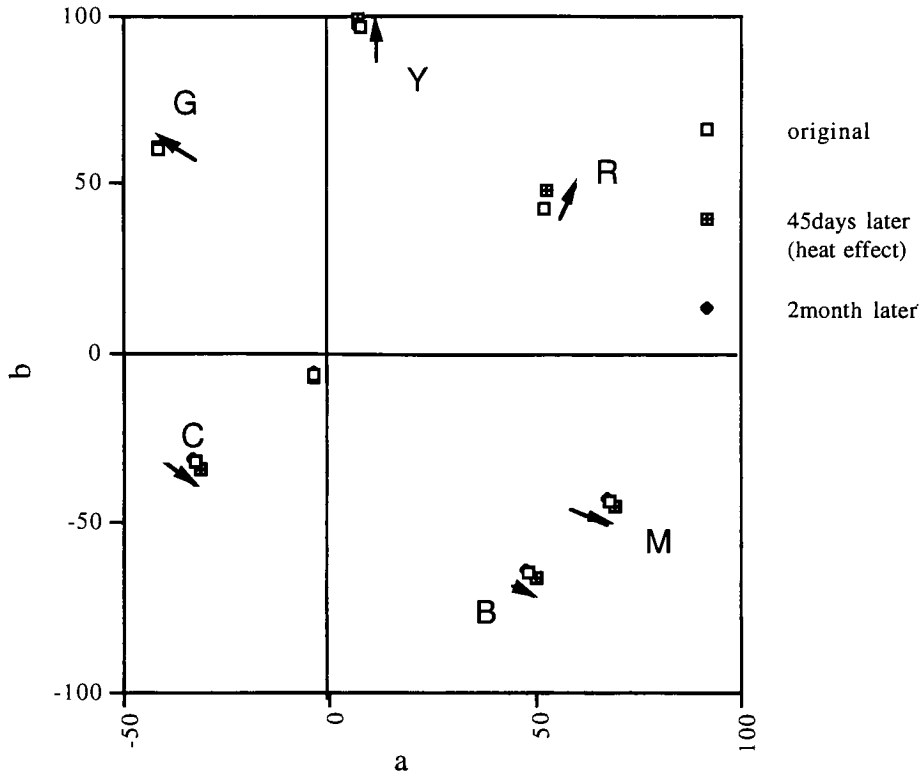

Fig. 2-12 Chroma changes compared with the first day of measurement as a function of time and heat.

Figure 2-13 shows the average and 2-sigma standard deviation of seven exposure densities within one roll of film. Figure 2-14 shows the average and standard deviation of nine different positions of the Dmin sample. This indicated the exposure variability of the film recorder in nine different positions. The Dmin sample was exposed seven times within one roll of film.

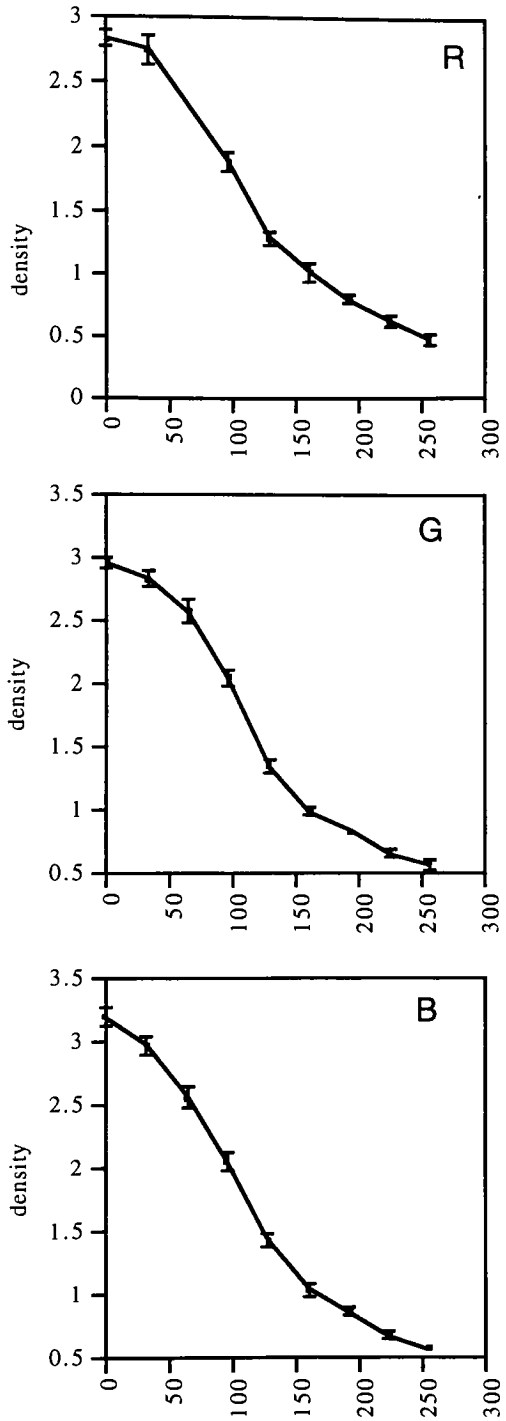

Fig.2-13 Average and 2σ Std. Dev. of 7 exposure densities within one roll of film.

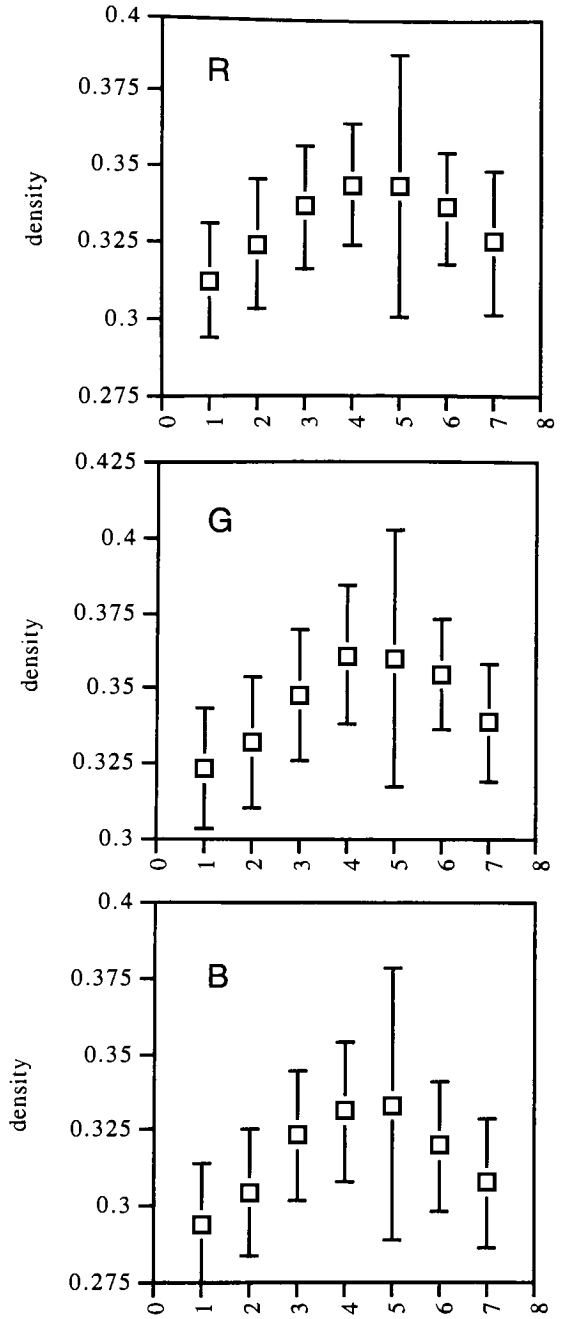

Fig. 2-14 Average and Std. Dev. of film densities in 9 positions within one roll of film as a function of exposures.

Figure 2-15 shows the average and standard deviation of seven exposure as a function of nine positions. This indicates the spatial variability of the slides upon different exposures. The film recorder has an average standard deviation of 0.02 in seven measurements. This variability was comprised of densitometer variability and processing variability within one roll of film. The spatial variability of the white samples was discounted by normalizing each sample by an average density of the white samples in the same position. Although the standard deviation of 0.02 was not large, this might contribute to modeling errors.

Second, the long term variability was examined on 3 different days. This is shown in Figure 2-16. The main gamma curves within 10 days are well matched. The main gamma curves after 23 days showed a little deviation, especially under red exposure. The variability seemed reasonable because it was a compilation of three different types of variability: long-term processing variability, densitometer variability, and film recorder variability.

2.4.3 Other Variability

It is important to allow an instrument time to warm-up in order to record accurate data. It is recommended that the film recorder should be turned on during the week and turned off during the weekend for self diagnosis when there is no exposure on the weekend. In this research, the film recorder was turned on at least a half day before exposing the film. The densitometer was also turned on at least one hour before measuring density values. The spectrophotometer was also turned on at least 30 minutes before measuring the transmittance data.

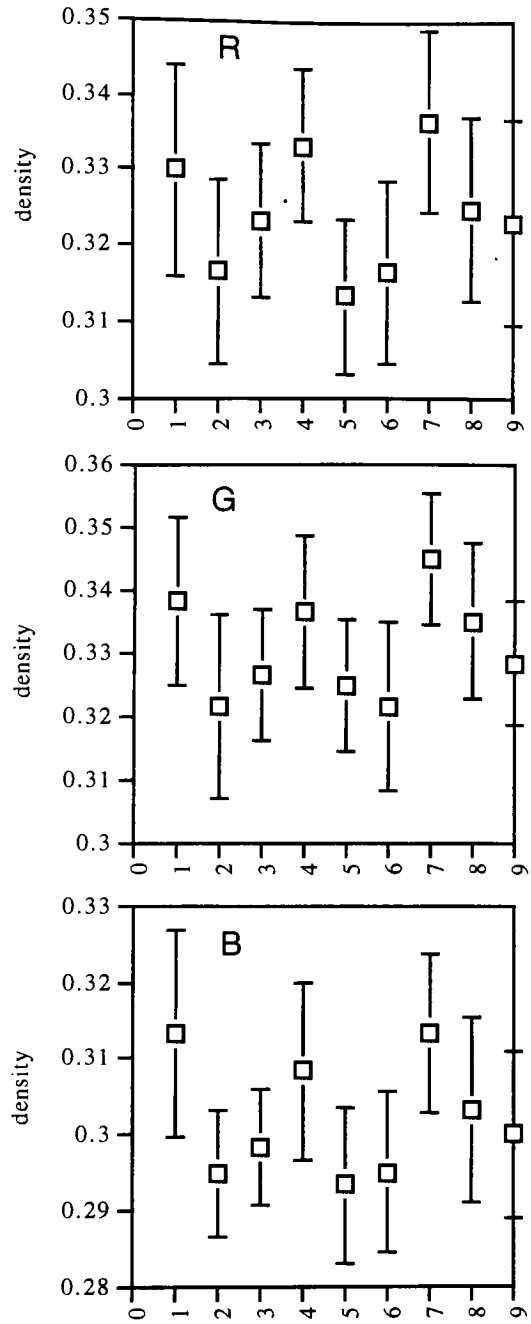

Fig. 2-15 Average and Std. Dev. of 7 exposures of Dmin sample as a function of 9 different positions within one slide.

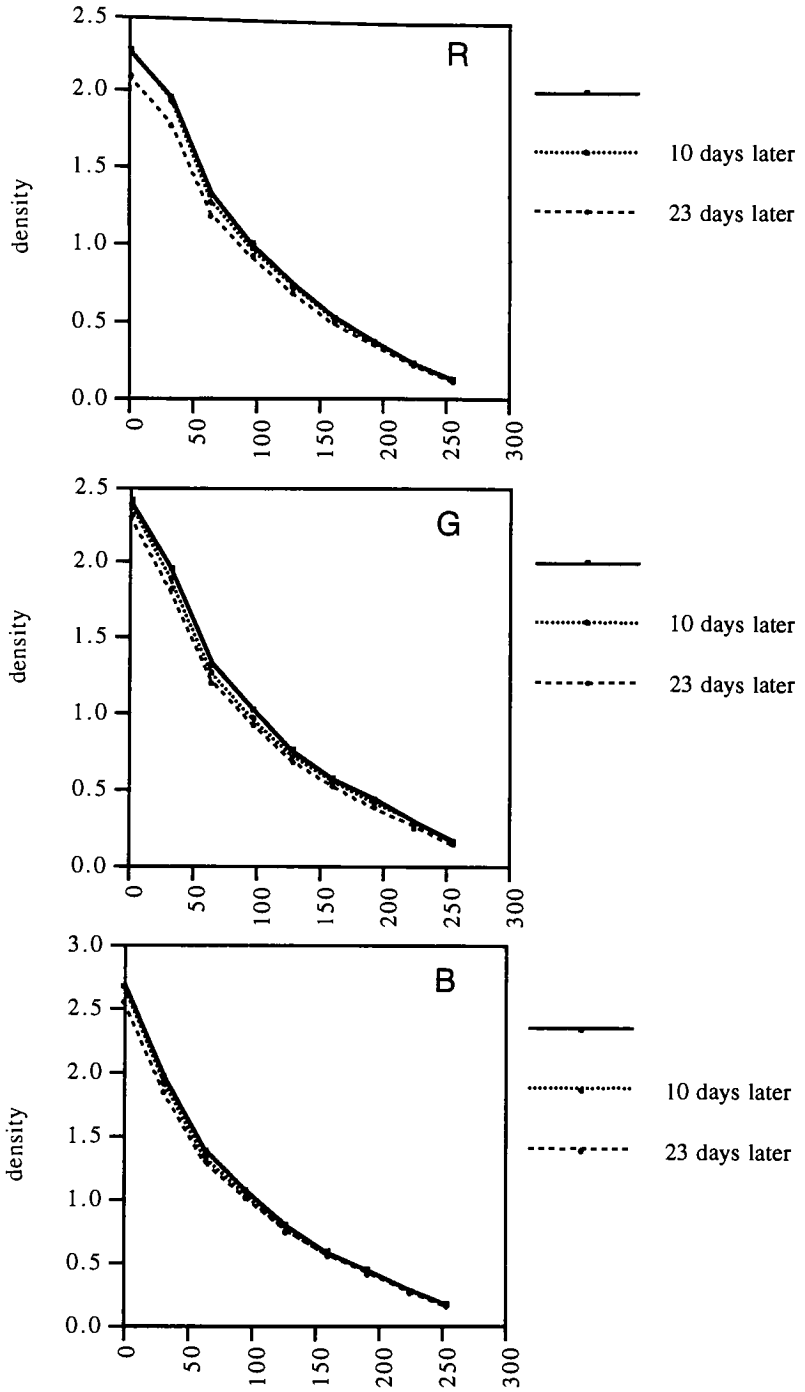

Fig. 2-16 Average density values of 7 exposures from three different days.

In this research, Kodak Ektachrome plus professional 100 film was used. The film used in this research came from the same batch (emulsion #091, production date: 7/27/93). The film was kept in a freezer. Before the film can be used by the film recorder, the film must sit in room temperature for at least 3 hours.

Because the variability of processing in color film is inherent, processing steps need to be controlled with precision. The processing variability results from the chemical composition of processing solutions, the temperature of the baths, time of immersion of the samples, and the agitation of each solution over the surface of the material.[11] In this research, processing variability was controlled by putting the images in the last hanger with control strips. The density values of the control strip give an indication of processing variability. Except for this condition, it is beyond the scope of this research.

Chapter III. Film Model

3.1 Background

It is important to understand the relationship between the transmitted light and the dyes in a film layer in order to predict color. As the light passes through the medium (film layer), some of the light is absorbed at a certain wavelength, and some of the light can be scattered. In this research, it was assumed that there was no scattering of light. If we only consider the light absorption, the light intensity is decreased by the amount of colorants. This was expressed by an absorption coefficient of the film. In order to specify color reproduction in color film, the absorption characteristics of the transparent colorants must first be known. The absorption of light in a film layer is directly proportional to the number of absorbing molecules. The greater the number of absorbing molecules, the greater the probability of absorption, and consequently, the greater the density to light.

3.1.1 Beer-Bouger Law

The transparent medium of interest is composed of dyes suspended in gelatin. Because of the special characteristics of gelatin, the gelatin behaved like a solution. Figure 3-1 shows the model for the passage of light in a transparent film medium.[7] A mathematical model for this medium considers a transparent film with total thickness **X**. The intensity of monochromatic light before passing through the film is $\mathbf{I_0}$; after passing through it is **I**. Assume the infinitesimal thickness **dx** inside the film and light intensity, **i** , passing through this element suffers a decrease of intensity, **di** that is proportional to its intensity.

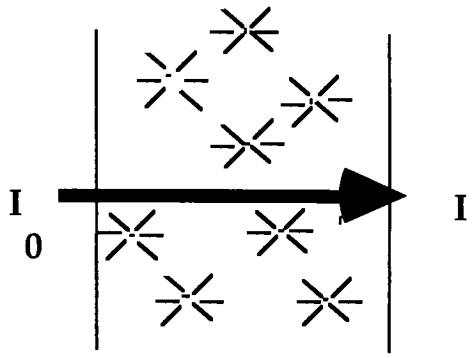

Fig. 3-1 Model for the passage of light in a transparent medium.

Therefore,

$$di/dx = -Ki$$

where **K** is the absorption coefficient of the film. The entire thickness of the film can be expressed as

$$I/I_0 = Ti = e^{-KX},$$

also,

$$-\log Ti = \log(1/Ti) = KX$$

where T_i is the internal transmittance of the film. By the Beer-Bouger law, the absorption coefficient K is proportional to the concentration of colorant causing absorption.

$$\log\left(1/Ti\right) = CkX$$

where **C** is the concentration of the colorant, and **k** is the unit absorption coefficient. When we have 3 colorants that are cyan, magenta, and yellow, the above equation can be expressed as

$$\log\left(1/Ti\right) = \left(k_t + Cck_c + Cmk_m + Cyk_y\right)X$$

where k_t is the absorption coefficient of the film base without colorant, and k_c, k_m, and k_y are the unit absorption coefficients of each dye. The optical density, **D**, is defined using the ratio of input flux density, I_0 and output flux density, **I**.

$$D = -\log\left(I/I_0\right)$$

Therefore, the relationship between the density and the dye concentrations can be expressed as

$$D = -\log Ti = \left(k_t + Cck_c + Cmk_m + Cyk_y\right)X$$

Because the dyes in color film are spectrally selective, the equation can be expressed as a function of the wavelength.

$$D_\lambda = -\log Ti_\lambda = \left(k_{t,\lambda} + Cck_{c,\lambda} + Cmk_{m,\lambda} + Cyk_{y,\lambda}\right)X$$

This equation is the spectral density distribution. The Beer-Bouger law holds only for spectral densities measured with monochromatic radiation since $-\log \int_\lambda T\lambda d\lambda$ approximates $\int_\lambda -\log T\lambda d\lambda$ when $d\lambda$ is small. The law does not hold for wide-band filters (large $d\lambda$) in terms of their effects on photographic film.

However, in practice, we can approximate this relationship for 10 nm spectrophotometric data. In this thesis, the integral densities were measured by a spectrophotometer with 10 nm intervals, and a densitometer with 3 filters. Therefore, the relationship between the spectral transmittance and the amount of dyes in the film is described as

$$T_\lambda = 10^{-\left(k_{\lambda,t} + Cck_{\lambda,c} + Cmk_{\lambda,m} + Cyk_{\lambda,y}\right)}$$

However, it is not easy to obtain the film base without any residual dye since it is impossible to get zero density film output from the film recorder. If the measured transmittance of the film was normalized by the Dmin (Tmax) samples, we can also eliminate the effects of the film base relatively. Therefore, the Beer-Bouger law can be redefined as

$$T_\lambda = T_{\lambda,max} * 10^{-\left(Cck_{\lambda,c} + Cmk_{\lambda,m} + Cyk_{\lambda,y}\right)}$$

The measured transmittance was normalized by the T_λ max (D_λ min), and the internal transmittance was obtained by the equation above in this research.

3.2 Determination of Dye Absorption Curves

The absorption curves of each dye were estimated by means of principal component analysis using SYSTAT.[9] A 90-image target created in Photoshop was used to obtain the eigenvectors of each dye absorptivity for transparent color films. The digital values of a 90-image target was shown in Appendix A.

The methodology of the principal component analysis for the dye absorption curves has been described by Berns.[1] First of all, the covariance matrix with equamax rotation was used to estimate three eigenvectors using all of the data. The total variance of the three eigenvectors was 99.95%. Since the film is composed of three dyes, this result seemed reasonable. The eigenvectors are shown in Figure 3-2. The peak wavelengths for each eigenvector was 660 nm, 550 nm, and 440 nm.

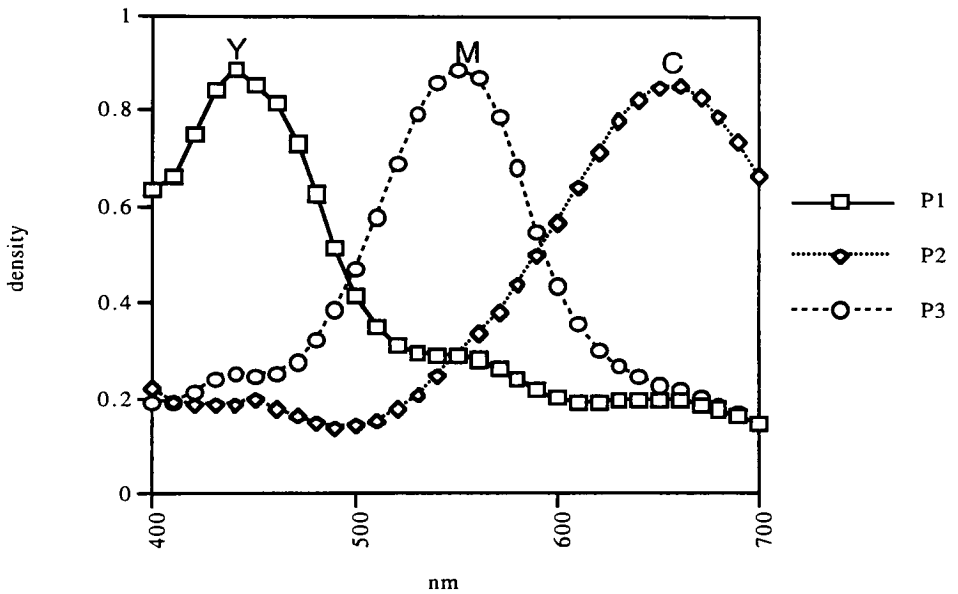

Fig. 3-2 C, M, and Y eigenvectors from equamax rotation.

Secondly, the eigenvectors of the cyan, yellow, and magenta ramps, from the 90-image data, were obtained by principal component analysis with covariance matrix without rotation. In this case, it was assumed that the first component of the cyan, magenta, and yellow dyes represented physical absorption

characteristics of each dye. The first eigenvector for each dye is shown in Figure 3-3. The peak wavelengths for cyan, magenta, and yellow dyes were 660 nm, 550 nm, and 440 nm respectively. These coincide with the equamax results.

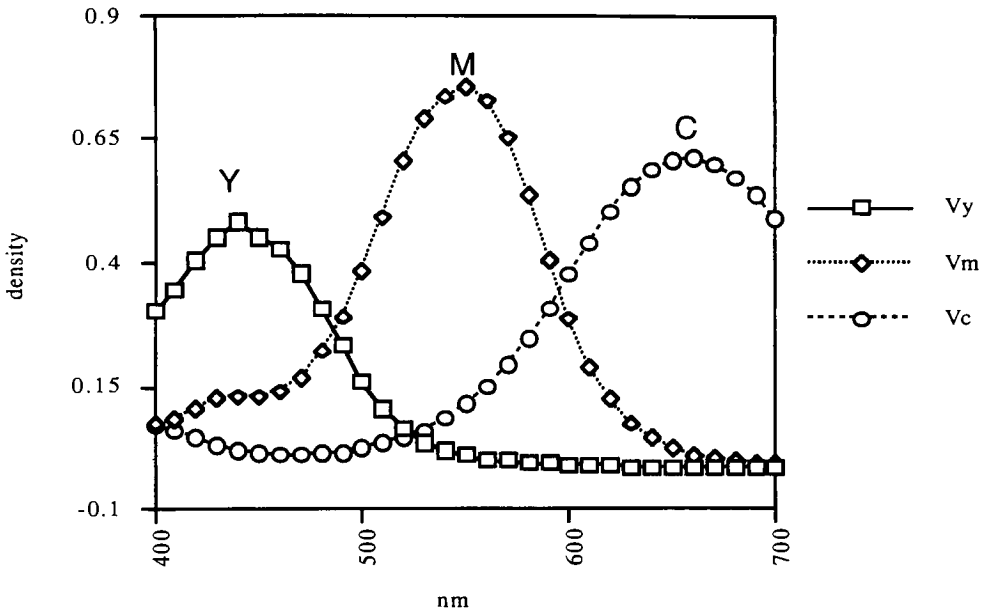

Fig. 3-3 Eigenvectors from C, M, and Y ramps.

Thirdly, the eigenvectors from equamax rotation and the eigenvectors without rotation were rotated by a three-by-three transformation. The reason for the rotation with the ramp eigenvectors was to acquire physically closely related cyan, magenta, and yellow dye absorption curves.

$$\begin{bmatrix} Vy \\ Vm \\ Vc \end{bmatrix} = \begin{bmatrix} 0.60023 & -0.14777 & -0.11840 \\ -0.08230 & 0.94968 & -0.20668 \\ -0.11955 & -0.08563 & 0.76916 \end{bmatrix} \begin{bmatrix} Py \\ Pm \\ Pc \end{bmatrix}$$

where **Vy, Vm,** and **Vc** are eigenvectors for the yellow, magenta, and cyan ramps respectively, and **Py, Pm,** and **Pc** are eigenvectors from the equamax rotation. The result is shown in Figure 3-4. These eigenvectors were used for determining the dye amounts. The data are listed in Appendix B.

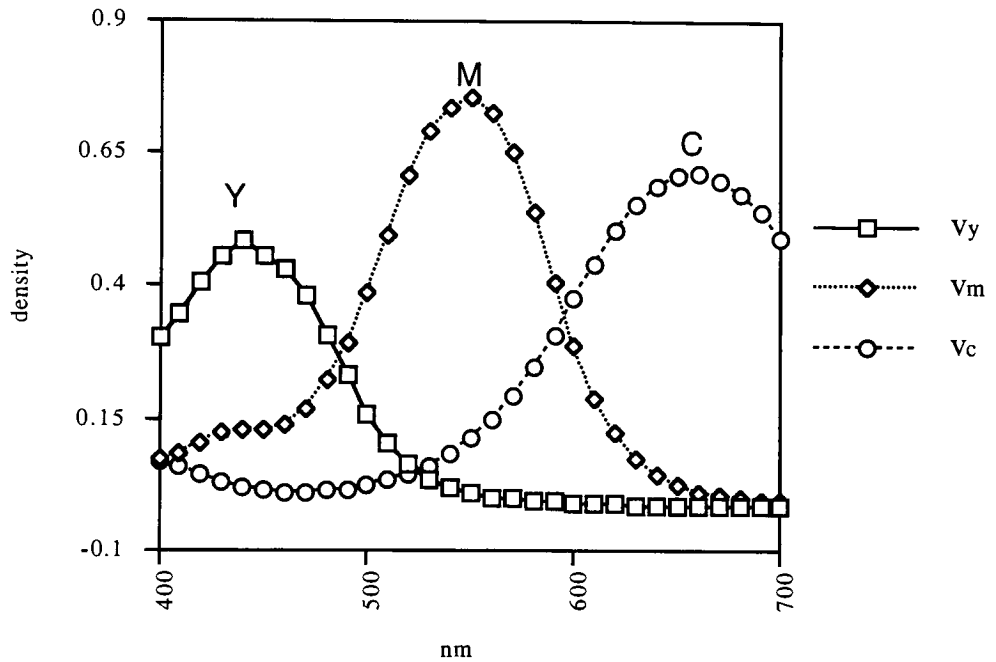

Fig. 3-4 Final eigenvectors from both equamax rotation and C, M, Y ramps.

3.3 Determination of the Dye Amounts

In this research, the amounts of cyan, magenta, and yellow dyes were determined by Allen's tristimulus matching algorithm.[7] Ohta[10,11,12] also described metameric color matching with Newton-Raphson algorithm in color photography. Berns[13] discussed these two algorithms and showed that Allen's

algorithm gave an accurate first estimation when the spectral transmittance of the dye was known. The tristimulus value matching software was used to calculate the concentrations. This software was based on Allen's algorithm and the optimization method was the Newton-Raphson method. The software was translated in C language from Fortran. The C version of this software is listed in Appendix C. If the Beer-Bouger law holds, eigenvectors that represent the unit absorptivity of each dye and the estimated concentrations from the tristimulus value match the predicted transmittance. Spectral matching, which minimizes the difference between measured transmittance and predicted transmittance, will cause the tristimulus value to match. In this program, the Newton-Raphson method was applied between the concentrations of each dye and the tristimulus values.

The tristimulus matching algorithm was based on the assumptions that the absorption properties of the slide were the sum of the absorption properties of each of the dyes.

$$\mathbf{D}_{\lambda,\mathbf{max}} = \mathbf{D}_{\lambda,\mathbf{cyan}} + \mathbf{D}_{\lambda,\mathbf{magenta}} + \mathbf{D}_{\lambda,\mathbf{yellow}}$$

and

$$\mathbf{D}_{\lambda,\mathbf{cyan}} = \mathbf{CcD}_{\lambda,\mathbf{cyan,max}}$$
$$\mathbf{D}_{\lambda,\mathbf{magenta}} = \mathbf{CmD}_{\lambda,\mathbf{magenta,max}}$$
$$\mathbf{D}_{\lambda,\mathbf{yellow}} = \mathbf{CcD}_{\lambda,\mathbf{yellow,max}}$$

By Allen's Conventions, the matrices and vectors are defined as:[7]

$$\mathbf{T} = \begin{bmatrix} \overline{x_{380}} & \overline{x_{390}} & \cdots & \overline{x_{760}} \\ \overline{y_{380}} & \overline{y_{390}} & \cdots & \overline{y_{760}} \\ \overline{z_{380}} & \overline{z_{390}} & \cdots & \overline{z_{760}} \end{bmatrix}$$

where $\overline{x_\lambda}$, $\overline{y_\lambda}$, and $\overline{z_\lambda}$ are the CIE color matching functions,

$$\mathbf{E} = \begin{bmatrix} E_{380} & 0 & \cdots & 0 \\ 0 & E_{390} & \cdots & 0 \\ \vdots & \vdots & & \vdots \\ 0 & 0 & \cdots & E_{760} \end{bmatrix}$$

where E represents the relative spectral power distribution of the light source,

$$\mathbf{F}^a = \begin{bmatrix} f(T)^a_{380} \\ f(T)^a_{390} \\ \vdots \\ f(T)^a_{760} \end{bmatrix}$$

where T represents spectral transmittance of the transparent samples, and a represents the sample being matched where f(T) is log(Tmax/T),

$$\mathbf{D} = \begin{bmatrix} d_{380} & 0 & \cdots & 0 \\ 0 & d_{390} & \cdots & 0 \\ \vdots & \vdots & & \vdots \\ 0 & 0 & \cdots & d_{760} \end{bmatrix}$$

where d = [dT/df(T)],

$$\Phi = \begin{bmatrix} \Phi^c_{380} & \Phi^m_{380} & \Phi^y_{380} \\ \vdots & \vdots & \vdots \\ \Phi^c_{760} & \Phi^m_{760} & \Phi^y_{760} \end{bmatrix}$$

where Φ represents the unit absorption coefficients for the dyes, and

$$\mathbf{C} = \begin{bmatrix} Cc \\ Cm \\ Cy \end{bmatrix}$$

where Cc, Cm, and Cy are the concentrations of the three colorants. The first estimate of concentrations can be calculated by Allen's algorithm.

$$\mathbf{C} = (\mathbf{TED\Phi})^{-1}\mathbf{TEDF}^{a}$$

Because there was a difference between tristimulus values from the absorption spectra and from the transmittance spectra, the first estimate must be iterated to attain colorimetric matching. The Allen's algorithm iterates using the Newton-Raphson method.

$$\begin{bmatrix} \Delta Cc \\ \Delta Cm \\ \Delta Cy \end{bmatrix} = \mathbf{TED\Phi}^{-1} \begin{bmatrix} \Delta X \\ \Delta Y \\ \Delta Z \end{bmatrix}$$

The final concentration will be expressed as

$$\mathbf{C} = \begin{bmatrix} Cc + \Delta Cc \\ Cm + \Delta Cm \\ Cy + \Delta Cy \end{bmatrix}$$

This algorithm was constrained under illuminant A and iterated using the Newton- Raphson method in order to achieve tristimulus matching. Most of the samples were matched in less than five iterations. The fitness of tristimulus

matching was specified by the degree of metamerism under illuminant D50 and illuminant A.

By using rotated eigenvectors, concentrations were estimated from the measured transmittance of 60 samples (a 90-image without the C, M, and Y ramp). The results are shown in Table 3-2. The ΔE^*_{ab} distributions from tristimulus matching algorithm are shown in Figure 3-5.

Comparing the results in Table 3-2 with Berns' test results in Table 3-1, this was a good improvement for the tristimulus value matching algorithm. This improvement resulted from the redefinition of transmittance. In Berns' article[1] it was assumed that the transmittance of the film base was unity. Normalizing each sample by the $\mathbf{D_{\lambda,min}}$ samples eliminated the errors of determining the dye density.

$$\mathbf{f(T)^a = -\log T_\lambda \quad \Rightarrow \quad f(T)^a = -\log T_\lambda / T_{\lambda,max}}$$

Table 3-1 Berns' result for tristimulus value matching algorithm.[1]

eigenvectors	average ΔE^*_{ab} for illuminant A	average ΔE^*_{ab} for illuminant D50	maximum ΔE^*_{ab} for illuminant D50
rotated vectors	0	0.82	
vectors from C, M, Y dyes	0	2.38	
vectors from equamax using all data	0	1.70	

Table 3-2 Tristimulus value matching algorithm result.

eigenvectors	average ΔE^*_{ab} for illuminant A	maximum ΔE^*_{ab} for illuminant A	average ΔE^*_{ab} for illuminant D50	maximum ΔE^*_{ab} for illuminant D50
rotated vectors	0.00	0.00	0.15	0.50
vectors from C, M, Y dyes	0.00	0.00	0.20	0.52
vectors from equamax using all data	0.00	0.00	0.15	0.50

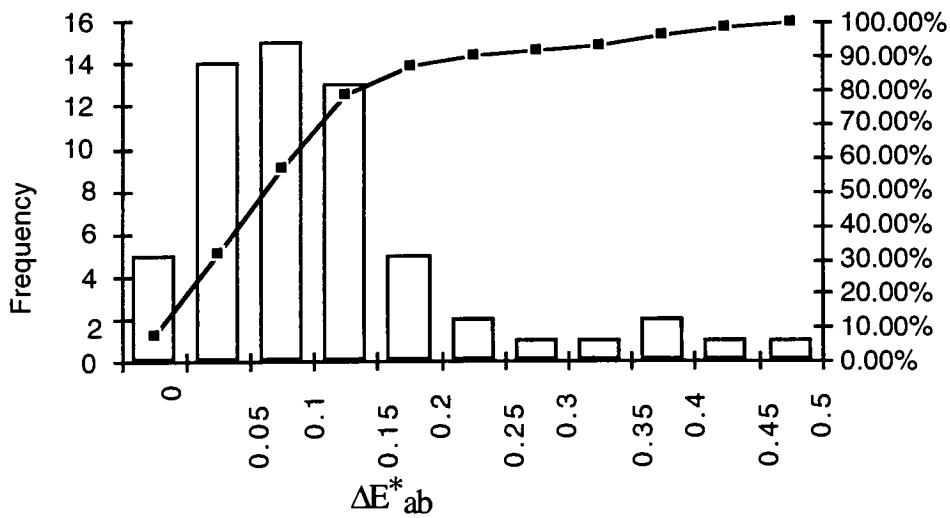

Fig. 3-5 ΔE^*_{ab} histogram for tristimulus matching algorithm for illuminant D50.

Chapter IV. Conversion Between Integral Density and Analytical Density

4.1 Background of Density Measurements

Density measurements can be divided into two groups: integral density and analytical density. Density in color photography depends on the absorption of the three dyes as well as the wavelength distribution of the radiant energy. Integral density is the measurement of the combined image absorption of the three dyes while analytical density is the measurement of the amounts of dye in the individual layers. The methods used to compute analytical densities from integral densities have been discussed in several articles. The data from the measurement of the three integral densities (C,M, and Y) were transformed to the three analytical densities. Figure 4-1 shows typical three dye spectral density curves and the neutral grey density curve.

4.1.1 Integral Density

According to the American National Standard PH2.1-1952, there are four types of integral densities: printing, visual, photoelectric, and spectral density.[14] In this research, the spectral density was used as an integral density. By definition, spectral density is a density measured with the monochromatic energy of wavelength. In practice, the measurement of spectral density is accomplished by the use of radiant energy covering a narrow band of wavelengths. The spectral density was also used as a function of wavelength over the whole range of the visible spectrum. This can be measured with a spectrophotometer.

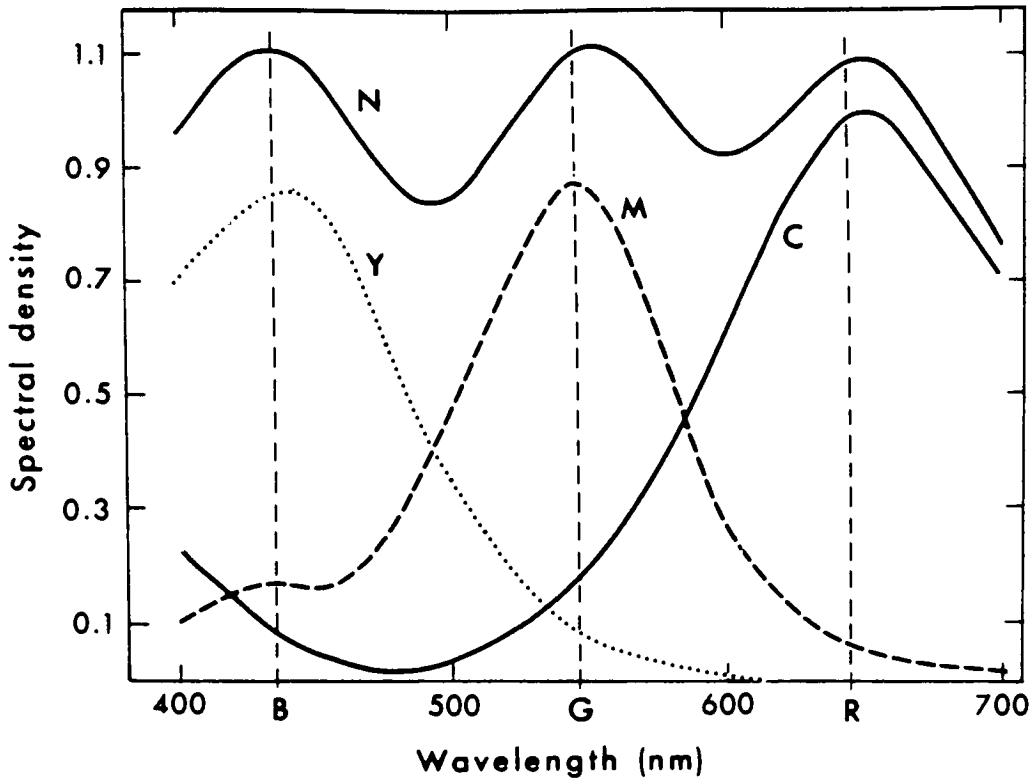

Fig. 4-1 C, M, and Y dyes, and the composite neutral dye spectral density distributions as a function of wavelength.[15]

According to Dawson and Voglesong[16] the integrated densitometer response can be written as

$$\mathbf{i} = \int_{350nm}^{800nm} \mathbf{J}_\lambda \mathbf{e}_\lambda \mathbf{f}_\lambda \mathbf{S}_\lambda \mathbf{d}\lambda$$

where $\mathbf{J}\lambda$ is the spectral emittance of the light source, $\mathbf{e}\lambda$ is the relative overall spectral efficiency, $\mathbf{f}\lambda$ is the spectral filter transmittance, $\mathbf{S}\lambda$ is the spectral photodetector response, and **i** is the photocathode current. The response function can be separated by the instrument response and filter response because

different filter sets are used according to the color materials. In the measurement of color reversal film, a status A densitometer with AA filters is recommended (Wratten filters W29+W25, W74, W98+W98+ W2E). The status A densitometer responses are shown in Figure 4-2. The measured density from a densitometer can be used as a measuring concentration if there is any relationship between analytical density and the measured density.

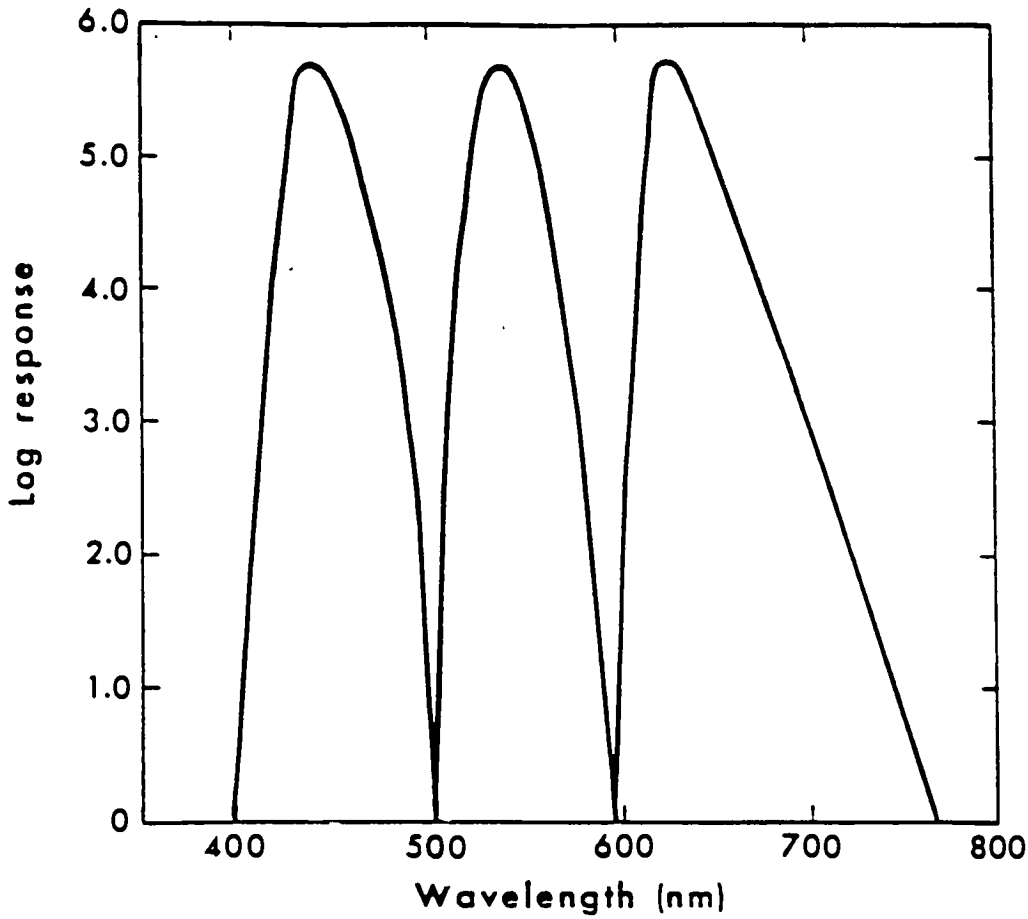

Fig. 4-2 Spectral densitometer responses for status A densitometry.[15]

4.1.2 Analytical Density

Analytical density provides information between the dye concentrations and their effects on the output image. For color reproduction purposes, the analytical density of color photography must be calculated from the integral density. The calculation of analytical density was based on the assumptions of the Beer-Bouger law. When the Beer-Bouger law is valid for the dyes in color films, it is possible to convert from integral density to analytical density. The Beer-Bouger law does not hold when scattering is caused by the impurities in the dyes. It also fails when there is an association of the absorbing molecules at a higher concentration or when there is a fluorescing of the dyes. This is called Beer's law failure. When additivity of the spectral densities is assumed, the spectral integral densities can be written as a component of analytical densities. Thus, the relationship between analytical density and integral density can be expressed as

$$\begin{bmatrix} Cc \\ Cm \\ Cy \end{bmatrix} = \begin{bmatrix} K_{11} & K_{12} & K_{13} \\ K_{21} & K_{22} & K_{23} \\ K_{31} & K_{32} & K_{33} \end{bmatrix} \begin{bmatrix} Dr \\ Dg \\ Db \end{bmatrix}$$

Two approaches were used to convert integral density to analytical density. First, the spectral transmittances from the spectrophotometer were converted to analytical densities based on the Beer-Bouger law. Second, the measured integral densities from the densitometer were transformed to the analytical densities. Even though the densitometer has wide spectral bands, the relationship between densities from the densitometer and the analytical densities showed a linear transformation in this research. The concentrations of each dye were estimated

by the tristimulus value matching algorithm described in Chapter 3. The spectral densities, D_λ , can be measured directly from transmittance, T_λ, using a spectrophotometer.

4.2 Linear Regression Model Between Measured Density and Analytical Density

Using the regression analysis in SYSTAT, several multiple regression models were tested. The relationships between the measured densities (Dr, Dg, and Db) and the concentrations (Cc, Cm, and Cy) for neutral samples were plotted in Figure 4-3. These plots show the linear transformation between the measured density and the analytical density (three-by-three transformation). Figure 4-3 indicates that the measured density can be directly used in the color matching algorithm. The conversion from the density to the concentration and then XYZ can be obtained through three-by-three transformations. The relationship between the concentration and the measured density using all 60 samples are shown in Figure 4-4. These plots also show a reasonably linear relationship between the two density spaces.

First, a three-by-three transformation between the concentration and the density was performed. The relationship can be expressed as

$$\begin{bmatrix} C_y \\ C_m \\ C_c \end{bmatrix} = \begin{bmatrix} 3*3 \end{bmatrix} \begin{bmatrix} D_R \\ D_G \\ D_B \end{bmatrix}$$

The transformation matrix is shown below:

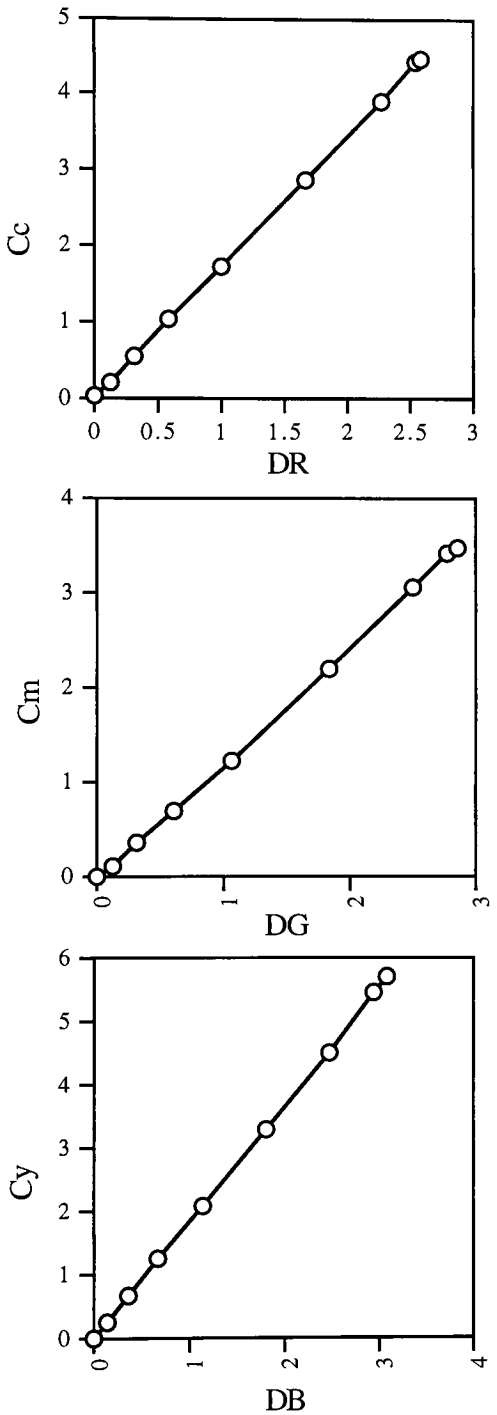

Fig. 4-3 Concentration vs. measured density for grey samples.

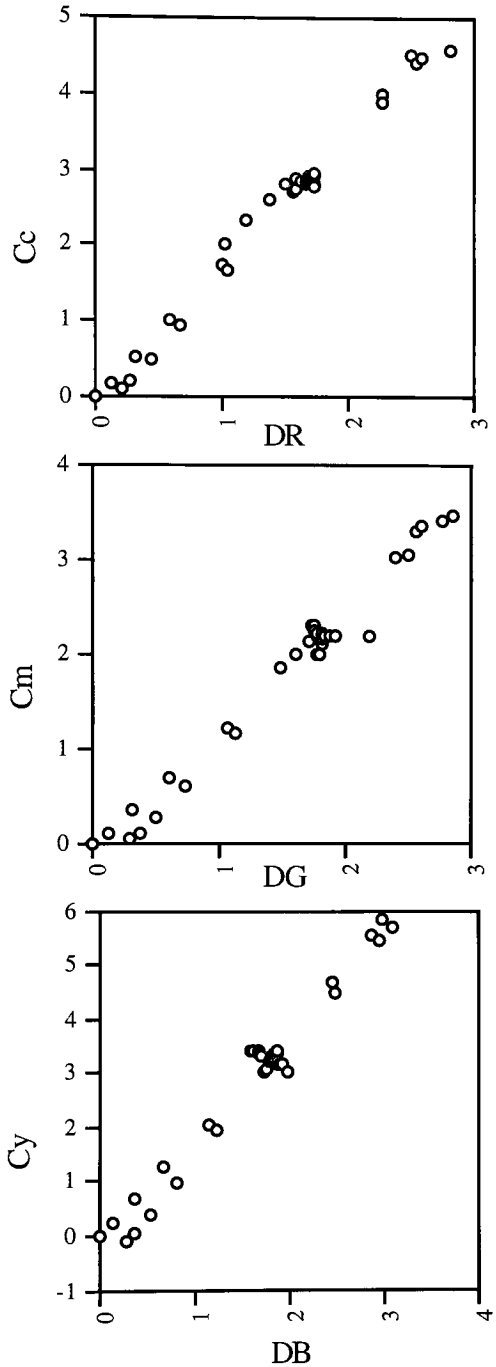

Fig. 4-4 Concentration vs. measured density for 60 color samples.

$$\begin{bmatrix} \hat{C}_y \\ \hat{C}_m \\ \hat{C}_c \end{bmatrix} = \begin{bmatrix} 0.00997 & -0.17463 & 1.94820 \\ -0.42063 & 1.47407 & -0.26176 \\ 2.21254 & -0.11542 & 0.06511 \end{bmatrix} \begin{bmatrix} D_R \\ D_G \\ D_B \end{bmatrix} \quad \textbf{Equation 4-1}$$

The squared multiple correlations are 0.99968, 0.99973, and 0.99993 for yellow, magenta, and cyan respectively. The residual plots from Equation 4-1 are shown in Figure 4-5. These residual plots show normality with most of the samples are ranging between -0.1 and +0.1. There were some outliers outside of this range; however, these outliers might have been caused by the normalization of the spatial variability in density units or from measurement errors. The ANOVA Tables for the three-by-three and three-by-four models are shown in Tables 4-1, and 4-2. In the three-by-four model including constant terms, the constant terms were not statistically significant. The three-by-three model showed better regression and residual coefficients. With the predicted concentrations from the above three-by-three transformation and the concentrations from Allen's algorithm, the perceived color difference was obtained under illuminant A and illuminant D50. The results are shown in Figure 4-6. Because the outliers had appreciable leverage, these data points were removed and the regressions were repeated resulting in Equation 4-2.

$$\begin{bmatrix} \hat{C}_y \\ \hat{C}_m \\ \hat{C}_c \end{bmatrix} = \begin{bmatrix} -0.00868 & -0.17861 & 1.95072 \\ -0.40573 & 1.47983 & -0.26383 \\ 2.22001 & -0.11896 & 0.06309 \end{bmatrix} \begin{bmatrix} D_R \\ D_G \\ D_B \end{bmatrix} \quad \textbf{Equation 4-2}$$

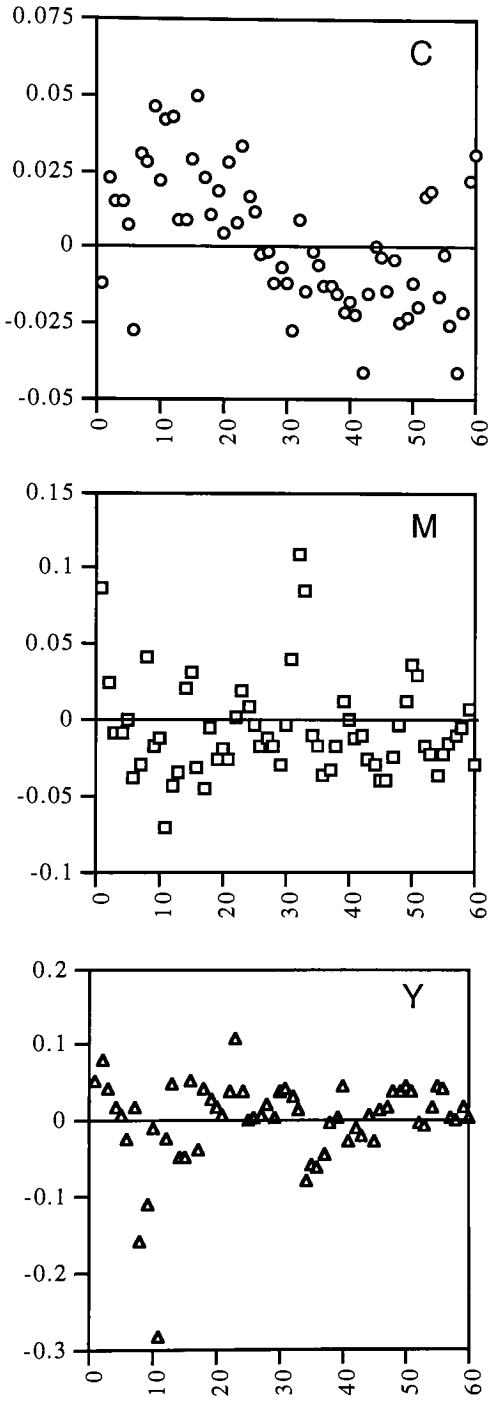

Fig. 4-5 Residual plots for the 3x3 transformation for predicted concentrations.

Table 4-1 The ANOVA table for the three-by-three regression model.

variable	Source	S.S.	D.F.	M.S.	F-ratio
Cy	regression	594.72803	2	297.36401	88230.02406
	residual	0.19548	58	0.00337	
Cm	regression	239.35274	3	79.78425	69407.30987
	residual	0.06552	57	0.00115	
Cc	regression	401.53656	3	133.84552	.264618E+06
	residual	0.02883	57	0.00051	

Table 4-2 The ANOVA table for the three-by-four regression model.

variable	Source	S.S.	D.F.	M.S.	F-ratio
Cy	regression	118.21850	3	39.40617	80773.954
	residual	0.02732	56	0.00049	
Cm	regression	74.33824	3	24.77941	27143.824
	residual	0.05112	56	0.00091	
Cc	regression	184.50785	2	92.25392	27046.168
	residual	0.19443	57	0.00341	

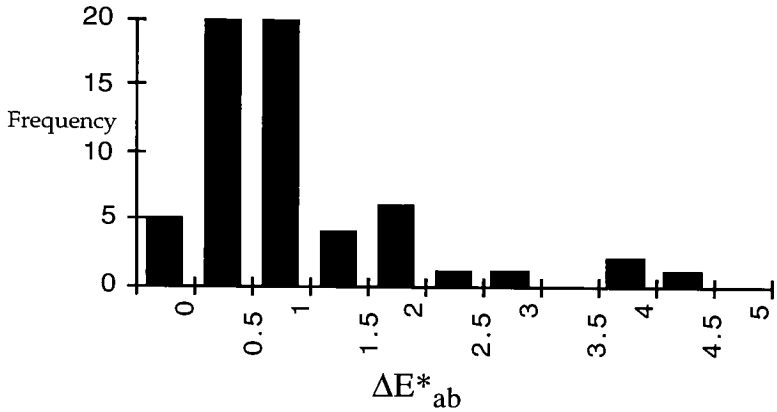

Fig. 4-6-1 ΔE^*_{ab} histogram for the predicted concentration from the three-by-three transformation and the concentration from Tristimulus matching algorithm under illuminant A.

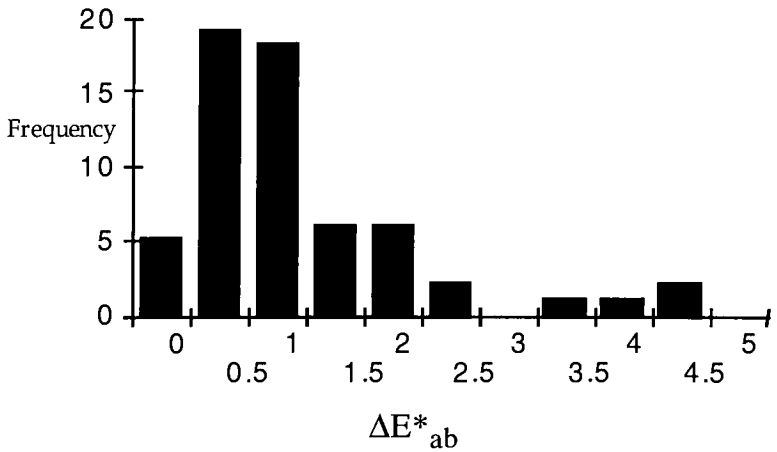

Fig. 4-6-2 ΔE^*_{ab} histogram for the predicted concentration from the three-by-three transformation and the concentration from Tristimulus matching algorithm under illuminant D50.

The squared multiple correlations for yellow, magenta, and cyan are 0.99990, 0.99978, and 0.99994 respectively. The residual plots after the outliers were taken out are shown in Figure 4-7. As for the residual plots in Figure 4-7, the cyan residual plot shows systematic error but the range is relatively small (the range of -0.05 ~ +0.05). The magenta and yellow plots are quite random. The ANOVA table is shown in Table 4-3. The color difference between the predicted concentrations from Equation 4-2 and the concentrations from tristimulus value matching algorithm under illuminant A and D50 are shown in Figures 4-8-1 and 4-8-2. These results showed that most of the samples had a ΔE^*_{ab} of less than 1. The three-by-three rotation between the integral density and the analytical density was fairly well achieved. Since the whole modeling scheme from spectral transmittance to the predicted concentration using interimage effects is quite complex, the conversion between the two densities was kept as simple as possible. Therefore, the simple three-by-three approximation was applied rather than a larger matrix.

Table 4-3 The ANOVA table after taking out outliers (three-by-three).

variable	Source	S.S.	D.F.	M.S.	F-ratio
Cc	regression	353.83092	3	117.94364	.2694E+06
	residual	0.02233	51	0.00044	
Cm	regression	206.45283	3	68.81761	78256.835
	residual	0.04485	51	0.00088	
Cy	regression	512.36704	2	256.18352	.2567E+06
	residual	0.05189	52	0.00100	

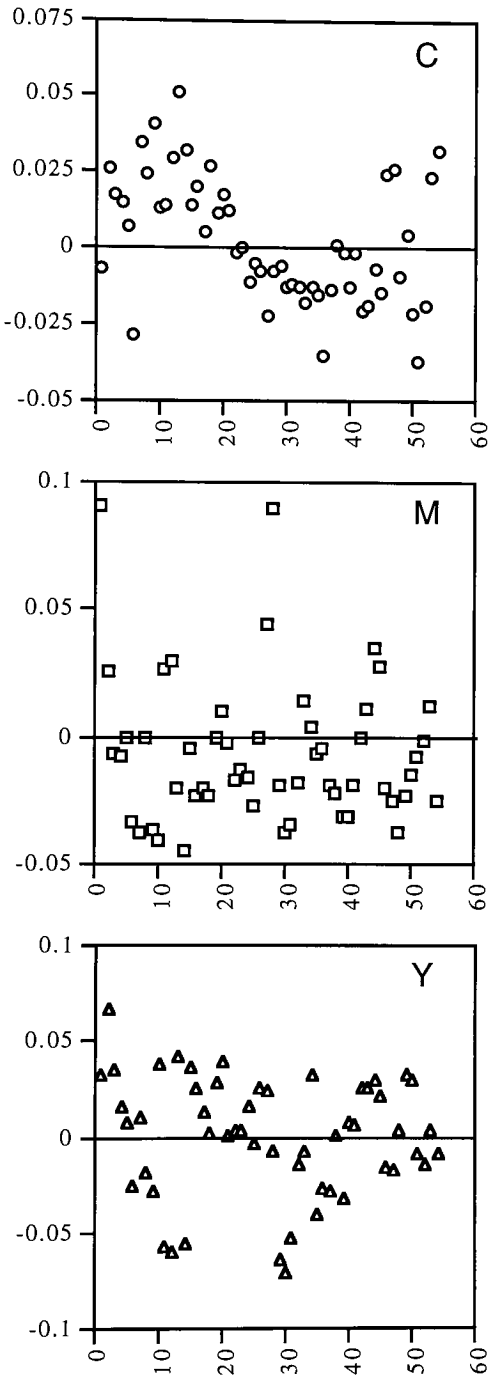

Fig. 4-7 Residual plots for predicted concentrations after taking out the outliers.

The relationship between the RGB exposure levels and the measured densities is shown in Figure 4-9, and the relationship between the exposure levels and the concentrations is shown in Figure 4-10. From these two graphs, the trend for the interimage effects in Figure 4-9 was similar to that in Figure 4-10. This justifies the rational to transform with a three-by-three matrix between the two densities. The interimage effects will be discussed in Chapter 5.

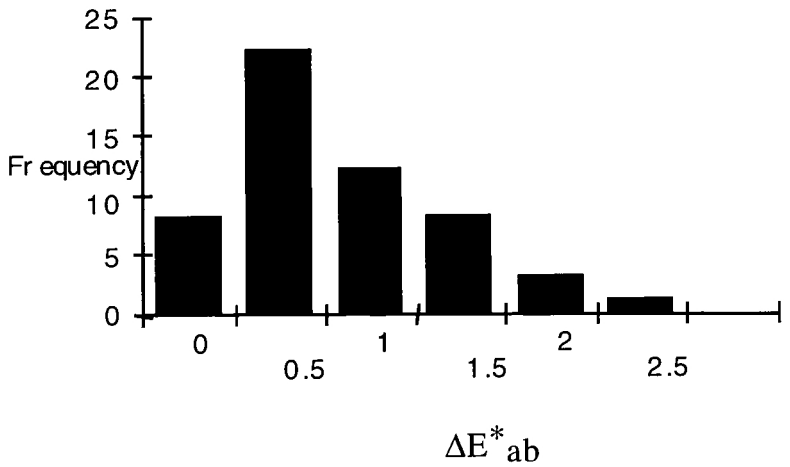

Fig. 4-8-1 ΔE^*_{ab} for the predicted concentrations from Equation 4-2 and concentrations from Tristimulus matching algorithm under illuminant A.

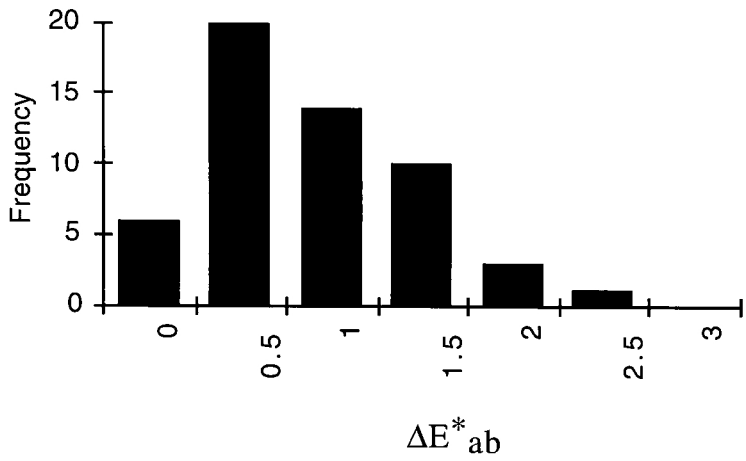

Fig. 4-8-2 ΔE^*_{ab} for the predicted concentrations from Equation 4-2 and concentrations from TSV algorithm under illuminant D50.

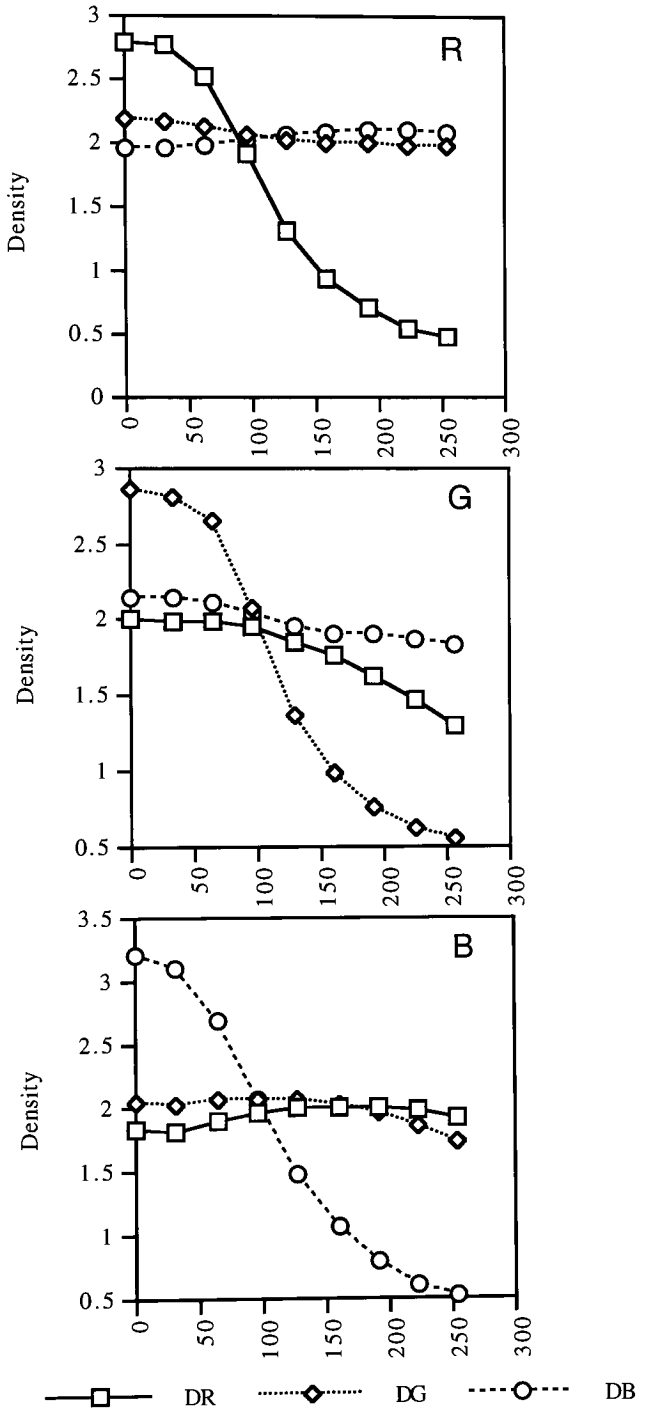

Fig. 4-9 Red, green, and blue densities as a function of input digital values.

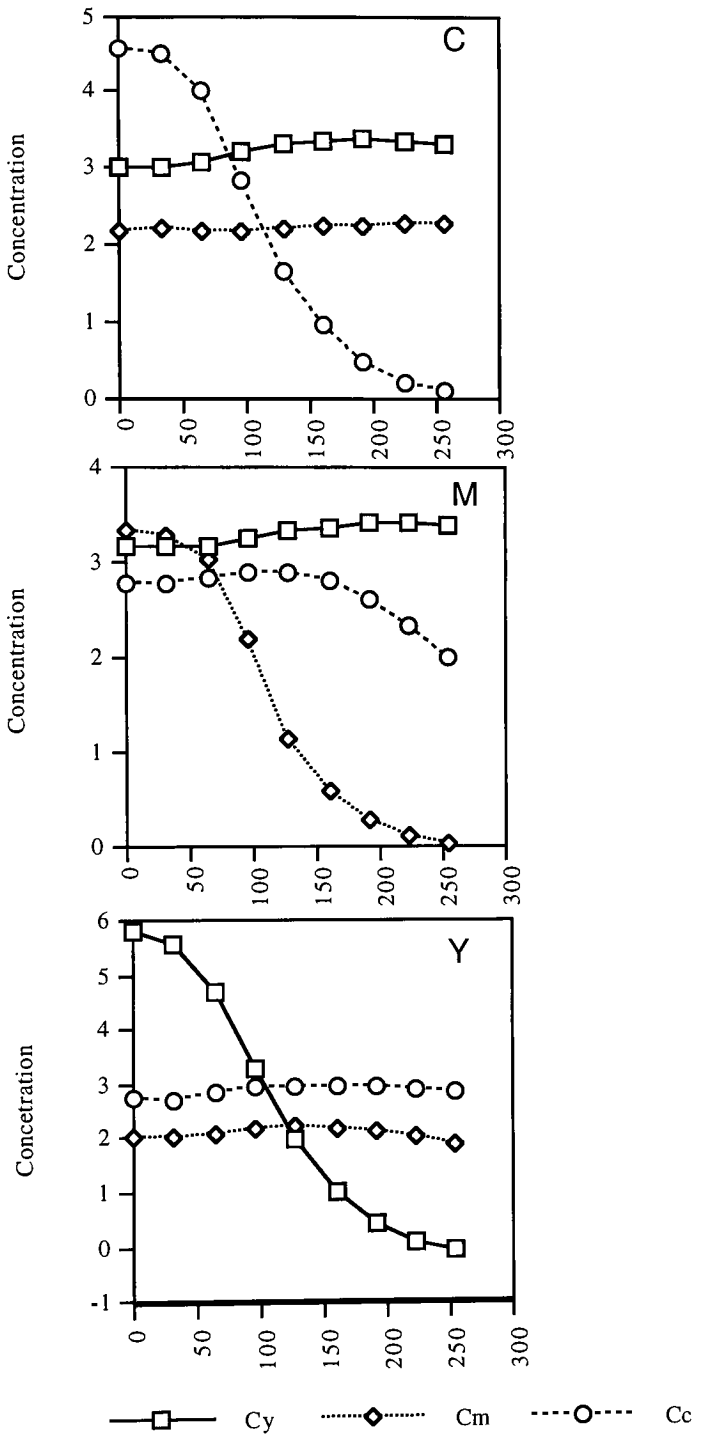

Fig. 4-10 C, M, and Y concentrations as a function of input digital values.

Chapter V. Interimage Effects Model

5.1 Background of Interimage Effects

To achieve the color reproduction of subtractive color photography, two deficiencies have to be compensated for[8]: 1) the lack of negative spectral sensitivities in the color seperation steps, and 2) the presence of secondary absorption in the spectra of the image dyes. The solution to these problems is a technique known as masking. In practice the masking corrections are incorporated into the process in the form either of interimage effects or of colored couplers. The presence of colored couplers in light areas gives a severe orange cast, and this is beyond the limitation of eye adaptation. For this reason colored couplers can be used in the materials designed to be printed or duplicated, not in normal reversal processes intended for viewing. Therefore the interimage effects are used to obtain masking effects in transparency films.[14] When image components of this films are exposed and processed, each of them influences the development of the components in the adjacent layers to some extent. Therefore, the amount of dye formed in one layer depends also on the degree of exposure of the other layers. The resulting reactions are called interimage effects.[8] The correction obtained from these effects can be used to offset an unwanted dye absorption. The correction for the interimage effects may written as

$$\begin{bmatrix} Cc \\ Cm \\ Cy \end{bmatrix} = \begin{bmatrix} Kcr & Kcg & Kcb \\ Kmr & Kmg & Kmb \\ Kyr & Kyg & Kyb \end{bmatrix} \begin{bmatrix} Dr \\ Dg \\ Db \end{bmatrix}$$

where **Cc, Cm** and **Cy** are the dye concentrations, and **Kcr, Kmg**, and **Kyb** are the main gamma of the characteristic curves. **Kcg, Kcb** represent the interimage effects upon the cyan dye from the green and blue sensitive layers, **Kmr, Kmb** upon the magenta dye from the red and blue sensitive layers, and **Kyr, Kyg** upon the yellow dye from the red and green sensitive layers.

Even though the actual chemical mechanism that produces the interimage effects is hard to specify, previous investigations have shown that interimage effects result from the development process.[14] When developer penetrates multi-layer color material, there might be speed differences between when all layers are exposed and when only one layer is exposed. Interimage effects can also be caused by the degree of development in one layer being affected by the release from a neighboring layer of development-inhibiting agents. Interimage effects may be caused by the dye of the wrong color when the oxidized developer wandered from one layer to another in a coupler-incorporated material. Also development in an unexposed layer might be occurred if an adjacent layer is very highly exposed.

There are several ways of examining the existence of interimage effects through dye density comparisons. First, expose white light and plot the amount of cyan, magenta and yellow dyes and then compare that cyan dye to the cyan dye formed when only the red exposure is given. Second, expose two layers along a given exposure scale from 0 to 255 while the remaining layer has uniform exposure at different intensities. Third, two layers have uniform exposures, and

one layer has an exposure scale. In this thesis, the data set for interimage effects was based on this third method.

5.2 Interimage Effects Model

It is known that color corrections are achieved by modeling the interimage effects in color photography. The amounts of each dye are the functions of red, green, and blue exposures. Usually the interimage effects have been modeled empirically using regression methods.[8, 14] A simple three-by-three matrix has been used to describe interimage effects. However, a three-by-three matrix is not an exact description of interimage effects due to the nonlinear characteristics of film. Clapper[8] used a three-by-ten matrix representing a second order polynomial to explain the nonlinearity. This is an purely empirical approach. Therefore, it is hard to relate the matrix elements with the film's chemistry. The interimage effects may differ slightly from the general description of a three-by-three matrix containing nonlinear exposure density terms.[8] In this research, the interimage effects of the film were explained by the characteristic vectors of the variability of the film density using principal component analysis.

The sample set was generated by increments of one exposure scale by 32 digital counts (0, 32, 64, 96, 128, 160, 192, 224, 255), while the two other layers had uniform intensity levels from 0 to 255. One of the slide samples for interimage effects is shown in Figure 5-1. The data set for interimage effects was shown in Appendix B.

dr = 0 dg = 96 db = 96	dr = 32 dg = 96 db = 96	dr = 64 dg = 96 db = 96
dr = 96 dg = 96 db = 96	dr =128 dg = 96 db = 96	dr =160 dg = 96 db = 96
dr =192 dg = 96 db = 96	dr = 224 dg = 96 db = 96	dr = 255 dg = 96 db = 96

Fig. 5-1 One of the samples for the interimage effects model.

The density plots for these samples are shown in Figures 5-2, 5-3, and 5-4. If there is no crosstalk between the layers, the green and blue densities must be uniform while the red channel changes exposure levels. However, the green density has a slightly negative slope as shown in Figure 5-2. This means that the formation of magenta dye was enhanced by red exposure even though green exposure levels remained uniform. This phenomenon is similar to Figure 5-3. When the green channel changed exposure levels, the red density showed an obviously negative slope especially in high red exposure levels. As a result, cyan dye increased from green exposure even though red exposure levels were uniform. The blue density also shows a negative slope with the uniform green exposure level in Figure 5-4. When the blue channel changed exposure levels, the green density showed a slightly negative slope. Therefore, the blue exposure enhanced the formation of magenta dye. Considering the structure of the film layers in Figure 5-5, these phenomena can be easily understood.

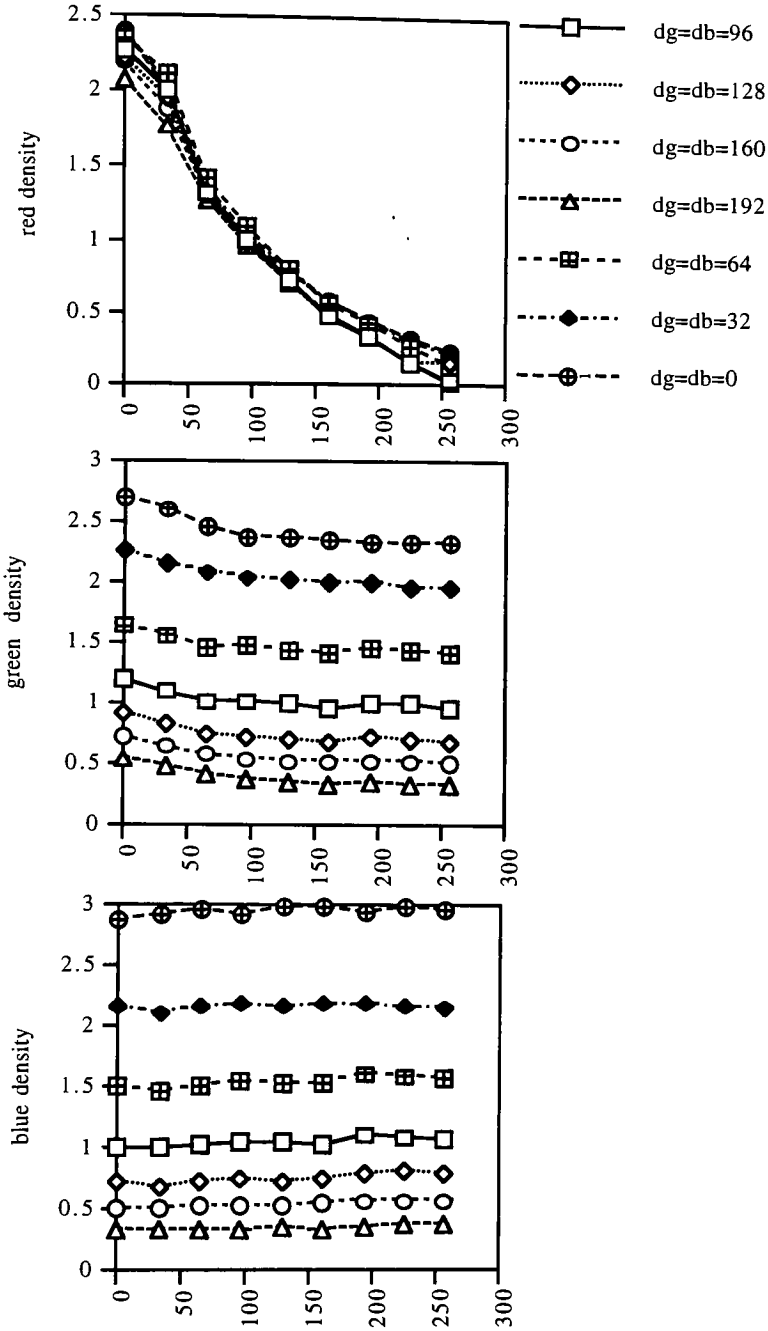

Fig. 5-2 Red, green, and blue densities with uniform green and blue exposure levels as a function of red exposure levels.

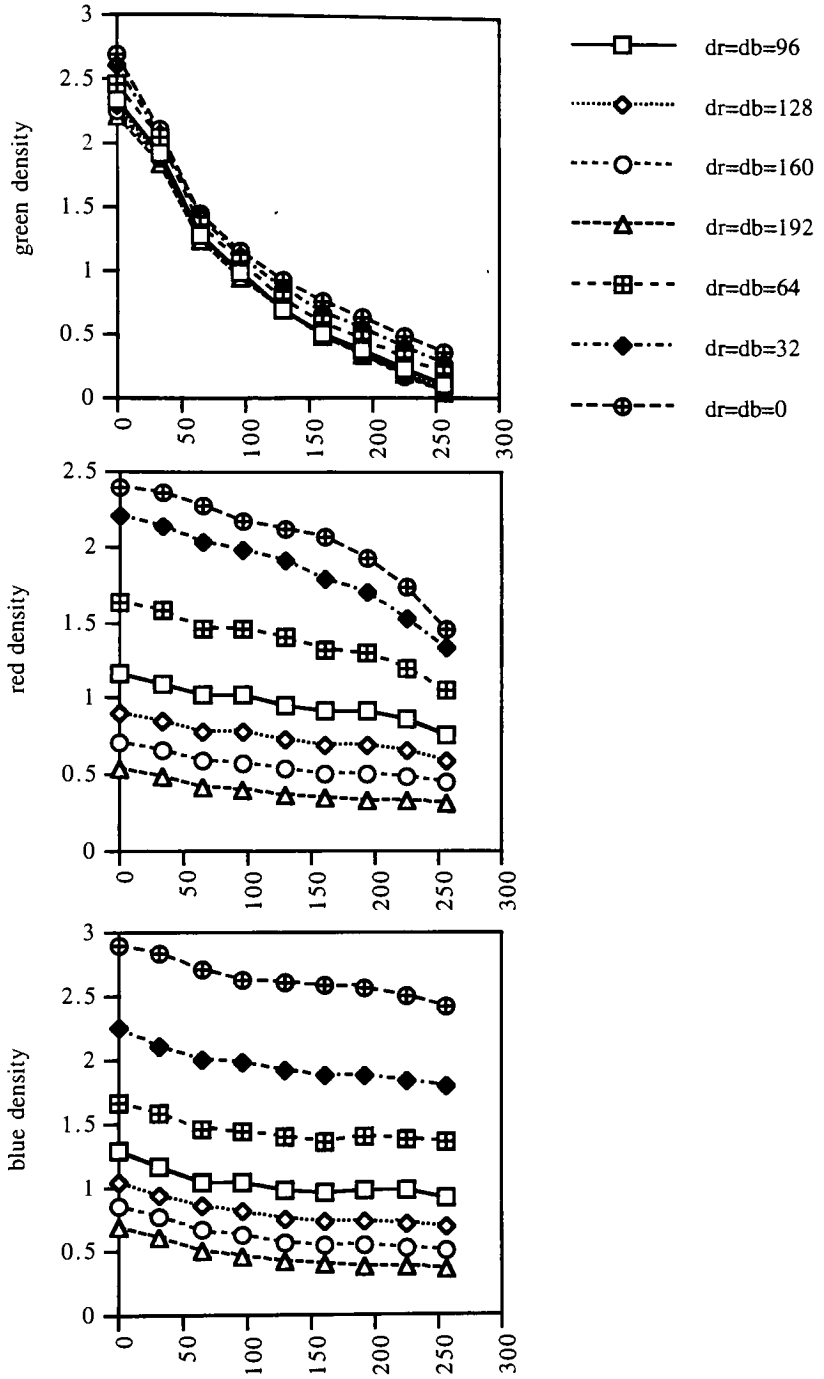

Fig. 5-3 Red, green, and blue densities with uniform red and blue exposure levels as a function of green exposure levels.

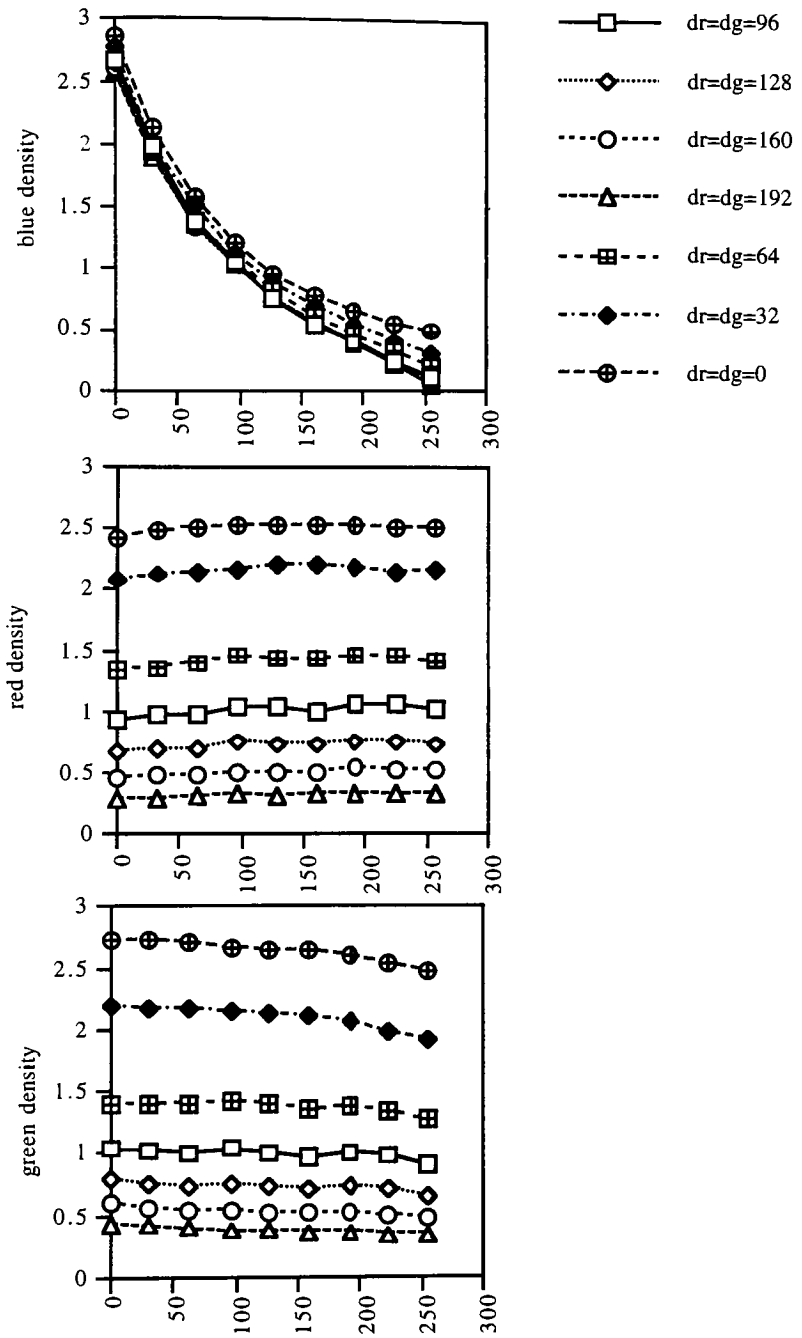

Fig. 5-4 Red, green, and blue densities with uniform red and green exposure levels as a function of blue exposure levels.

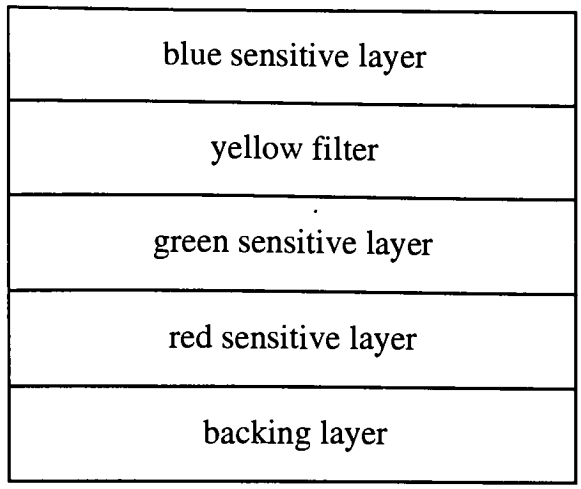

Fig. 5-5 The general structure of color film.

The crosstalk was obvious when an adjacent layer was exposed. The blue exposure may affect the green layer and also slightly affect the blue sensitive layer. This explains the negative slope of the green density. The green exposure affected the red sensitive layer. The slope of the red densities appeared to be the most negative. The red exposure might affect the green sensitive layer as well as the red sensitive layer. Since the green sensitive layer is in the middle, the formation of magenta dye can be influenced by the exposure to red, blue and green lights.

5.2.1 Interimage Effects Model using Principal Component Analysis

In regards to Figures 5-2, 5-3, and 5-4, it is difficult to describe the interimage effects by a simple three-by-three matrix form. The TRCs of red densities changed along several levels of uniform green and blue exposure levels. The uniform green and blue densities also changed although exposure levels were

constant. The same effects were shown in the case of green and blue densities. In reference to the effect of the exposure levels of adjacent layers, there are functions to explain these characteristics.

$$\Delta D\ (\mathbf{Dmean} - \mathbf{Dr(dg = db)}) = \mathbf{S_1(dg = db)V_1(dr)}$$

where **Dr** is the red density, and **dr, dg**, and **db** are the input R, G, B digital values. The red TRCs are compared with the red TRCs in the grey samples in Figure 5-6. These plots show the TRCs with different off-diagonal exposure levels. The variability was explained by the difference between the mean vector and each gamma. In order to understand the characteristics of the main gamma variability, principal component analysis was used. The eigenvector anaysis results are listed in Appendix C. The first set of eigenvectors contained the variability of 96.19%, 97.47% and 95.79% for red, green, and blue densities respectively. The second set of eigenvectors was comprised of 3.15%, 2.35%, and 2.86% for red, green, and blue densities respectively. The third eigenvectors showed 0.51%, 0.10%, and 0.95% for red, green, and blue respectively. It seemed that the third set of vectors contained some measurement errors since there were no uniform characteristics among the vectors. Two of the three sets of vectors were used for the model because the third set of vectors was insignificant (0.51%, 0.10%, 0.95% for red, green, and blue respectively) and indicated noise in the density measurement. The eigenvector analysis for red, green and blue densities are shown in Figures 5-7, 5-8 and 5-9. From these vector sets, the coefficients are obtained based on Equation 5-1 and 5-2.

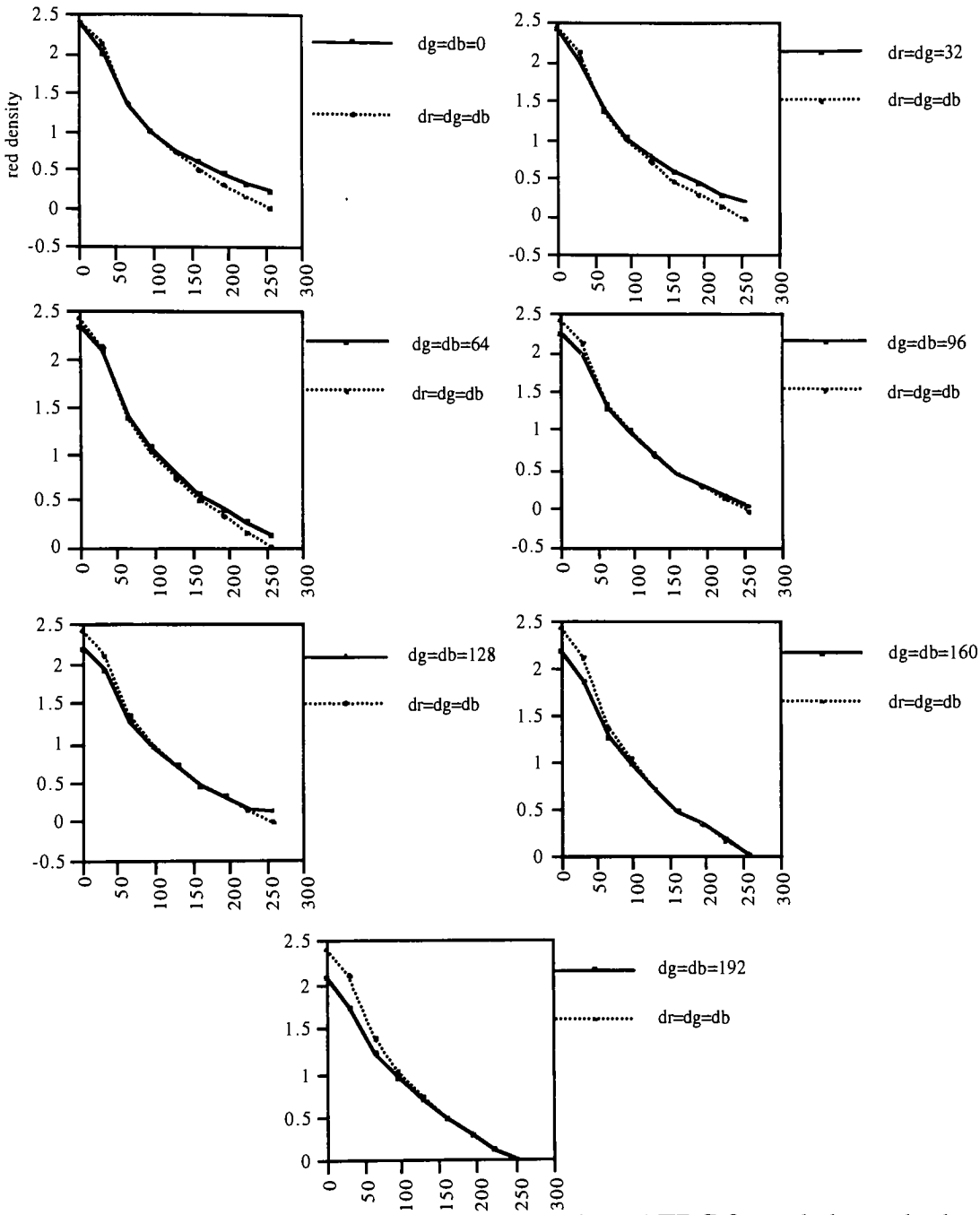

Fig. 5-6 Difference between TRC for grey sample and TRC for red channel when blue and green channels have uniform exposure levels.

Equation 5-1

$$\Delta D\ (\mathbf{Dmean} - \mathbf{Dr(dg = db)}) = S_1(\mathbf{dg = db})V_1(\mathbf{dr})$$

and

Equation 5-2

$$\Delta D\ (\mathbf{Dmean} - \mathbf{Dr(dg = db)}) = S_1(\mathbf{dg = db})V_1(\mathbf{dr}) + S_2(\mathbf{dg = db})V_2(\mathbf{dr})$$

where **S1** and **S2** indicate the red scalars for the first and second components upon the different green and blue exposure levels. The coefficients of the main gamma variabilities with different exposure levels were calculated from each vector using least-squares fit. The scalar components for each channel are shown in Figure 5-10. The model containing two vectors yielded a better least-squares fit compared to the model one vector. The regression analysis results using two vectors are listed in Appendix D. Each coefficient with different off-diagonal digital counts was used as scalars in interimage effects model. Table 5-1 shows the coefficients and squared multiple R values. The squared multiple correlations are plotted for each channel in Figure 5-12. The plots show that the middle range (64 ~ 128) of exposure levels had a smaller deviation of the interimage variability than the high and the low ranges. There might be a need for another vector to explain the middle range of deviation. However, the scalars and vectors for interimage effects are already considerably complex and they explained interimage effects well along the whole range. In this thesis, the cubic spline interpolation method was used to interpolate nine data points in each vector.

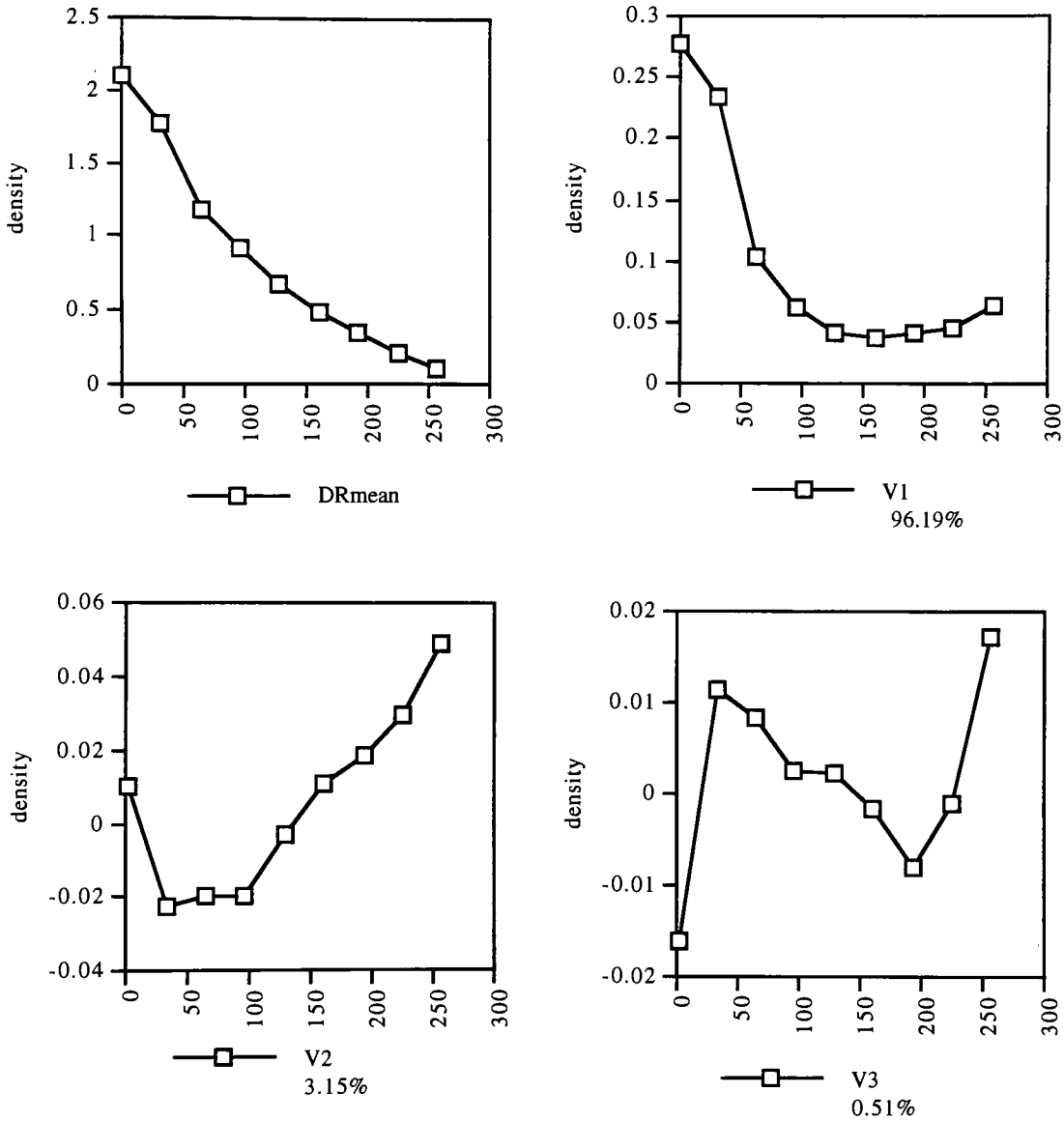

Fig. 5-7 Eigenvectors for red density variability.

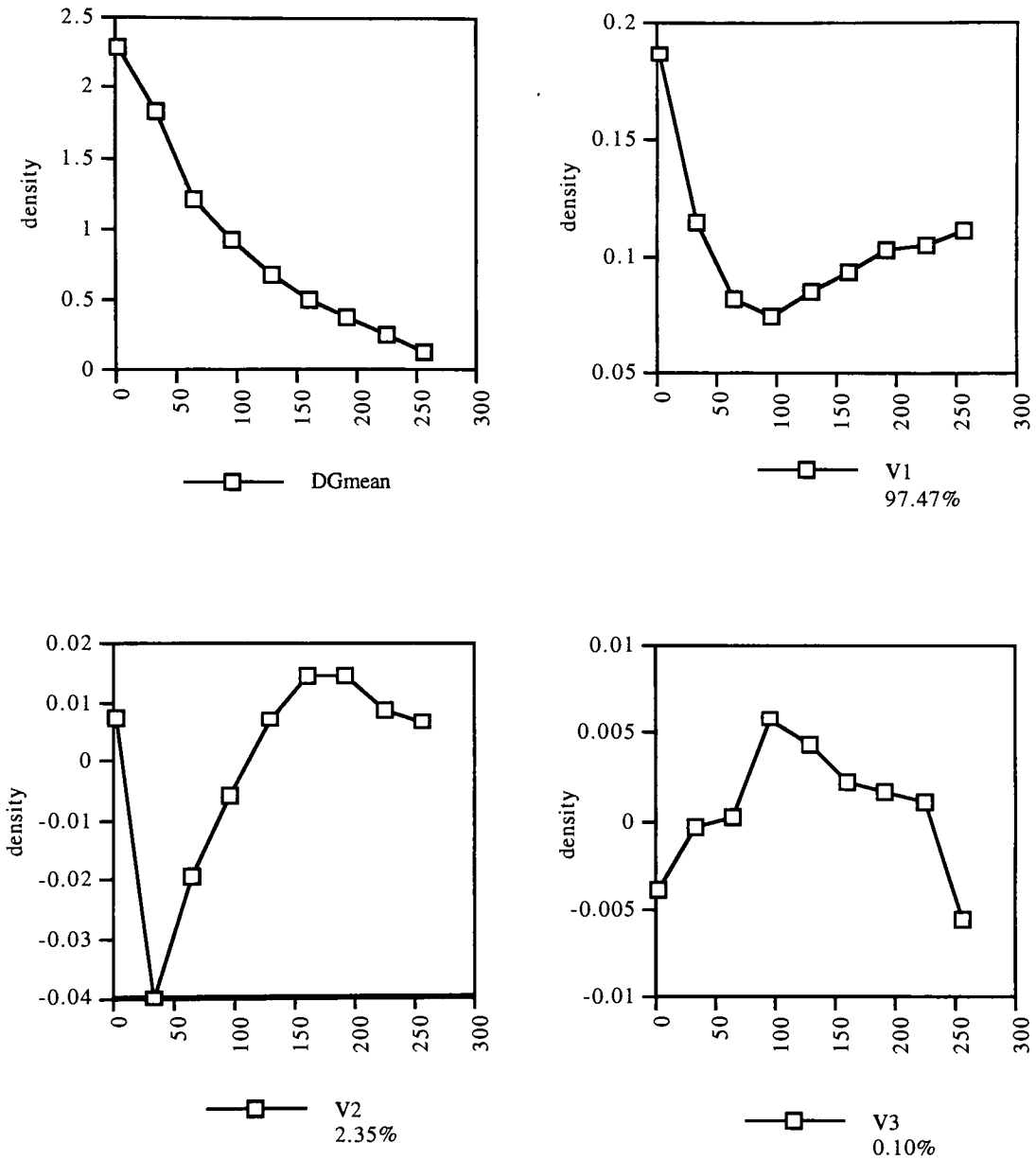

Fig. 5-8 Eigenvectors for green density variability using one vector.

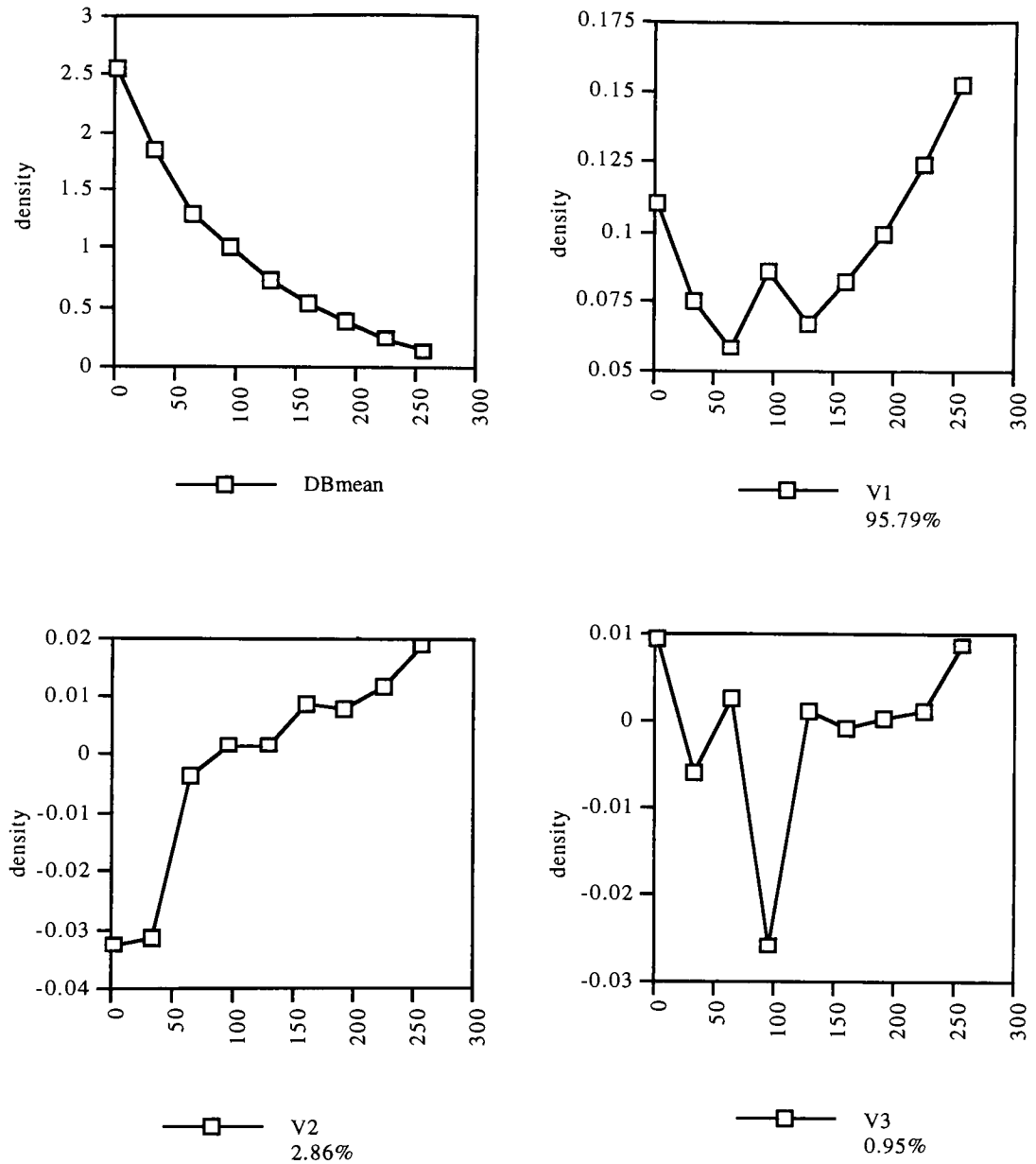

Fig. 5-9 Eigenvectors for blue density variability.

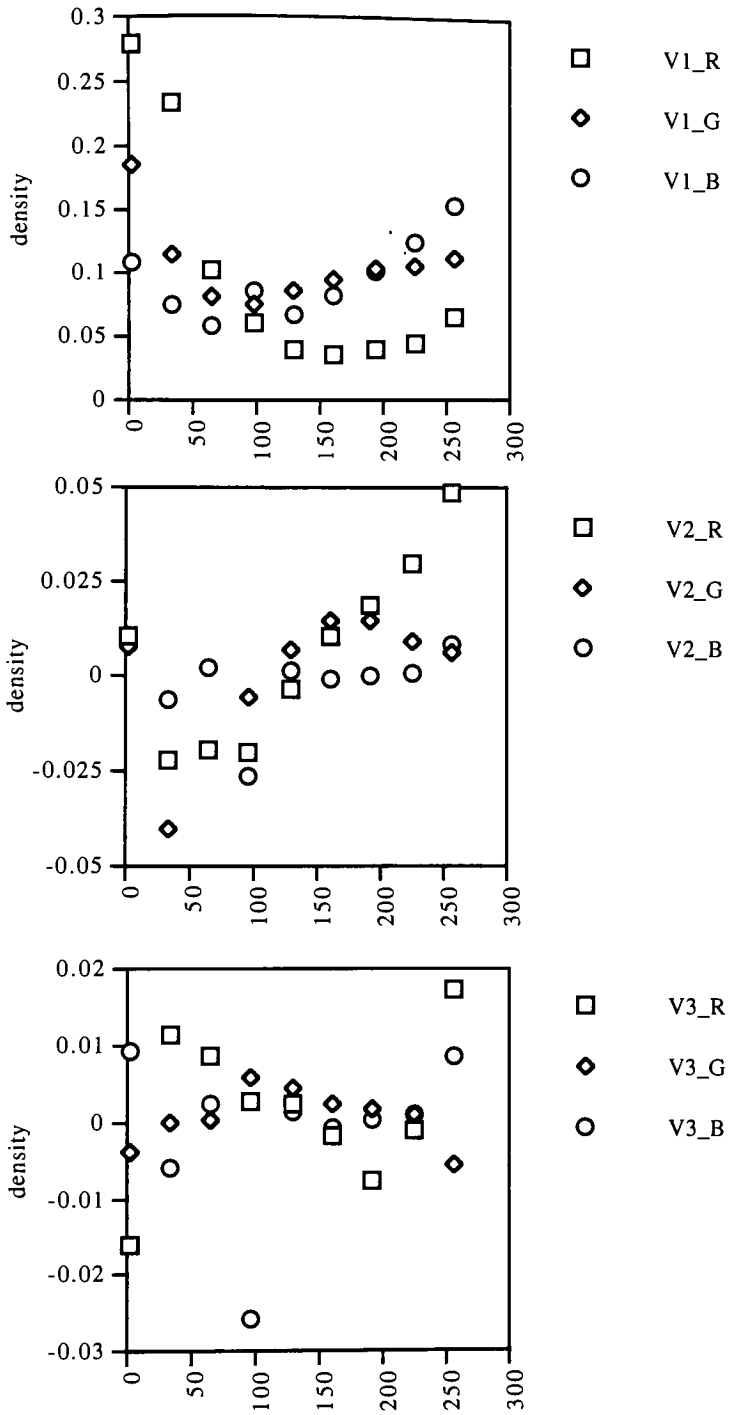

Fig.5-10 Eigenvector comparison for red, green, and blue main gamma variability.

Table 5-1 Coefficients with different off-diagonal digital counts using least-square fit based on Equation 5-2 model.

DR	S1	S2	R^2
DR0	-0.76213	-1.76707	0.998
DR32	-0.67769	-1.18742	0.988
DR64	-0.81495	0.72965	0.994
DR96	-0.6628	1.29759	0.998
DR128	-0.50669	-0.09382	0.899
DR160	-0.11	0.84705	0.842
DR192	0.37138	0.5401	0.98
DR224	1.10823	0.10558	0.999
DR255	2.05467	-0.47166	0.999
DG			
DG0	-1.74904	-1.20561	0.999
DG32	-1.15099	-0.47925	0.998
DG64	-0.50096	0.8556	0.994
DG96	-0.08183	1.09837	0.943
DG128	0.14194	0.7873	0.985
DG160	0.39555	0.74514	0.995
DG192	0.61444	0.31058	0.995
DG224	0.95586	-0.39461	0.998
DG255	1.37503	-1.71753	0.999
DB			
DB0	-2.03663	-0.51081	0.995
DB32	-1.07724	-0.52176	0.984
DB64	-0.06684	-0.61455	0.343
DB96	-0.00936	1.50855	0.944
DB128	0.29505	0.51819	0.922
DB160	0.28758	1.17248	0.978
DB192	0.54945	0.42605	0.973
DB224	0.80775	-0.27035	0.977
DB255	1.25023	-1.70779	0.998

Contrary to the polynomial regression analysis which needs many data points, this function needed only four points for curve fitting. Using the cubic spline

interpolation function, 8 bit LUTs were generated for each channel using nine points. The nine LUTs were generated into nine vectors: V_0^r, V_1^r, V_2^r, V_0^g, V_1^g, V_2^g, V_0^b,V_1^b, V_2^b, where V_0's are the mean vectors for each channel, V_1's are the first characteristic vector components for each channel, and V_2's are the second characteristic vector components. The six LUTs were generated into six scalars: S_1^r(dg=db), S_2^r(dg=db), S_1^g(dr=db), S_2^g(dr=db), S_1^b(dr=dg), S_2^b(dr=dg), where S_1 and S_2 are coefficients for different exposure levels. The LUTs are shown in Figures 5-13, 5-14, and 5-15.

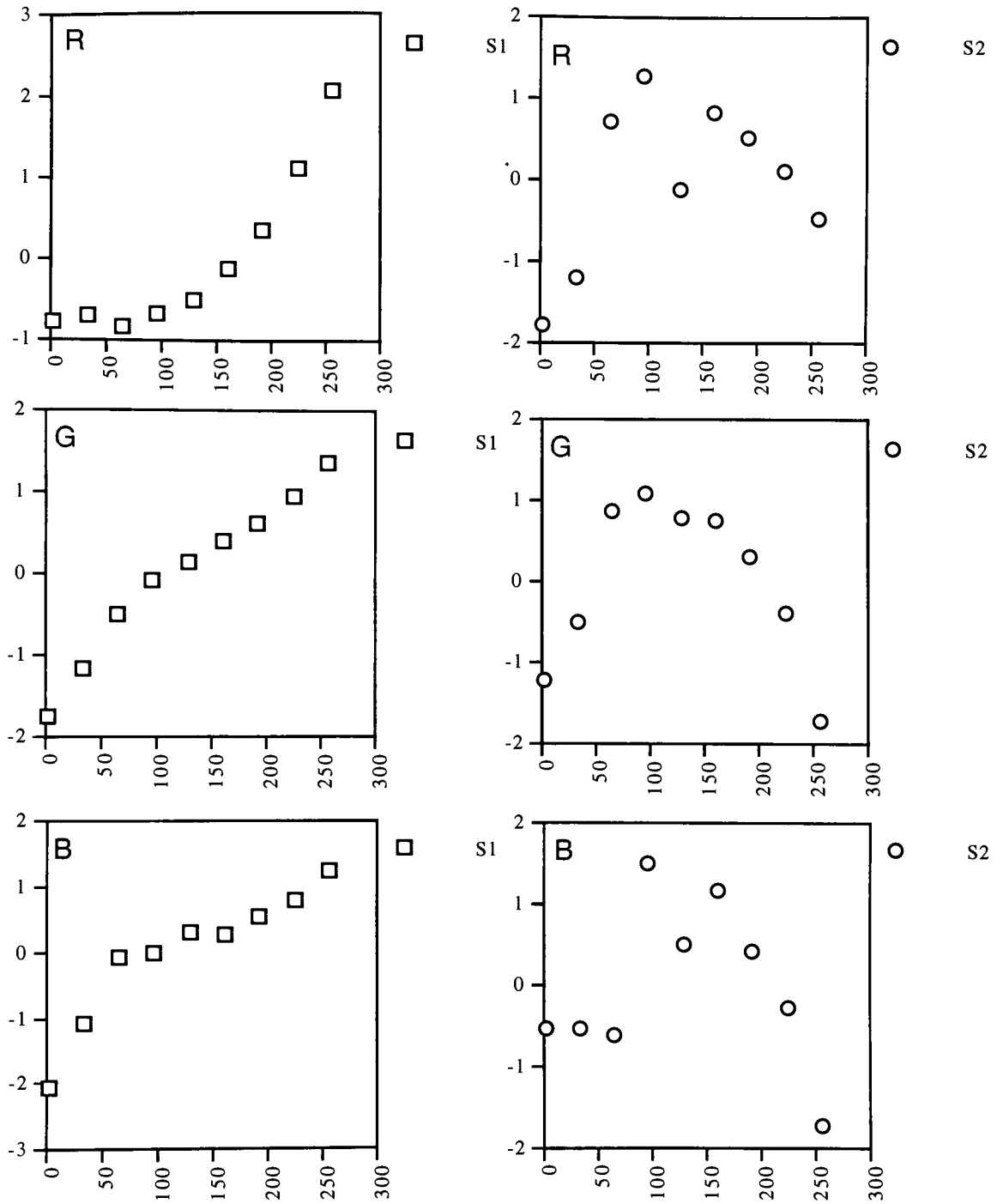

Fig. 5-11 Least-squares fit coefficients for interimage effects.

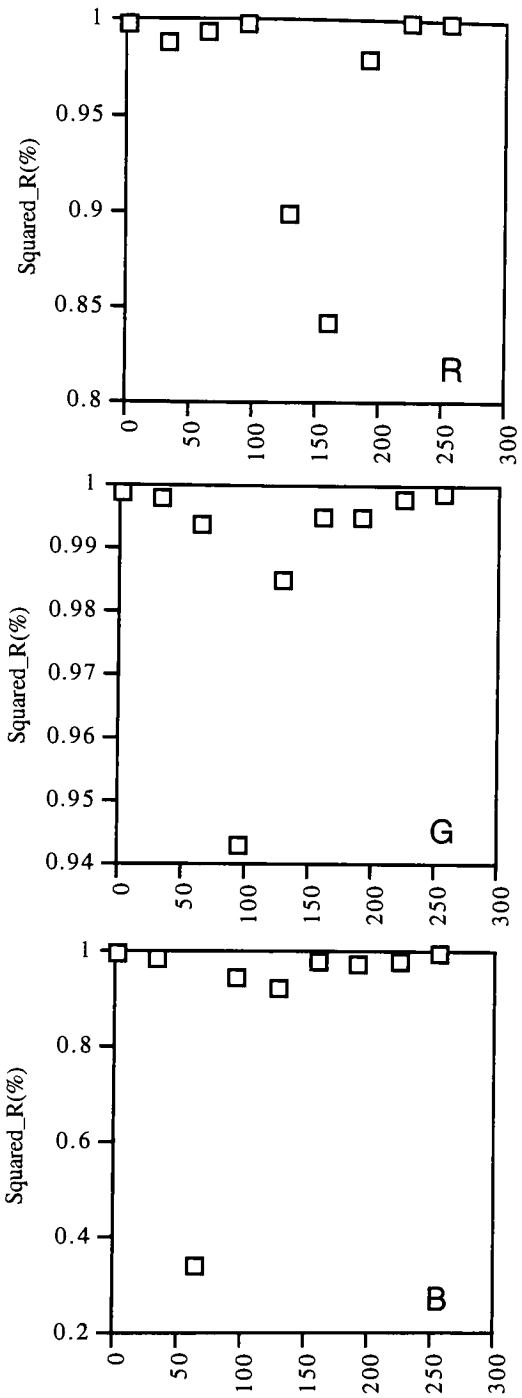

Fig. 5-12 Squared_R plots for predicted densities using 2 vectors and 2 scalars.

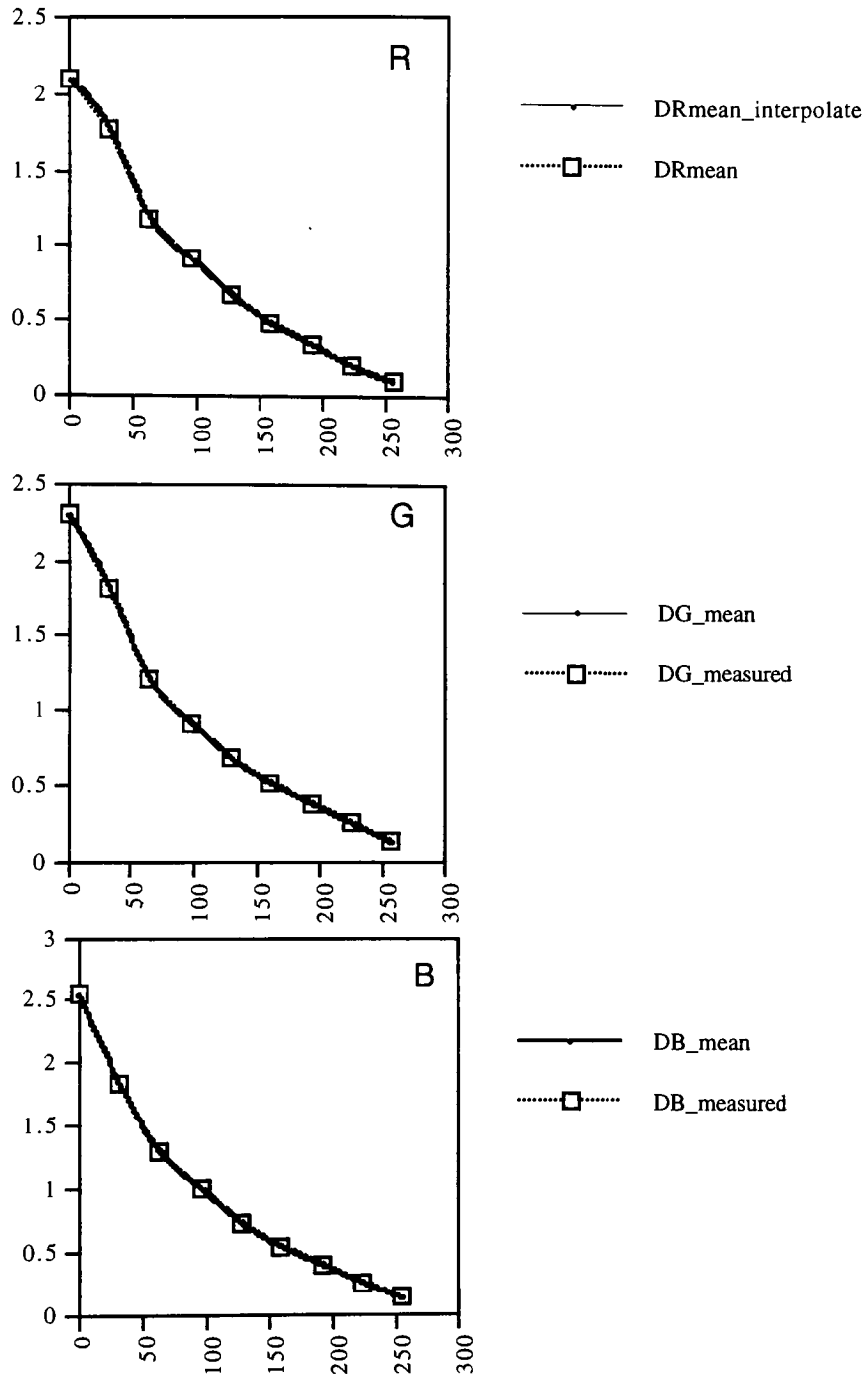

Fig. 5-13 LUT for red, green, and blue mean vectors using the cubic spline interpolation method with 9 data points.

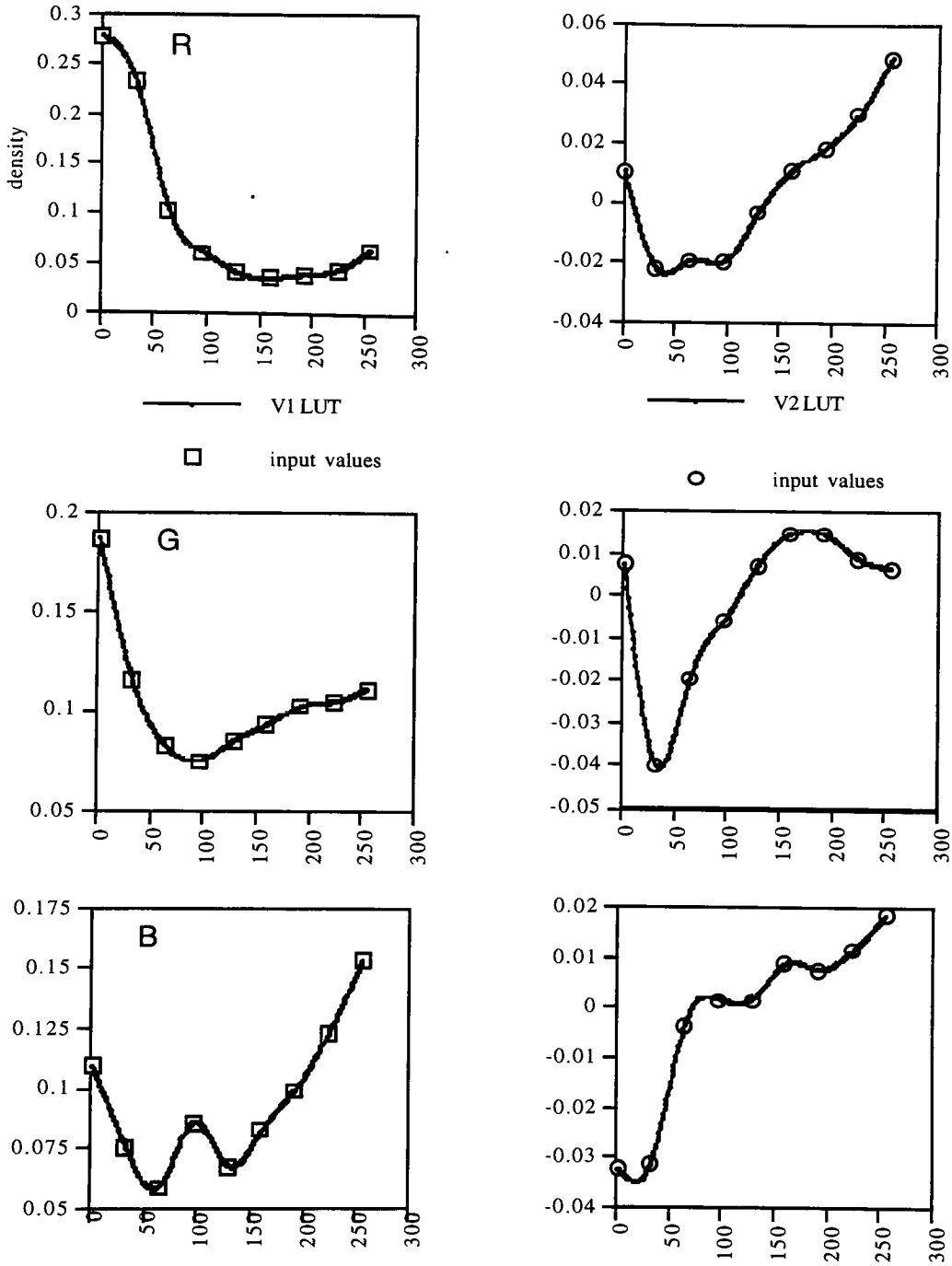

Fig. 5-14 LUT for red, green, and blue eigenvectors using cubic spline interpolation.

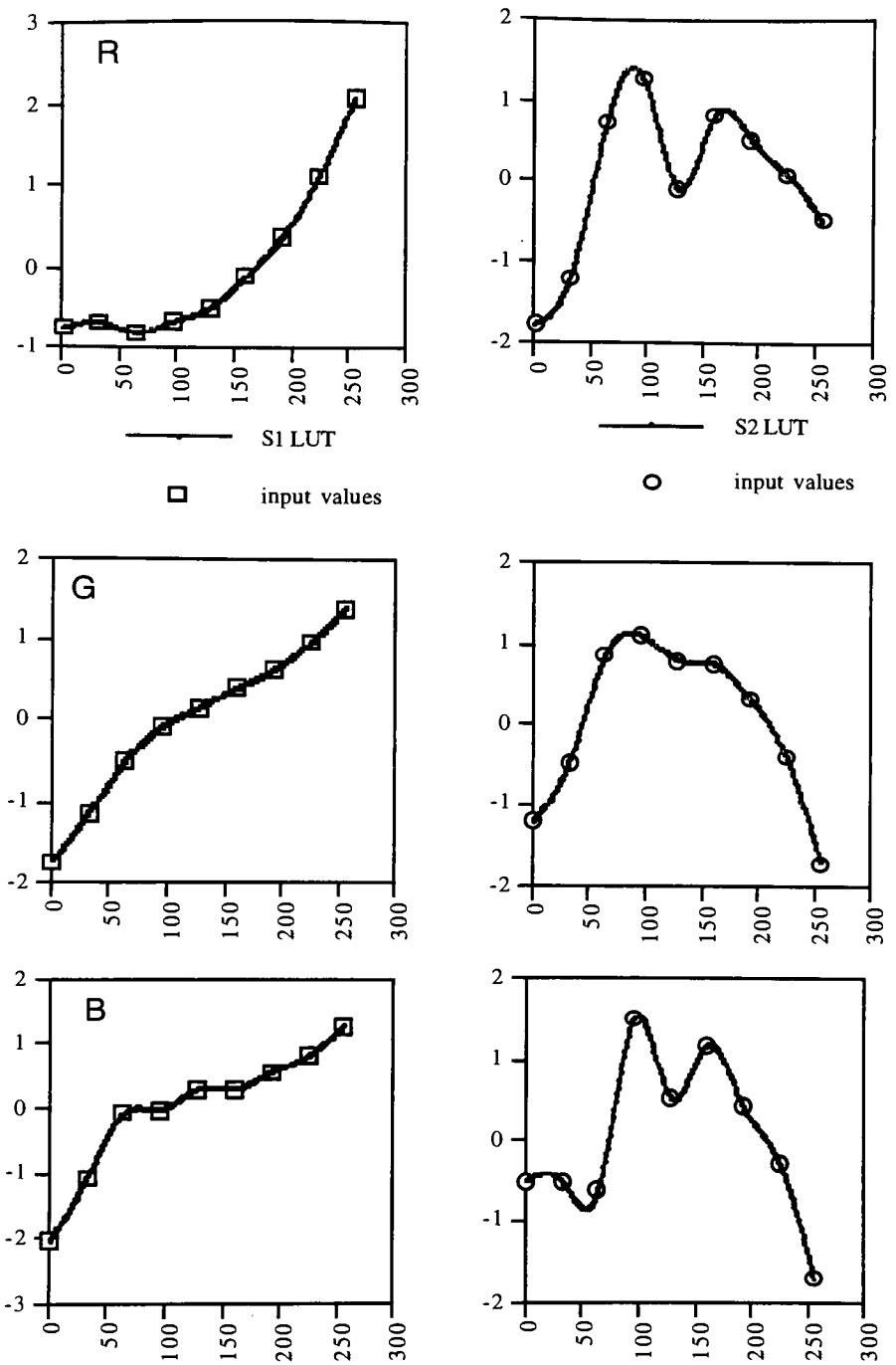

Fig. 5-15 LUT for least-squares fit coefficients for predicted densities.

Chapter VI. Forward Film Recorder Model

The characterization of the film recorder was based on the relationship between the input digital counts and the tristimulus values of the slide. The tristimulus values of the slide were obtained before and after projection. The model was mainly focused on the tristimulus values of the slide before projection. Once the relationship was defined, this model can be directly applied to the projected slide. The tristimulus values are obtained from the spectral transmittances of the slide. The image path for the characterization of a film recorder is shown in Figure 6-1. First, the concentrations of C, M, and Y dyes were defined from spectral transmittance measurements using Allen's tristimulus matching algorithms with Newton-Raphson method. Second, the relationship between concentrations of dyes and status A density was defined using a three-by-three transformation. Third, tone reproduction curves were defined and corrected by a gamma of 2.2. Fourth, the color correction LUT was developed based on the TRCs. In this thesis, the color correction LUT was defined by the interimage effects model with principal component analysis. In this thesis, the forward relationship was only considered. However, to complete colorimetric characterization of the film recorder, the reverse of this path must be defined.

Especially in this thesis, the interimage effects were determined by the variability of main gamma (Kcr, Kmg, Kyb) on the off-diagonal exposure levels. When the digital counts for main gamma terms kept changing from 0 to 255 (8 bits), the digital counts for the off-diagonal terms remained constant in certain

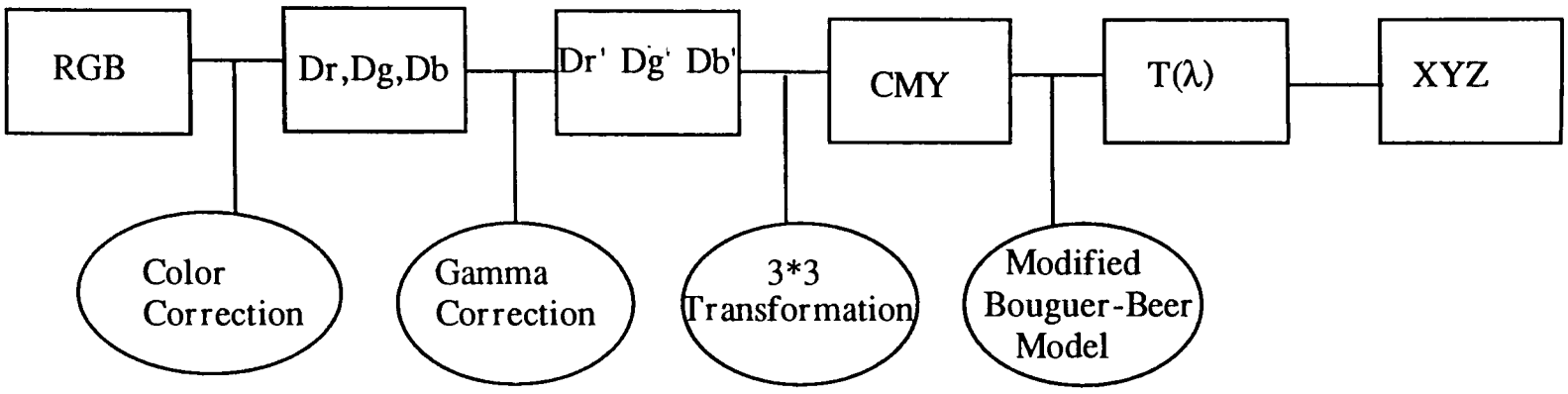

Fig. 6-1 Image Path for Characterization of a Film Recorder

levels. Since the main gammas changed along the off-diagonal exposure levels, it is necessary to explain this variability along the off-diagonal terms as well as the off-diagonal coefficient itself. It was assumed that the variability of main gamma includes the variability of the off-diagonal terms as well.

When light passed through the red filter, the red sensitive layer was exposed and the amount of cyan dye decreased. However, the red exposure affected the green sensitive layer as well as the blue sensitive layer. The green sensitive layer was more affected by the red exposure than the blue sensitive layer. These phenomena coincide with the interimage effects plots in Figure 5-6. Therefore, the green scalars were used to show the interimage effects for the red exposure density. Green and red scalars were used to show the effects for the blue and green exposure densities, respectively. The red off-diagonal terms and the blue off-diagonal terms had obviously negative slopes, especially for the green exposure density. Therefore, these two scalars were considered equally in the model.

The color correction LUTs were generated using one scalar and two scalars of the interimage effects model. The inputs were the digital image counts for each channel (dr, dg, and db). The outputs were the status A densities (D_R, D_G, and D_B). The model using one scalar and two scalars are shown below:

One scalar model:

$$D_R(dr) = V_0{}^R(dr) + V_1{}^R(dr) * S_1{}^R(dg) + V_2{}^R(dr) * S_2{}^R(dg)$$

$$D_G(dg) = V_0{}^G(dg) + V_1{}^G(dg) * S_1{}^G(dr) + V_2{}^G(dg) * S_2{}^G(dr)$$

$$D_B(db) = V_0{}^B(db) + V_1{}^B(db) * S_1{}^B(dg) + V_2{}^B(db) * S_2{}^B(dg)$$

Two scalar model:

$$D_R(dr) = V_0^R(dr) + V_1^R(dr) * \{S_1^R(dg) + S_1^R(db)\} / 2 + V_2^R(dr) * \{S_2^R(dg) + S_2^R(db)\} / 2$$

$$D_G(dg) = V_0^G(dg) + V_1^G(dg) * \{S_1^G(dr) + S_1^G(db)\} / 2 + V_2^G(dg) * \{S_2^G(dr) + S_2^G(db)\} / 2$$

$$D_B(db) = V_0^B(db) + V_1^B(db) * \{S_1^B(dr) + S_1^B(dg)\} / 2 + V_2^B(db) * \{S_2^B(dr) + S_2^B(dg)\} / 2$$

The ΔD between the predicted densities from these two models and the measured densities from the densitometer were calculated.

$$\Delta D = |\text{predicted D} - \text{measured D}|$$

The results are shown in Table 6-1. The red and blue densities show better results (small ΔD) using one scalar as opposed to two scalars. However, the green density yielded a better result when two scalars were used.

Table 6-1 ΔD using the interimage effects model.

ΔD	ΔD_R	ΔD_G	ΔD_B
1_scalar aver.	0.039	0.039	0.033
1_scalar max.	0.270	0.273	0.185
2_scalars aver.	0.061	0.030	0.055
2_scalars max.	0.549	0.206	0.293

Thus, the final color correction model using the interimage effects is shown below:

$$D_R(dr) = V_0{}^R(dr) + V_1{}^R(dr) * S_1{}^R(dg) + V_2{}^R(dr) * S_2{}^R(dg)$$
$$D_G(dg) = V_0{}^G(dg) + V_1{}^G(dg) * \{S_1{}^G(dr) + S_1{}^G(db)\} / 2 + V_2{}^G(dg) * \{S_2{}^G(dr) + S_2{}^G(db)\} / 2$$
$$D_B(db) = V_0{}^B(db) + V_1{}^B(db) * S_1{}^B(dg) + V_2{}^B(db) * S_2{}^B(dg)$$

Based on this model, the LUT was generated. The software for the color correction LUT is listed in Appendix G. Using the forward color correction model, the predicted densities were compared with the measured densities using all the samples. The results for the grey samples are shown in Figure 6-2. The results for all colors are also shown in Figures 6-3, 6-4, and 6-5.

After the status A density was corrected colorimetrically, the concentration was converted from the corrected density using the three-by-three transformation. The transformation matrix is shown below:

$$\begin{bmatrix} C_y \\ C_m \\ C_c \end{bmatrix} = \begin{bmatrix} 0.00997 & -0.17463 & 1.94820 \\ -0.42063 & 1.47407 & -0.26176 \\ 2.21254 & -0.11542 & 0.06511 \end{bmatrix} \begin{bmatrix} D_R(dr) \\ D_G(dg) \\ D_B(db) \end{bmatrix}$$

After the status A density was transformed to the concentration, the color correction model was applied using the concentration.

$$\Delta C = |[3x3] \times \text{predicted } C - [3x3] \times \text{measured } C|$$

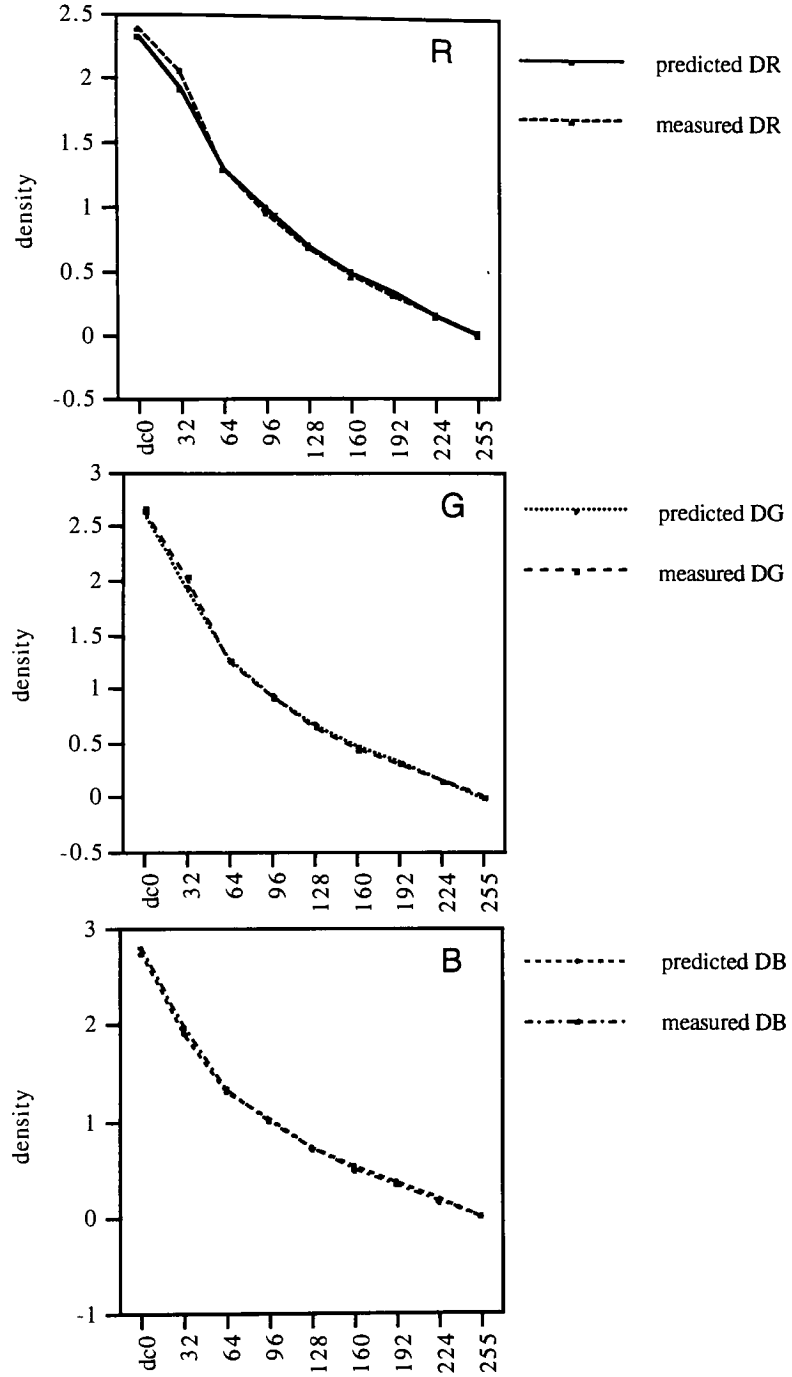

Fig. 6-2 Predicted density vs. measured density using the interimage effects model for grey samples.

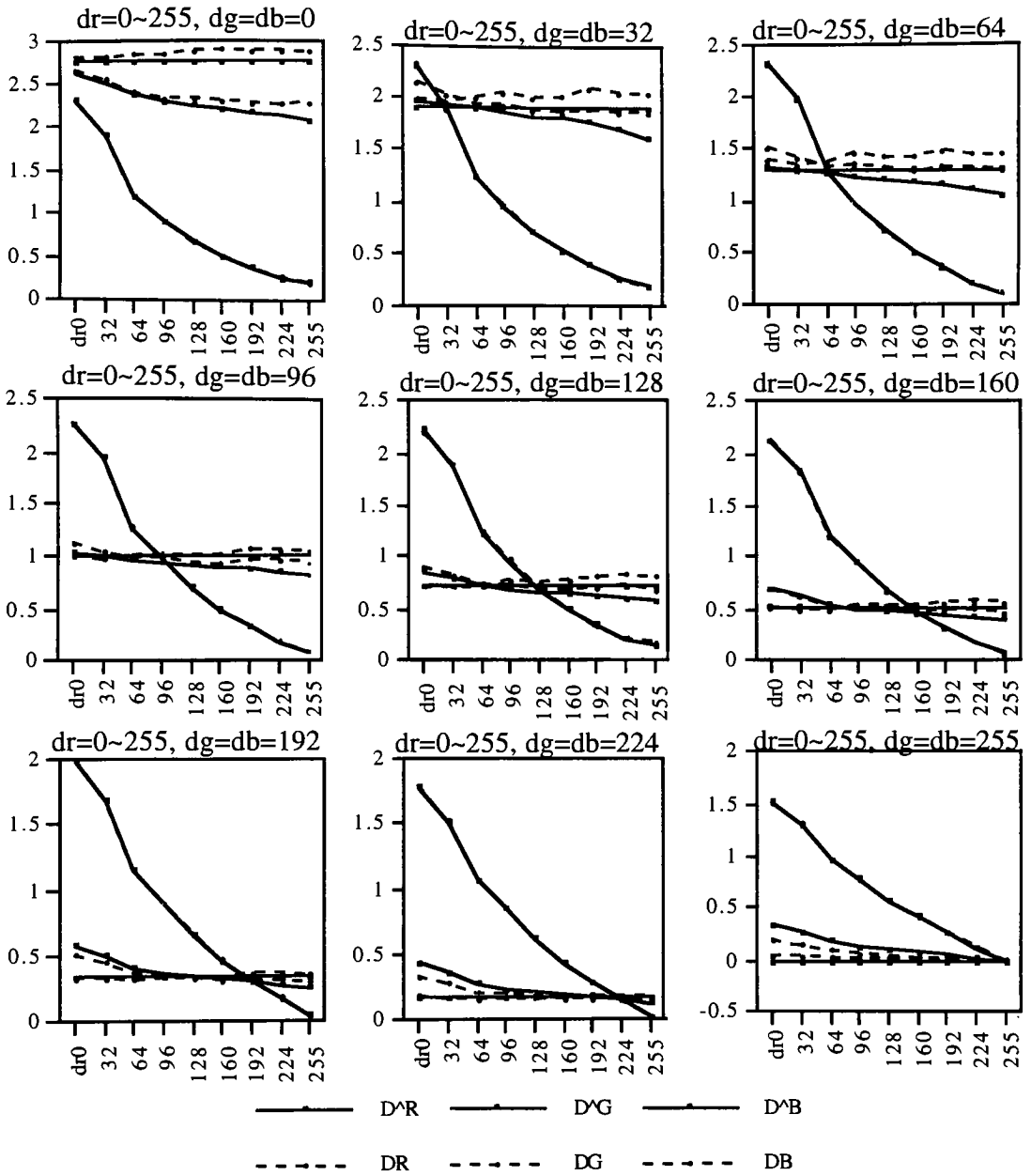

Fig. 6-3 Predicted density vs. measured density using the interimage effects model as a function of red exposure.

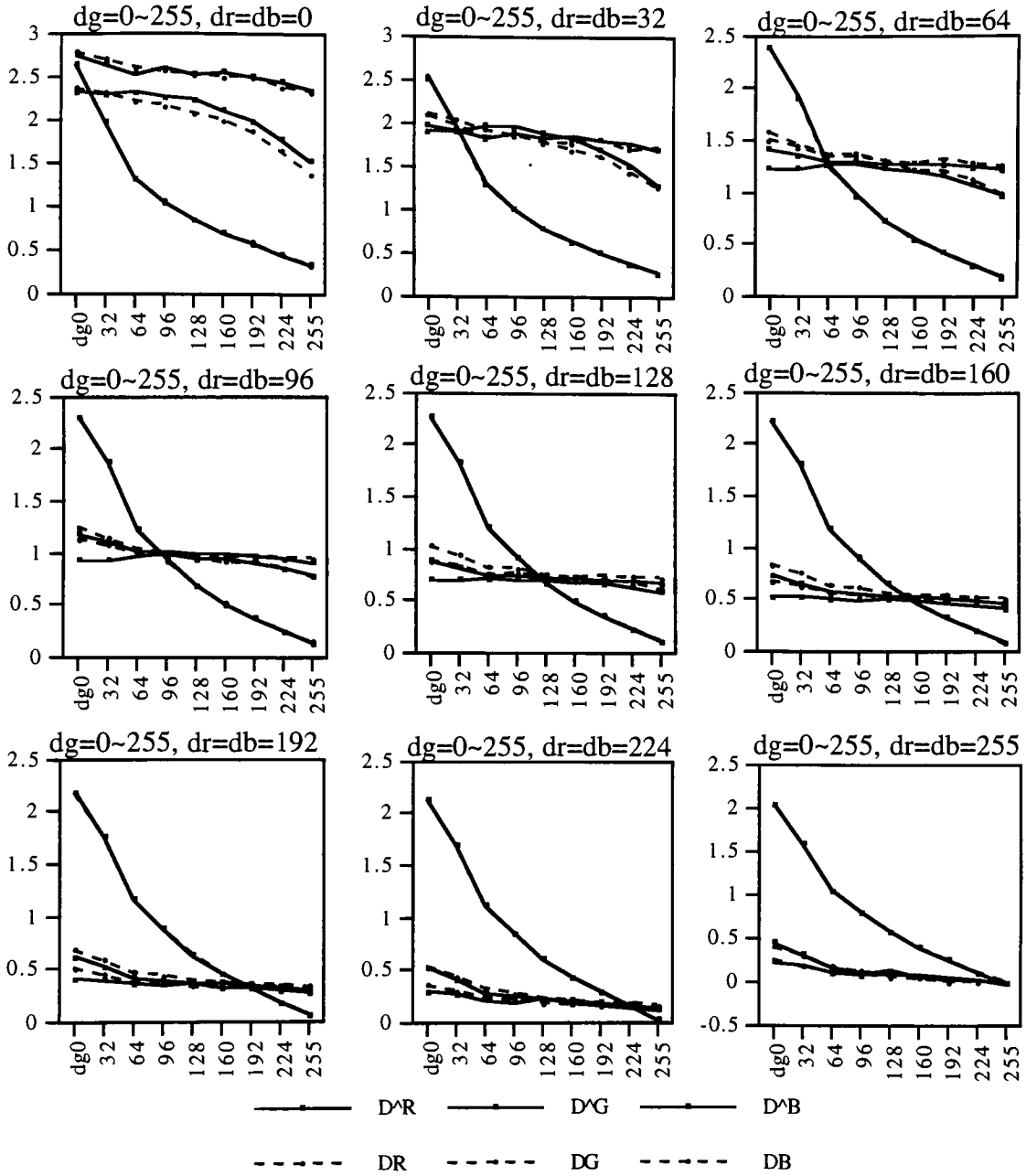

Fig. 6-4 Predicted density vs. measured density using the interimage effects model as a function of green exposure.

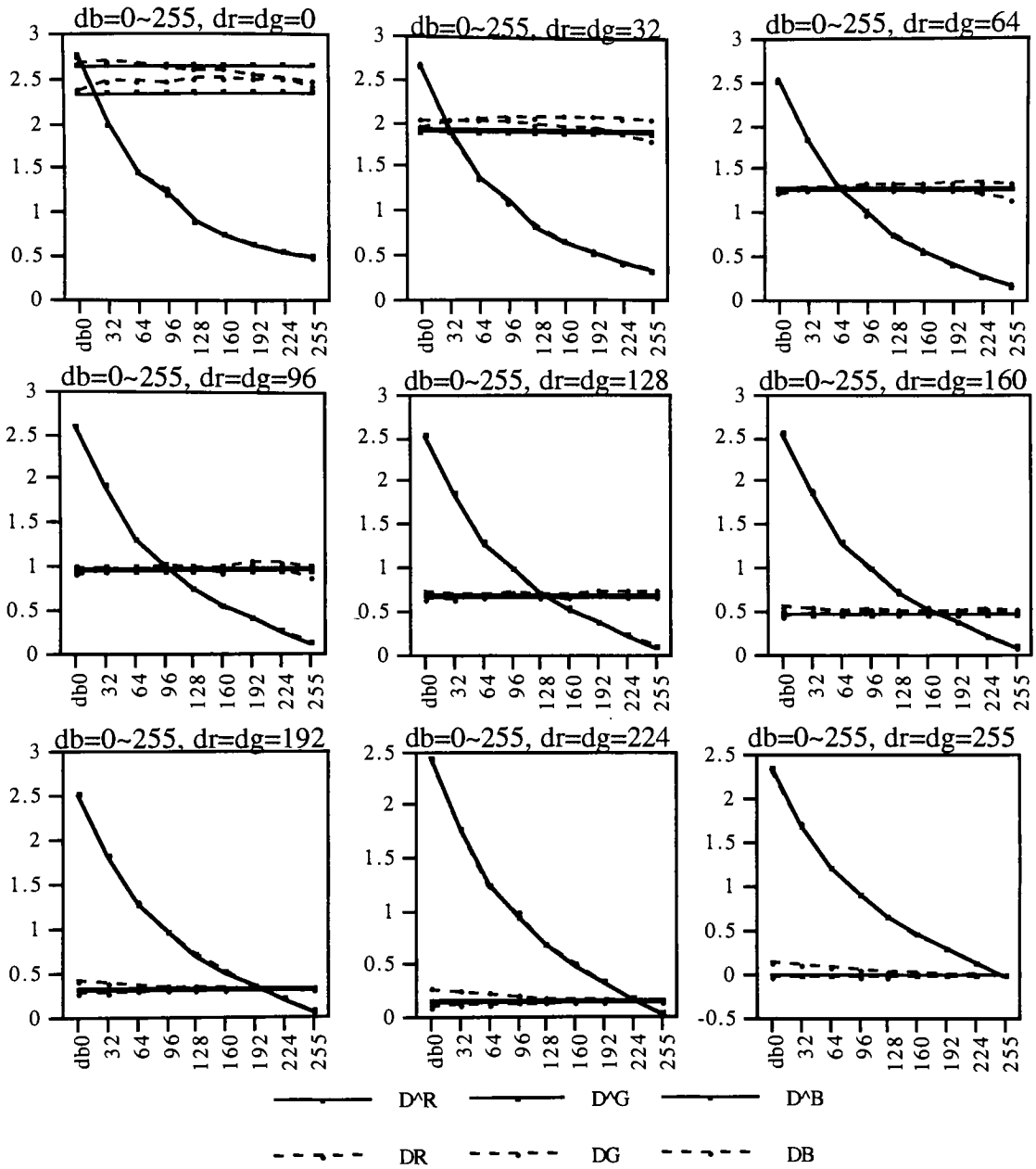

Fig. 6-5 Predicted density vs. measured density using the interimage effects model as a function of blue exposure.

The ΔC for each dye is listed in Table 6-2 using one and two scalars.

Table 6-2 ΔC using the interimage effects model and the three-by-three transformation.

ΔC	ΔCc	ΔCm	ΔCy
1_scalar aver.	0.075	0.059	0.073
1_scalar max.	0.536	0.389	0.387
2_scalars aver.	0.118	0.043	0.122
2_scalars max.	1.083	0.296	0.673

Using the predicted concentrations of cyan, magenta, and yellow (Cc, Cm, and Cy) after a three-by-three transformation, the spectral transmittance of the film was derived by the modified Beer-Bouger model. The tristimulus values of the slide before projection were calculated using these spectral transmittance values under Illuminant A. First, the measured density was transformed to concentrations using the three-by-three transformation and the spectral transmittance was calculated using the Beer-Bouger model. Second, the predicted densities from the color correction model were transformed to concentrations and the spectral transmittance was then calculated. The color difference was calculated using these two sets of spectral transmittance in CIELAB space. Figure 6-6 shows the histogram of the color difference. The average ΔE^*_{ab} under Illuminant A was 3.09 and the maximum ΔE^*_{ab} was 10.30. For the grey samples only, the average ΔE^*_{ab} was 1.46 and the maximum ΔE^*_{ab} was 2.51. The concentrations and the ΔE^*_{ab} values for 252 samples are listed in Appendix F.

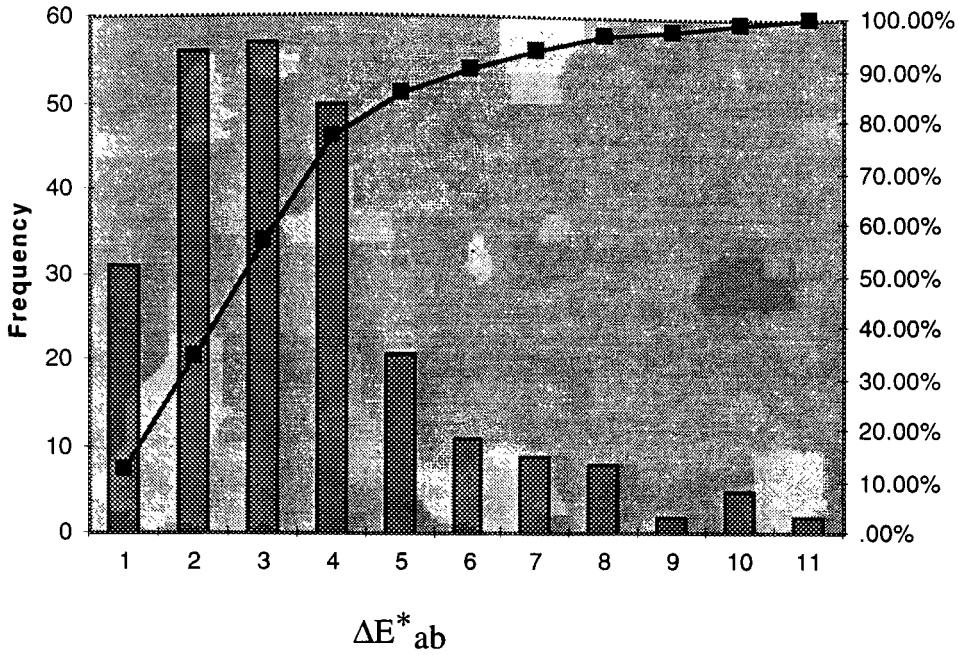

Fig. 6-6 ΔE^*_{ab} using the interimage effects model under Illuminant A.

The results were reasonable for the grey samples, in particular. When the off-diagonal terms have high exposure levels compared to main gamma levels, ΔE^*_{ab} becomes larger. The color correction model was derived from the variability of the main gammas which were dependent on the off-diagonal exposure levels. Since the model was defined by only one off-diagonal level (dr 0~255, dg=db=k), the high variability between the off-diagonal terms may have caused substantial error. However, 96% of the samples have ΔE^*_{ab} under 8. Only nine samples among the 252 samples have ΔE^*_{ab} over 8. Considering this LUT was not 3D, these results were fairly promising. Table 6-3 shows the cumulative percentages for color difference.

Table 6-3 The cumulative ΔE^*_{ab} for the interimage effects model.

Interval	Frequency	Cumulative %
1	31	12.30%
2	56	34.52%
3	57	57.14%
4	50	76.98%
5	21	85.32%
6	11	89.68%
7	9	93.25%
8	8	96.43%
9	2	97.22%
10	5	99.21%
11	2	100.00%

The delta graphs for the a*b* plane and L* vs. C^*_{ab} are shown in figure 6-7 and 6-8. CIE94 color difference formula was also calculated to compare the color difference values from CIELAB formula. The results are listed in Table 6-4 and figure 6-9. The average ΔE^*_{94} under illumimant A was 1.89 for 252 samples and the maximum ΔE^*_{94} was 6.66. 96% of the samples have ΔE^*_{94} under 5. These results were very good. The CIE94 color difference formula is shown below:

$$\Delta E^*_{94} = \left[\left(\frac{\Delta L^*}{k_L S_L} \right)^2 + \left(\frac{\Delta C^*_{ab}}{k_c S_c} \right)^2 + \left(\frac{\Delta H^*_{ab}}{k_H S_H} \right)^2 \right]^{1/2}$$

$$S_L = 1$$

$$S_C = 1 + 0.045 C^*_{ab}$$

$$S_H = 1 + 0.015 C^*_{ab}$$

$$C^*_{ab} = \sqrt{C^*_{ab,Std} C^*_{ab,Trial}}$$

$k_L = k_C = k_H = 1$ for basis conditions

$k_L = 2k_C = k_H = 1$ for textiles

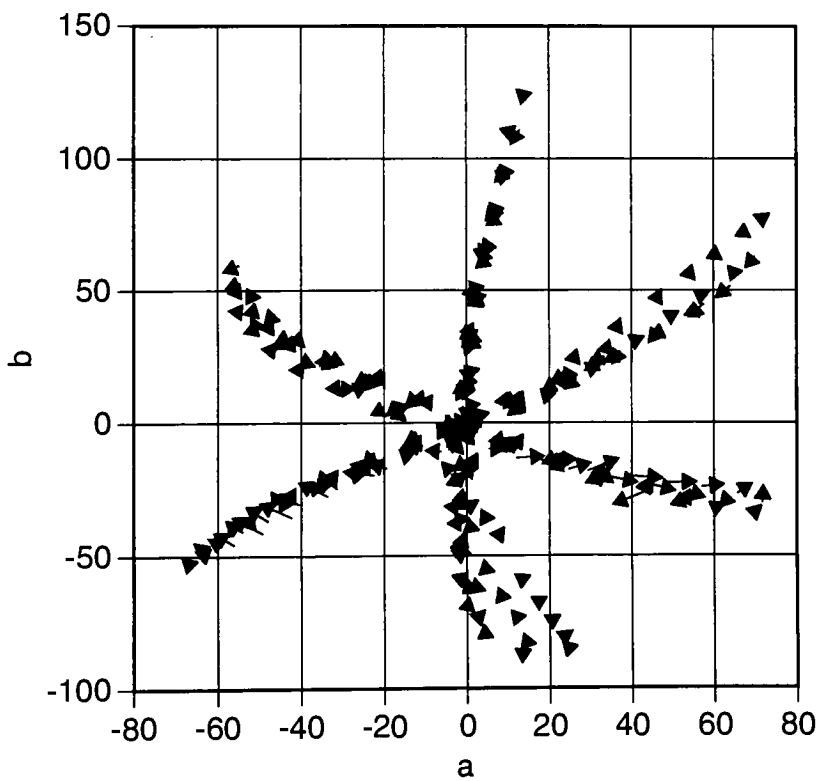

Fig.6-7 Hue plane(a*b*) delta plot under illuminant A.

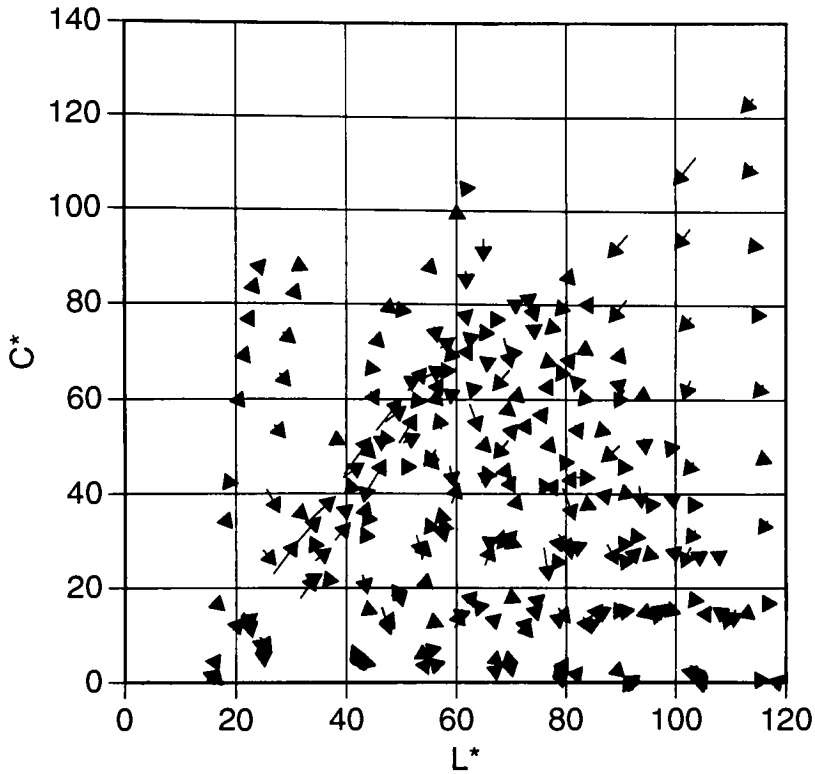

Fig.6-8 Lightness vs. Chroma delta plot under illuminant A.

Table 6-4 The cumulative ΔE^*_{94} using interimage effects model.

Bin	Frequency	Cumulative %
1	54	21.43%
2	112	65.87%
3	52	86.51%
4	15	92.46%
5	9	96.03%
6	5	98.02%
7	5	100.00%

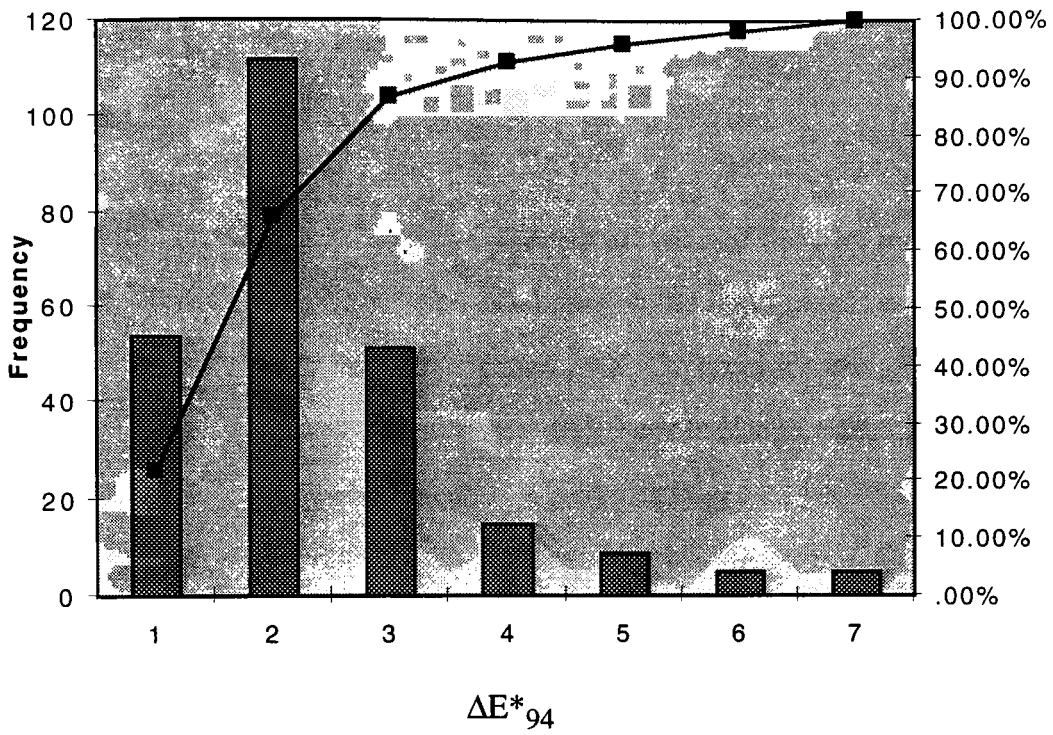

Fig. 6-9 ΔE^*_{94} using interimage effects model under illuminant A.

Chapter VII. Conclusions

In this thesis, the colorimetric characterization of the film recorder was achieved. Specifically, the relationship between the input pixel values and the spectral transmittance of the film exposed by a film recorder was modeled by one dimensional LUTs for tone reproduction and the interimage effects matrix for the color correction. The interimage effects were explained by the characteristic vectors using principal component analysis. It is known that characteristic vectors are used to find dye absorptive curves for color film. However, the principal component analysis has never been used for the interimage effects model. This interimage effects model approach can also be applied to printers, such as dye diffusion printers, that have the cross-talk problems.

It is crucial to find the relationship between the integral density and the analytical density (concentrations) in order to achieve color reproduction of film. The relationship is shown in Figures 4-3 and 4-4. Since the plots were reasonably linear and the transformation between the input RGB and the status A density based on interimage effects model is complicated, transformations beyond three-by-three were not considered in this thesis. The ΔE^*_{ab} between the real dye concentrations and the predicted dye concentrations were compared in order to find the errors caused by the three-by-three transformation. The error was an average ΔE^*_{ab} of 1.0.

The integral density is measured by either a spectrophotometer or a densitometer. The density values from a spectrophotometer were used to

characterize film with the spectral data. If the dye concentrations and dye absorptivities of film are specified, a densitometer can be used as a device for calibrating film recorders. This is similar to the characterization of CRTs. In order to characterize a CRT correctly, either a monitor colorimeter or a spectroradiometer should be used. However, if the CRT phosphors are characterized correctly, a photometer can be used for calibration. Using a densitometer as a calibration device provides some advantages. A densitometer is usually much less expensive than a spectrophotometer. Also, the aperture of a densitometer is usually much smaller than that of a transmission spectrophotometer. In this thesis, 252 samples were generated from one roll of film for the densitometer while 36 samples were generated for the transmission spectrophotometer. This reduced the variability of process as well as the film cost.

In this thesis, the color correction LUTs for a film recorder were generated in status A density space, and it was followed by the transformation between the status A density and the analytical density (dye concentrations). Allen's tristimulus matching algorithm with the Newton-Raphson method was used to estimate the dye concentrations. The tone reproduction curves were corrected by a gamma of 2.2. The color correction matrix was generated using the principal component analysis. The color correction model were generated by the interimage effects matrix using the one dimensional characteristic vector LUTs based on extensive mesurements (252 samples). The results from this model were fairly reasonable. The average ΔE^*_{ab} for grey samples was 1.46 and for all samples was 3.09. The maximum ΔE^*_{ab} for grey samples was 2.51 and for all samples was 10.30. 96% of all the samples were below a ΔE^*_{ab} of 8.0.

7.1 Future Research

The characterization of the film recorder can be improved by considering the following factors. The interimage effects were explained by keeping two off-diagonal terms the same while the main gamma terms changed over the whole range of exposures. For example, the red exposure changed up to maximum and the green and blue exposure levels remained the same (dr 0~255, dg=db=k). In order to apply the interimage effects to all the colors, the sample that contains different green and blue exposure levels also must be considered (dr 0~255, dg=i db=j).

In this thesis, the transformation between the integral density and concentrations was modeled by a three-by-three transformation. However, the transformation beyond three-by three may need to be considered.

In the color correction modeling, the determination of characteristic vectors are critical. In this thesis, the three sets of 252-samples were generated for characteristic vector analysis. There are three different methods of generating TRCs which are: adjustment of gamma, linear in density, and linear in lightness. This thesis used a gamma adjustment of 2.2 which was applied to the LUT. The gamma approach was used because the TRC from a gamma 2.2 yielded better gray balanced neutral samples than the TRC from the linear-in-density method. The linear-in-lightness method was not considered in this thesis because it involves more human perception rather than colorimetric matching which is done before projection. Although the other TRCs yielded less gray balanced neutrals than that of the gamma adjustment, the LUTs may match the colors with more accuracy.

This thesis focused on the forward relationship between input RGB and output tristimulus values, XYZ, before the slide is projected. Since the slide is viewed by projection under a dark surround, the colorimetry of the projected slides must be accounted for as well. Based on the matrix of the interimage effects, the colorimetry of the projected slide may be revealed. To complete this model for the application of color correction, inversion of the interimage model must be defined.

References

1) R. S. Berns, Colorimetric Characterization of the Solitaire 16 Film Recorder for Kodak Ektachrome Plus Professional 100: A Pilot Study, Munsell Color Science Laboratory, Technical Report, Rochester, NY (May 1993).

2) J.O. Hamblen and A.Parker, Visual Communication Technogies for Computer Graphics, *IEEE Transactions Professional Communication* **31(3)**, 135-141 (September, 1988)

3) G. MacNicol, Film Recorders at the High End, *Computer Graphics World*, 103-110 (1990).

4) R. H. Wallis, Film Recording of Color Digital Images, *USCIPI Report 570*, Image Processing Institute, University of Southern Califonia, Los Angeles (1975).

5) W. L. Rogers and J. W. Keyes, Jr., Techniques for precise recording of gray-scale images from computerized scintigraphic displays, *J.Nucl.Med.* **22**, 283-286 (1981).

6) J. Rosenbaum, Semi-Automatic Generation of Film Compensation Tables, *Color Res. Appl.* **13**, 187-192 (1988).

7) F. Grum and C. J. Bartleson, Chapter 7: Colorant Formulation and Shading, *Optical Radiation Measurements*, Vol. 2, Academic Press, Inc, New York (1984).

8) F. R. Clapper, Chapter 19: Tone and Color Reproduction II.Color Reproduction of Color Films, T.H.James, *The Theory of the Photographic Process*, 4th Ed., Macmillian Publishing Co. Inc, New York (1977).

9) Wilkinson, L.., *SYSTAT: The System for Statistics.* , SYSTAT Inc. (1986).

10) N. Ohta, Metameric Color Matching by Dye Systems Deviating from the Lambert-Beer Law, *DK535.626, 778.66*.

11) N. Ohta, Metameric color matching in subtractive color photography, I. Dye system in obedience to Lambert-Beer law, *Photographic Sci. and Eng.*, **16**, 136-143 (1972).

12) N. Ohta, Estimating Absorption Bands of Component Dyes by Means of Principal Component Analysis, *Anal. Chem.*, **45**, 553-557 (1973).

13) R. S. Berns, Spectral modeling of a dye diffusion thermal transfer printer., *J. of Electronic Imaging*, **2**, 359-370 (1993).

14) R. W. G. Hunt, *The Reproduction of Color in Photography, Printing & Television*, 4th Ed., Chapter 14, Fountain Press, England (1987).

15) P.Kowaliski, Chapter 18: Sensitometry of Color Films and Papers, T.H.James, *The Theory of the Photographic Process*, 4th Ed. Macmillian Publishing Co. Inc, New York (1977).

16) G. H. Dawson and W. F. Voglesong, *Photogr. Sci. Eng.*, **17**, 31 (1973).

Bibliography

D. S. Aframe, *Graphics and Color Hardcopy: Software and Standards Drive a Major New Printer Market*, A Datek Information Services, Inc. Industry Report.

J. P. Allebach, J. Z. Chang and C. A. Bouman, Efficient Implementation of Nonlinear Color Transformations, *IS&T and SID's Color Imaging Conference Proceeding*, 143-148 (1993).

C. J. Bartleson, *Optical Radiation Measurements*, Vol. 5, Academic Press, Inc., Orlando, Florida (1984).

R. S. Berns, Colorimetric Characterization of the Solitaire 16 Film Recorder for Kodak Ektachrome Plus Professional 100: A Pilot Study, Munsell Color Science Laboratory, Technical Report, Rochester NY (May 1993).

CIE (*Commission Internationale deEclairage*) Publication 15.2, *Colorimetry*, 2nd Ed, Vienna, Austria (1986).

M. D. Fairchild, R. S. Berns, A. A. Lester and H. K. Shin, Accurate Color Reproduction of CRT Displayed Images as Projected 35mm Slides, *The Second IS&T/SID Proceedings*, 69-73 (1994).

M. D. Fairchild, A Simple Printer Calibration Technique for "Good Enough" Color Reproduction of Color Images, Munsell Color Science Laboratory, Technical Report, Rochester, New York (January 1994).

M. D. Fairchild, Some Hidden Requirements For Device-Independent Color Imaging, *SID Int'l Symposium Digest of Technical Papers* XXV, 865-868 (1994).

S. W. Grotta & D. Grotta, Digital to Silver: How Film Recorders Bridge Two Technologies, *Photo>Electronic Imaging*, 20-23 (July 1993).

Franc Grum and C. J. Bartleson, *Optical Radiation Measurements*, Vol. 2, Academic Press, Inc, New York (1984).

R. Gschwind, Restoration of Faded Colour Photographs by Digital Image Processing, *J. of Photo. Sci.* **38**, 193-196 (1990).

W. T. Hanson, Jr., & C.A. Horton, Subtractive Color Reproduction: Interimage Effects, *J. of the Opt. Soc..Am.* **42**, 663 (1952).

A. C. Hardy & F. L. Wurzburg, Jr., The Theory of Three-Color Reproduction, *J. Opt. Soc.Am.* **27**, 227-240 (1937).

P. C. Hung, Colorimetric Calibration in Electronic Imaging Devices Using a Look-up-table Model and Interpolations, *J. of Electronic Imag.* **2**, 53-61 (1993).

P. C. Hung, Colorimetric Calibration for Scanners and Media, *S.P.I.E.Proceeding 1448*, 164-174 (1991).

R. W. G. Hunt, *The Reproduction of Color in Photography, Printing & Television*, 4th Ed., Fountain Press, England (1987).

T. H. James, *The Theory of the Photographic Process*, 4th Ed., Macmillian Publishing Co. Inc, New York (1977).

N. Ohta, Colorimetric Analysis in the Design of Color Films: A Perspective. *J. of Imaging Sci. and Tech.* **36**, 63-72 (1992).

N. Ohta, Interrelation between Spectral Sensitivities and Interimage Effects, *J. of Imag. Sci.* **35**, 94-103 (1991).

N. Ohta, Optimum Absorption Bands of Subtractive Dyes for Color Photography, *Nature Physical Science* **235**, 24-26 (1972).

N. Ohta, The Color Gamut Obtainable by the Combination of Subtractive Color Dyes, 1. Actual Dyes in Color Film. (2) Influence of Unwanted Secondary Absorption Peak, *Photo. Sci. and Eng.* **15**, 416-422 (1971).

J. D. Panning, *Interimage Effects and The MTF of A Color Reversal Film*, Masters Thesis, Rochester Institute of Technology, Rochester, New York (1978).

S. A. Rajala and A. P. Kakodkar, Interpolation of Color Data, *IS&T and SID's Color Imaging Conference Proceedings*, 180-183 (1993).

S. P. Robinson & L. S. Horst, Color Film Recording from T.V., *S.P.I.E. Journal* **9**, 196-200 (1971).

M. A. Rodriguez, Producing Colorimetric Data From Densitometric Scans, *IS&T/SPIE Int'l Symposium on Electronic Imaging Proceedings*, 1913-1933 (1993).

S. A. Teukolsky, William T. Vetterling and B. P. Flannery, *Numerical Recipies in C, 2nd Ed., The Art of Scientific Computing*, W. H. Press,

J. A. S. Viggiano, C. J. Wang, A Novel Method for Colorimetric Calibration of Color Digitizing Scanners, *TAGA* (1993).

M. J. Vrhel, H. J. Trussell, Color Correction Using Principal Components, *Color Res. Appl.* **17** (1992).

J. E. Wurtz & F. J. Marshall, The Application of Cathode Ray Tubes to Film Recording and Scanning, *S.P.I.E. Journal* **9**, 186-195 (1971).

G. Wyszecki and W. S. Stiles, *Color Science*, 2nd Ed., John Wiley & Sons Inc., New York (1982).

Appendix A. The digital values of a 90-image target for the eigenvector analysis and final eigenvector data.

	dr	dg	db
1	50	50	50
2	100	100	100
3	150	150	150
4	200	200	200
5	250	250	250
6	50	250	250
7	250	50	250
8	250	250	50
9	50	50	250
10	50	250	50
11	250	50	50
12	50	150	150
13	150	50	150
14	150	150	50
15	50	50	150
16	50	150	50
17	150	50	50
18	200	150	150
19	150	200	150
20	150	150	200
21	100	150	150
22	150	100	150
23	150	150	100
24	255	255	255
25	0	0	0
26	32	32	32
27	64	64	64
28	96	96	96
29	128	128	128
30	160	160	160
31	192	192	192
32	224	224	224
33	255	255	255
34	0	96	96
35	32	96	96
36	64	96	96
37	96	96	96
38	128	96	96
39	160	96	96
40	192	96	96
41	224	96	96

42	255	96	96
43	96	0	96
44	96	32	96
45	96	64	96
46	96	96	96
47	96	128	96
48	96	160	96
49	96	192	96
50	96	224	96
51	96	255	96
52	96	96	0
53	96	96	32
54	96	96	64
55	96	96	96
56	96	96	128
57	96	96	160
58	96	96	192
59	96	96	224
60	96	96	255
61	0	75	75
62	0	95	95
63	0	115	115
64	0	135	135
65	0	155	155
66	0	175	175
67	0	195	195
68	0	215	215
69	0	235	235
70	0	255	255
71	75	0	75
72	95	0	95
73	115	0	115
74	135	0	135
75	155	0	155
76	175	0	175
77	195	0	195
78	215	0	215
79	235	0	235
80	255	0	255
81	75	75	0
82	95	95	0
83	115	115	0
84	135	135	0
85	155	155	0
86	175	175	0
87	195	195	0

88	215	215	0
89	235	235	0
90	255	255	0

Final eigenvector data

	V^c	V^m	V^y
400	0.07925	0.08715	0.32767
410	0.0554	0.08744	0.34667
420	0.03848	0.10148	0.39762
430	0.02566	0.12072	0.44898
440	0.01702	0.12797	0.47525
450	0.02852	0.12614	0.45372
460	0.02049	0.13852	0.42864
470	0.01353	0.17185	0.37947
480	0.0127	0.22449	0.31112
490	0.01523	0.29348	0.2339
500	0.02036	0.3816	0.16356
510	0.02876	0.48769	0.1066
520	0.04101	0.59579	0.06466
530	0.05898	0.68677	0.03637
540	0.08244	0.74071	0.01881
550	0.11386	0.76209	0.00927
560	0.15068	0.73135	0.00334
570	0.19429	0.65089	-0.00254
580	0.24989	0.53502	-0.00612
590	0.31015	0.40117	-0.00826
600	0.37662	0.28152	-0.01011
610	0.44233	0.18851	-0.0115
620	0.50326	0.12247	-0.01232
630	0.55224	0.07639	-0.01307
640	0.59019	0.04667	-0.01354
650	0.60902	0.02663	-0.01347
660	0.61395	0.01409	-0.0135
670	0.59838	0.00493	-0.01325
680	0.57009	-0.00082	-0.0129
690	0.53096	-0.00381	-0.01208
700	0.48118	-0.00532	-0.0111

Appendix B. Digital count data for interimage effects.

	dr	dg	db		dr	dg	db		dr	dg	db
slide 1	0	0	0	12	0	0	0	23	0	0	0
	32	0	0		0	32	0		0	0	32
	64	0	0		0	64	0		0	0	64
	96	0	0		0	96	0		0	0	96
	128	0	0		0	128	0		0	0	128
	160	0	0		0	160	0		0	0	160
	192	0	0		0	192	0		0	0	192
	224	0	0		0	224	0		0	0	224
	255	0	0		0	255	0		0	0	255
slide 2	0	32	32	13	32	0	32	24	32	32	0
	32	32	32		32	32	32		32	32	32
	64	32	32		32	64	32		32	32	64
	96	32	32		32	96	32		32	32	96
	128	32	32		32	128	32		32	32	128
	160	32	32		32	160	32		32	32	160
	192	32	32		32	192	32		32	32	192
	224	32	32		32	224	32		32	32	224
	255	32	32		32	255	32		32	32	255
slide 3	0	64	64	14	64	0	64	25	64	64	0
	32	64	64		64	32	64		64	64	32
	64	64	64		64	64	64		64	64	64
	96	64	64		64	96	64		64	64	96
	128	64	64		64	128	64		64	64	128
	160	64	64		64	160	64		64	64	160
	192	64	64		64	192	64		64	64	192
	224	64	64		64	224	64		64	64	224
	255	64	64		64	255	64		64	64	255
slide 4	0	96	96	15	96	0	96	26	96	96	0
	32	96	96		96	32	96		96	96	32
	64	96	96		96	64	96		96	96	64
	96	96	96		96	96	96		96	96	96
	128	96	96		96	128	96		96	96	128
	160	96	96		96	160	96		96	96	160
	192	96	96		96	192	96		96	96	192
	224	96	96		96	224	96		96	96	224
	255	96	96		96	255	96		96	96	255
slide 5	0	128	128	16	128	0	128	27	128	128	0
	32	128	128		128	32	128		128	128	32
	64	128	128		128	64	128		128	128	64
	96	128	128		128	96	128		128	128	96
	128	128	128		128	128	128		128	128	128
	160	128	128		128	160	128		128	128	160
	192	128	128		128	192	128		128	128	192
	224	128	128		128	224	128		128	128	224
	255	128	128		128	255	128		128	128	255
slide 6	0	160	160	17	160	0	160	28	160	160	0
	32	160	160		160	32	160		160	160	32

	64	160	160		160	64	160		160	160	64
	96	160	160		160	96	160		160	160	96
	128	160	160		160	128	160		160	160	128
	160	160	160		160	160	160		160	160	160
	192	160	160		160	192	160		160	160	192
	224	160	160		160	224	160		160	160	224
	255	160	160		160	255	160		160	160	255
slide 7	0	192	192	18	192	0	192	29	192	192	0
	32	192	192		192	32	192		192	192	32
	64	192	192		192	64	192		192	192	64
	96	192	192		192	96	192		192	192	96
	128	192	192		192	128	192		192	192	128
	160	192	192		192	160	192		192	192	160
	192	192	192		192	192	192		192	192	192
	224	192	192		192	224	192		192	192	224
	255	192	192		192	255	192		192	192	255
slide 8	0	224	224	19	224	0	224	30	224	224	0
	32	224	224		224	32	224		224	224	32
	64	224	224		224	64	224		224	224	64
	96	224	224		224	96	224		224	224	96
	128	224	224		224	128	224		224	224	128
	160	224	224		224	160	224		224	224	160
	192	224	224		224	192	224		224	224	192
	224	224	224		224	224	224		224	224	224
	255	224	224		224	255	224		224	224	255
slide 9	0	255	255	20	255	0	255	31	255	255	0
	32	255	255		255	32	255		255	255	32
	64	255	255		255	64	255		255	255	64
	96	255	255		255	96	255		255	255	96
	128	255	255		255	128	255		255	255	128
	160	255	255		255	160	255		255	255	160
	192	255	255		255	192	255		255	255	192
	224	255	255		255	224	255		255	255	224
	255	255	255		255	255	255		255	255	255
slide 10	0	0	0	21	0	0	0	32	0	0	0
	32	32	32		32	32	32		32	32	32
	64	64	64		64	64	64		64	64	64
	96	96	96		96	96	96		96	96	96
	128	128	128		128	128	128		128	128	128
	160	160	160		160	160	160		160	160	160
	192	192	192		192	192	192		192	192	192
	224	224	224		224	224	224		224	224	224
	255	255	255		255	255	255		255	255	255
slide 11	255	255	255	22	255	255	255	33	255	255	255
	255	255	255		255	255	255		255	255	255
	255	255	255		255	255	255		255	255	255
	255	255	255		255	255	255		255	255	255
	255	255	255		255	255	255		255	255	255
	255	255	255		255	255	255		255	255	255
	255	255	255		255	255	255		255	255	255
	255	255	255		255	255	255		255	255	255
	255	255	255		255	255	255		255	255	255

Appendix C. Vector Analysis Results for Interimage Effects by Principal Component Analysis.

DR					
LATENT ROOTS (EIGENVALUES)					
1	2	3	4	5	
0.1571	0.00514	0.00083	0.00017	0.00005	
6	7	8	9		
0.00002	0.00001	0	0		
COMPONENT LOADINGS					
	1	2	3		
DR0	0.2787	0.01031	-0.01605		
DR32	0.23348	-0.02231	0.0114		
DR64	0.10236	-0.01938	0.00848		
DR96	0.06068	-0.01962	0.00266		
DR128	0.04086	-0.00327	0.0024		
DR160	0.03627	0.01085	-0.0017		
DR192	0.03995	0.01882	-0.00786		
DR224	0.04509	0.02995	-0.00107		
DR255	0.06432	0.04894	0.01722		
VARIANCE EXPLAINED BY COMPONENTS					
	1	2	3		
	0.1571	0.00514	0.00083		
PERCENT OF TOTAL VARIANCE EXPLAINED					
	1	2	3		
	96.18548	3.14667	0.51106		
DG					
LATENT ROOTS (EIGENVALUES)					
	1	2	3	4	5
	0.11073	0.00267	0.00011	0.00004	0.00002
	6	7	8	9	
	0.00002	0	0	0	
COMPONENT LOADINGS					
	1	2	3		
DG0	0.18624	0.00766	-0.00383		
DG32	0.11525	-0.03989	-0.00018		
DG64	0.08255	-0.01943	0.00034		
DG96	0.07549	-0.0057	0.00591		
DG128	0.08554	0.00725	0.00439		
DG160	0.0936	0.01483	0.00225		
DG192	0.10315	0.01455	0.00167		
DG224	0.10542	0.00897	0.00111		

DG255	0.11142	0.00674	-0.00553		
VARIANCE EXPLAINED BY COMPONENTS					
	1	2	3		
	0.11073	0.00267	0.00011		
PERCENT OF TOTAL VARIANCE EXPLAINED					
	1	2	3		
	97.4743	2.35006	0.09557		
DB					
LATENT ROOTS (EIGENVALUES)					
	1	2	3	4	5
	0.08864	0.00265	0.00088	0.0002	0.00009
	6	7	8	9	
	0.00006	0.00002	0.00001	0	
COMPONENT LOADINGS					
	1	2	3		
DB0	0.10974	-0.03223	0.00939		
DB32	0.07547	-0.03106	-0.00601		
DB64	0.05906	-0.00347	0.00246		
DB96	0.08611	0.00179	-0.02587		
DB128	0.06794	0.00181	0.00125		
DB160	0.08243	0.00889	-0.0008		
DB192	0.09968	0.00783	0.00046		
DB224	0.12369	0.01167	0.00106		
DB255	0.15283	0.01865	0.00857		
VARIANCE EXPLAINED BY COMPONENTS					
	1	2	3		
	0.08864	0.00265	0.00088		
PERCENT OF TOTAL VARIANCE EXPLAINED					
	1	2	3		
	95.7620	2.86007	0.94735		

Appendix D. Scalar analysis results using least square fit based on Equation 5-2.

DR

DEP VAR: DR0 N: 9 MULTIPLE R: 0.999 SQUARED MULTIPLE R: 0.998
ADJUSTED SQUARED MULTIPLE R: 0.998 STANDARD ERROR OF ESTIMATE: 0.00516

VARIABLE	COEFFICIENT	STD ERROR	STD COEF	TOLERANCE	T	P(2 TAIL)
DR_V1	-0.76213	0.01301	-0.92139	1.00000	-.59E+02	0.00000
DR_V2	-1.76707	0.07194	-0.38640	1.00000	-.25E+02	0.00000

ANALYSIS OF VARIANCE

SOURCE	SUM-OF-SQUARES	DF	MEAN-SQUARE	F-RATIO	P
REGRESSION	0.10730	2	0.05365	2016.99968	0.00000
RESIDUAL	0.00019	7	0.00003		

DEP VAR: DR32 N: 9 MULTIPLE R: 0.994 SQUARED MULTIPLE R: 0.988
ADJUSTED SQUARED MULTIPLE R: 0.986 STANDARD ERROR OF ESTIMATE: 0.01188

VARIABLE	COEFFICIENT	STD ERROR	STD COEF	TOLERANCE	T	P(2 TAIL)
DR_V1	-0.67769	0.02997	-0.94740	1.00000	-.23E+02	0.00000
DR_V2	-1.18742	0.16569	-0.30024	1.00000	-7.16654	0.00018

ANALYSIS OF VARIANCE

SOURCE	SUM-OF-SQUARES	DF	MEAN-SQUARE	F-RATIO	P
REGRESSION	0.07940	2	0.03970	281.36779	0.00000
RESIDUAL	0.00099	7	0.00014		

DEP VAR: DR64 N: 9 MULTIPLE R: 0.997 SQUARED MULTIPLE R: 0.994
ADJUSTED SQUARED MULTIPLE R: 0.993 STANDARD ERROR OF ESTIMATE: 0.00945

VARIABLE	COEFFICIENT	STD ERROR	STD COEF	TOLERANCE	T	P(2 TAIL)
DR_V1	-0.81495	0.02383	-0.98427	1.00000	-.34E+02	0.00000
DR_V2	0.72965	0.13176	0.15939	1.00000	5.53781	0.00087

ANALYSIS OF VARIANCE

SOURCE	SUM-OF-SQUARES	DF	MEAN-SQUARE	F-RATIO	P
REGRESSION	0.10707	2	0.05354	600.03579	0.00000
RESIDUAL	0.00062	7	0.00009		

DEP VAR: DR96 N: 9 MULTIPLE R: 0.999 SQUARED MULTIPLE R: 0.998
ADJUSTED SQUARED MULTIPLE R: 0.997 STANDARD ERROR OF ESTIMATE: 0.00512

VARIABLE	COEFFICIENT	STD ERROR	STD COEF	TOLERANCE	T	P(2 TAIL)
DR_V1	-0.66280	0.01293	-0.94154	1.00000	-.51E+02	0.00000
DR_V2	1.29759	0.07146	0.33339	1.00000	.18E+02	0.00000

ANALYSIS OF VARIANCE

SOURCE	SUM-OF-SQUARES	DF	MEAN-SQUARE	F-RATIO	P
REGRESSION	0.07767	2	0.03883	1479.55691	0.00000
RESIDUAL	0.00018	7	0.00003		

DEP VAR: DR128 N: 9 MULTIPLE R: 0.948 SQUARED MULTIPLE R: 0.899
ADJUSTED SQUARED MULTIPLE R: 0.885 STANDARD ERROR OF ESTIMATE: 0.02540

VARIABLE	COEFFICIENT	STD ERROR	STD COEF	TOLERANCE	T	P(2 TAIL)
DR_V1	-0.50669	0.06409	-0.94783	1.00000	-7.90621	0.00010
DR_V2	-0.09382	0.35433	-0.03174	1.00000	-0.26477	0.79881

ANALYSIS OF VARIANCE

SOURCE	SUM-OF-SQUARES	DF	MEAN-SQUARE	F-RATIO	P
REGRESSION	0.04038	2	0.02019	31.28914	0.00032
RESIDUAL	0.00452	7	0.00065		

DEP VAR: DR160 N: 9 MULTIPLE R: 0.917 SQUARED MULTIPLE R: 0.842
ADJUSTED SQUARED MULTIPLE R: 0.819 STANDARD ERROR OF ESTIMATE: 0.01225

VARIABLE	COEFFICIENT	STD ERROR	STD COEF	TOLERANCE	T	P(2 TAIL)
DR_V1	-0.11000	0.03092	-0.53508	1.00000	-3.55800	0.00924
DR_V2	0.84705	0.17093	0.74524	1.00000	4.95543	0.00165

ANALYSIS OF VARIANCE

SOURCE	SUM-OF-SQUARES	DF	MEAN-SQUARE	F-RATIO	P
REGRESSION	0.00559	2	0.00279	18.60770	0.00158
RESIDUAL	0.00105	7	0.00015		

DEP VAR: DR192 N: 9 MULTIPLE R: 0.990 SQUARED MULTIPLE R: 0.980
ADJUSTED SQUARED MULTIPLE R: 0.977 STANDARD ERROR OF ESTIMATE: 0.00831

VARIABLE	COEFFICIENT	STD ERROR	STD COEF	TOLERANCE	T	P(2 TAIL)
DR_V1	0.37138	0.02098	0.95715	1.00000	.18E+02	0.00000

DR_V2 0.54010 0.11599 0.25177 1.00000 4.65659 0.00232

ANALYSIS OF VARIANCE

SOURCE	SUM-OF-SQUARES	DF	MEAN-SQUARE	F-RATIO	P
REGRESSION	0.02317	2	0.01158	167.53709	0.00000
RESIDUAL	0.00048	7	0.00007		

DEP VAR: DR224 N: 9 MULTIPLE R: 0.999 SQUARED MULTIPLE R: 0.999
ADJUSTED SQUARED MULTIPLE R: 0.998 STANDARD ERROR OF ESTIMATE: 0.00625

VARIABLE	COEFFICIENT	STD ERROR	STD COEF	TOLERANCE	T	P(2 TAIL)
DR_V1	1.10823	0.01578	0.99914	1.00000	.70E+02	0.00000
DR_V2	0.10558	0.08724	0.01722	1.00000	1.21018	0.26549

ANALYSIS OF VARIANCE

SOURCE	SUM-OF-SQUARES	DF	MEAN-SQUARE	F-RATIO	P
REGRESSION	0.19300	2	0.09650	2467.10659	0.00000
RESIDUAL	0.00027	7	0.00004		

DEP VAR: DR255 N: 9 MULTIPLE R: 1.000 SQUARED MULTIPLE R: 0.999
ADJUSTED SQUARED MULTIPLE R: 0.999 STANDARD ERROR OF ESTIMATE: 0.00774

VARIABLE	COEFFICIENT	STD ERROR	STD COEF	TOLERANCE	T	P(2 TAIL)
DR_V1	2.05467	0.01952	0.99882	1.00000	.11E+03	0.00000
DR_V2	-0.47166	0.10790	-0.04147	1.00000	-4.37142	0.00327

ANALYSIS OF VARIANCE

SOURCE	SUM-OF-SQUARES	DF	MEAN-SQUARE	F-RATIO	P
REGRESSION	0.66435	2	0.33218	5551.92364	0.00000
RESIDUAL	0.00042	7	0.00006		

DG

DEP VAR: DG0 N: 9 MULTIPLE R: 1.000 SQUARED MULTIPLE R: 0.999
ADJUSTED SQUARED MULTIPLE R: 0.999 STANDARD ERROR OF ESTIMATE: 0.00521

VARIABLE	COEFFICIENT	STD ERROR	STD COEF	TOLERANCE	T	P(2 TAIL)
DG_V1	-1.74904	0.01565	-0.99404	1.00000	-.11E+03	0.00000
DG_V2	-1.20561	0.10079	-0.10640	1.00000	-.12E+02	0.00001

ANALYSIS OF VARIANCE

SOURCE	SUM-OF-SQUARES	DF	MEAN-SQUARE	F-RATIO	P
REGRESSION	0.34261	2	0.17131	6315.66949	0.00000
RESIDUAL	0.00019	7	0.00003		

DEP VAR: DG32 N: 9 MULTIPLE R: 0.999 SQUARED MULTIPLE R: 0.998
ADJUSTED SQUARED MULTIPLE R: 0.998 STANDARD ERROR OF ESTIMATE: 0.00618

VARIABLE	COEFFICIENT	STD ERROR	STD COEF	TOLERANCE	T	P(2 TAIL)
DG_V1	-1.15099	0.01858	-0.99701	1.00000	-.62E+02	0.00000
DG_V2	-0.47925	0.11967	-0.06446	1.00000	-4.00483	0.00516

ANALYSIS OF VARIANCE

SOURCE	SUM-OF-SQUARES	DF	MEAN-SQUARE	F-RATIO	P
REGRESSION	0.14730	2	0.07365	1926.23604	0.00000
RESIDUAL	0.00027	7	0.00004		

DEP VAR: DG64 N: 9 MULTIPLE R: 0.997 SQUARED MULTIPLE R: 0.994
ADJUSTED SQUARED MULTIPLE R: 0.993 STANDARD ERROR OF ESTIMATE: 0.00526

VARIABLE	COEFFICIENT	STD ERROR	STD COEF	TOLERANCE	T	P(2 TAIL)
DG_V1	-0.50096	0.01580	-0.96346	1.00000	-.32E+02	0.00000
DG_V2	0.85560	0.10176	0.25552	1.00000	8.40810	0.00007

ANALYSIS OF VARIANCE

SOURCE	SUM-OF-SQUARES	DF	MEAN-SQUARE	F-RATIO	P
REGRESSION	0.02974	2	0.01487	537.88271	0.00000
RESIDUAL	0.00019	7	0.00003		

DEP VAR: DG96 N: 9 MULTIPLE R: 0.971 SQUARED MULTIPLE R: 0.943
ADJUSTED SQUARED MULTIPLE R: 0.935 STANDARD ERROR OF ESTIMATE: 0.00585

VARIABLE	COEFFICIENT	STD ERROR	STD COEF	TOLERANCE	T	P(2 TAIL)
DG_V1	-0.08183	0.01759	-0.42006	1.00000	-4.65115	0.00234
DG_V2	1.09837	0.11330	0.87549	1.00000	9.69408	0.00003

ANALYSIS OF VARIANCE

SOURCE	SUM-OF-SQUARES	DF	MEAN-SQUARE	F-RATIO	P
REGRESSION	0.00396	2	0.00198	57.80235	0.00004
RESIDUAL	0.00024	7	0.00003		

DEP VAR: DG128 N: 9 MULTIPLE R: 0.992 SQUARED MULTIPLE R: 0.985
ADJUSTED SQUARED MULTIPLE R: 0.982 STANDARD ERROR OF ESTIMATE: 0.00295

VARIABLE	COEFFICIENT	STD ERROR	STD COEF	TOLERANCE	T	P(2 TAIL)
DG_V1	0.14194	0.00887	0.75180	1.00000	.16E+02	0.00000
DG_V2	0.78730	0.05712	0.64754	1.00000	.14E+02	0.00000

ANALYSIS OF VARIANCE

SOURCE	SUM-OF-SQUARES	DF	MEAN-SQUARE	F-RATIO	P
REGRESSION	0.00389	2	0.00194	223.03760	0.00000
RESIDUAL	0.00006	7	0.00001		

DEP VAR: DG160 N: 9 MULTIPLE R: 0.997 SQUARED MULTIPLE R: 0.995
ADJUSTED SQUARED MULTIPLE R: 0.994 STANDARD ERROR OF ESTIMATE: 0.00369

VARIABLE	COEFFICIENT	STD ERROR	STD COEF	TOLERANCE	T	P(2 TAIL)
DG_V1	0.39555	0.01110	0.95734	1.00000	.36E+02	0.00000
DG_V2	0.74514	0.07145	0.28005	1.00000	.10E+02	0.00002

ANALYSIS OF VARIANCE

SOURCE	SUM-OF-SQUARES	DF	MEAN-SQUARE	F-RATIO	P
REGRESSION	0.01881	2	0.00940	689.81087	0.00000
RESIDUAL	0.00010	7	0.00001		

DEP VAR: DG192 N: 9 MULTIPLE R: 0.998 SQUARED MULTIPLE R: 0.995
ADJUSTED SQUARED MULTIPLE R: 0.994 STANDARD ERROR OF ESTIMATE: 0.00545

VARIABLE	COEFFICIENT	STD ERROR	STD COEF	TOLERANCE	T	P(2 TAIL)
DG_V1	0.61444	0.01637	0.99448	1.00000	.38E+02	0.00000
DG_V2	0.31058	0.10539	0.07806	1.00000	2.94694	0.02150

ANALYSIS OF VARIANCE

SOURCE	SUM-OF-SQUARES	DF	MEAN-SQUARE	F-RATIO	P
REGRESSION	0.04206	2	0.02103	709.13974	0.00000
RESIDUAL	0.00021	7	0.00003		

DEP VAR: DG224 N: 9 MULTIPLE R: 0.999 SQUARED MULTIPLE R: 0.998
ADJUSTED SQUARED MULTIPLE R: 0.998 STANDARD ERROR OF ESTIMATE: 0.00559

VARIABLE	COEFFICIENT	STD ERROR	STD COEF	TOLERANCE	T	P(2 TAIL)
DG_V1	0.95586	0.01681	0.99688	1.00000	.57E+02	0.00000

DG_V2 -0.39461 0.10823 -0.06391 1.00000 -3.64587 0.00822

ANALYSIS OF VARIANCE

SOURCE	SUM-OF-SQUARES	DF	MEAN-SQUARE	F-RATIO	P
REGRESSION	0.10158	2	0.05079	1623.90849	0.00000
RESIDUAL	0.00022	7	0.00003		

DEP VAR: DG255 N: 9 MULTIPLE R: 1.000 SQUARED MULTIPLE R: 0.999
ADJUSTED SQUARED MULTIPLE R: 0.999 STANDARD ERROR OF ESTIMATE: 0.00419

VARIABLE	COEFFICIENT	STD ERROR	STD COEF	TOLERANCE	T	P(2 TAIL)
DG_V1	1.37503	0.01258	0.98143	1.00000	.11E+03	0.00000
DG_V2	-1.71753	0.08103	-0.19036	1.00000	-.21E+02	0.00000

ANALYSIS OF VARIANCE

SOURCE	SUM-OF-SQUARES	DF	MEAN-SQUARE	F-RATIO	P
REGRESSION	0.21722	2	0.10861	6195.20197	0.00000
RESIDUAL	0.00012	7	0.00002		

DB

EP VAR: DB0 N: 9 MULTIPLE R: 0.997 SQUARED MULTIPLE R: 0.995
ADJUSTED SQUARED MULTIPLE R: 0.994 STANDARD ERROR OF ESTIMATE: 0.01635

VARIABLE	COEFFICIENT	STD ERROR	STD COEF	TOLERANCE	T	P(2 TAIL)
DB_V1	-2.03663	0.05492	-0.99654	1.00000	-.37E+02	0.00000
DB_V2	-0.51081	0.31788	-0.04319	1.00000	-1.60692	0.15211

ANALYSIS OF VARIANCE

SOURCE	SUM-OF-SQUARES	DF	MEAN-SQUARE	F-RATIO	P
REGRESSION	0.36837	2	0.18419	688.77037	0.00000
RESIDUAL	0.00187	7	0.00027		

DEP VAR: DB32 N: 9 MULTIPLE R: 0.992 SQUARED MULTIPLE R: 0.984
ADJUSTED SQUARED MULTIPLE R: 0.981 STANDARD ERROR OF ESTIMATE: 0.01575

VARIABLE	COEFFICIENT	STD ERROR	STD COEF	TOLERANCE	T	P(2 TAIL)
DB_V1	-1.07724	0.05289	-0.98828	1.00000	-.20E+02	0.00000
DB_V2	-0.52176	0.30613	-0.08271	1.00000	-1.70436	0.13209

ANALYSIS OF VARIANCE

SOURCE	SUM-OF-SQUARES	DF	MEAN-SQUARE	F-RATIO	P

REGRESSION	0.10358	2	0.05179	208.83484	0.00000
RESIDUAL	0.00174	7	0.00025		

DEP VAR: DB64 N: 9 MULTIPLE R: 0.586 SQUARED MULTIPLE R: 0.343
ADJUSTED SQUARED MULTIPLE R: 0.249 STANDARD ERROR OF ESTIMATE: 0.01953

VARIABLE	COEFFICIENT	STD ERROR	STD COEF	TOLERANCE	T	P(2 TAIL)
DB_V1	-0.06684	0.06560	-0.31210	1.00000	-1.01890	0.34217
DB_V2	-0.61455	0.37966	-0.49583	1.00000	-1.61870	0.14954

ANALYSIS OF VARIANCE

SOURCE	SUM-OF-SQUARES	DF	MEAN-SQUARE	F-RATIO	P
REGRESSION	0.00140	2	0.00070	1.82898	0.22961
RESIDUAL	0.00267	7	0.00038		

DEP VAR: DB96 N:9 MULTIPLE R: 0.972 SQUARED MULTIPLE R: 0.944
ADJUSTED SQUARED MULTIPLE R: 0.936 STANDARD ERROR OF ESTIMATE: 0.00715

VARIABLE	COEFFICIENT	STD ERROR	STD COEF	TOLERANCE	T	P(2 TAIL)
DB_V1	-0.00936	0.02400	-0.03487	1.00000	-0.38994	0.70817
DB_V2	1.50855	0.13891	0.97099	1.00000	.11E+02	0.00001

ANALYSIS OF VARIANCE

SOURCE	SUM-OF-SQUARES	DF	MEAN-SQUARE	F-RATIO	P
REGRESSION	0.00603	2	0.00302	59.04313	0.00004
RESIDUAL	0.00036	7	0.00005		

DEP VAR: DB128 N: 9 MULTIPLE R: 0.960 SQUARED MULTIPLE R: 0.922
ADJUSTED SQUARED MULTIPLE R: 0.910 STANDARD ERROR OF ESTIMATE: 0.01012

VARIABLE	COEFFICIENT	STD ERROR	STD COEF	TOLERANCE	T	P(2 TAIL)
DB_V1	0.29505	0.03397	0.91870	1.00000	8.68440	0.00005
DB_V2	0.51819	0.19663	0.27878	1.00000	2.63531	0.03365

ANALYSIS OF VARIANCE

SOURCE	SUM-OF-SQUARES	DF	MEAN-SQUARE	F-RATIO	P
REGRESSION	0.00843	2	0.00421	41.17911	0.00013
RESIDUAL	0.00072	7	0.00010		

DEP VAR: DB160 N: 9 MULTIPLE R: 0.989 SQUARED MULTIPLE R: 0.978

ADJUSTED SQUARED MULTIPLE R: 0.975 STANDARD ERROR OF ESTIMATE: 0.00588

VARIABLE	COEFFICIENT	STD ERROR	STD COEF	TOLERANCE	T	P(2 TAIL)
DB_V1	0.28758	0.01975	0.80870	1.00000	.15E+02	0.00000
DB_V2	1.17248	0.11428	0.56968	1.00000	.10E+02	0.00002

ANALYSIS OF VARIANCE

SOURCE	SUM-OF-SQUARES	DF	MEAN-SQUARE	F-RATIO	P
REGRESSION	0.01097	2	0.00548	158.67761	0.00000
RESIDUAL	0.00024	7	0.00003		

DEP VAR: DB192 N: 9 MULTIPLE R: 0.986 SQUARED MULTIPLE R: 0.973
ADJUSTED SQUARED MULTIPLE R: 0.969 STANDARD ERROR OF ESTIMATE: 0.01040

VARIABLE	COEFFICIENT	STD ERROR	STD COEF	TOLERANCE	T	P(2 TAIL)
DB_V1	0.54945	0.03494	0.97766	1.00000	.16E+02	0.00000
DB_V2	0.42605	0.20221	0.13098	1.00000	2.10694	0.07312

ANALYSIS OF VARIANCE

SOURCE	SUM-OF-SQUARES	DF	MEAN-SQUARE	F-RATIO	P
REGRESSION	0.02724	2	0.01362	125.87341	0.00000
RESIDUAL	0.00076	7	0.00011		

DEP VAR: DB224 N: 9 MULTIPLE R: 0.988 SQUARED MULTIPLE R:0.977
ADJUSTED SQUARED MULTIPLE R: 0.974 STANDARD ERROR OF ESTIMATE: 0.01398

VARIABLE	COEFFICIENT	STD ERROR	STD COEF	TOLERANCE	T	P(2 TAIL)
DB_V1	0.80775	0.04695	0.98676	1.00000	.17E+02	0.00000
DB_V2	-0.27035	0.27174	-0.05706	1.00000	-0.99487	0.35294

ANALYSIS OF VARIANCE

SOURCE	SUM-OF-SQUARES	DF	MEAN-SQUARE	F-RATIO	P
REGRESSION	0.05803	2	0.02902	148.47627	0.00000
RESIDUAL	0.00137	7	0.00020		

DEP VAR: DB255 N: 9 MULTIPLE R: 0.999 SQUARED MULTIPLE R: 0.998
ADJUSTED SQUARED MULTIPLE R: 0.998 STANDARD ERROR OF ESTIMATE: 0.00609

VARIABLE	COEFFICIENT	STD ERROR	STD COEF	TOLERANCE	T	P(2 TAIL)
DB_V1	1.25023	0.02045	0.97237	1.00000	.61E+02	0.00000
DB_V2	-1.70779	0.11838	-0.22950	1.00000	-.14E+02	0.00000

ANALYSIS OF VARIANCE

SOURCE	SUM-OF-SQUARES	DF	MEAN-SQUARE	F-RATIO	P
REGRESSION	0.14628	2	0.07314	1972.29073	0.00000
RESIDUAL	0.00026	7	0.00004		

Appendix E. Data points for Spline Interpolation in Interimage Effects Model (1-D LUTs).

dc	DR_mean	DR_V1	DR_V2	DR_S1	DR_S2
0	2.0975	0.2787	0.0103	-0.7621	-1.7671
32	1.7717	0.2335	-0.0223	-0.6777	-1.1874
64	1.1839	0.1024	-0.0194	-0.8150	0.7297
96	0.9167	0.0607	-0.0196	-0.6628	1.2976
128	0.6703	0.0409	-0.0033	-0.5067	-0.0938
160	0.4822	0.0363	0.0109	-0.1100	0.8471
192	0.3433	0.0400	0.0188	0.3714	0.5401
224	0.2003	0.0451	0.0300	1.1082	0.1056
255	0.1011	0.0643	0.0489	2.0547	-0.4717
	DG_mean	DG_V1	DG_V2	DG_S1	DG_S2
0	2.3022	0.1862	0.0077	-1.7490	-1.2056
32	1.8217	0.1153	-0.0399	-1.1510	-0.4793
64	1.2042	0.0826	-0.0194	-0.5010	0.8556
96	0.9225	0.0755	-0.0057	-0.0818	1.0984
128	0.6856	0.0855	0.0073	0.1419	0.7873
160	0.5131	0.0936	0.0148	0.3956	0.7451
192	0.3814	0.1032	0.0146	0.6144	0.3106
224	0.2486	0.1054	0.0090	0.9559	-0.3946
255	0.1308	0.1114	0.0067	1.3750	-1.7175
	DB_mean	DB_V1	DB_V2	DB_S1	DB_S2
0	2.5475	0.1097	-0.0322	-2.0366	-0.5108
32	1.8425	0.0755	-0.0311	-1.0772	-0.5218
64	1.2936	0.0591	-0.0035	-0.0668	-0.6146
96	1.0103	0.0861	0.0018	-0.0094	1.5086
128	0.7397	0.0679	0.0018	0.2951	0.5182
160	0.5542	0.0824	0.0089	0.2876	1.1725
192	0.4103	0.0997	0.0078	0.5495	0.4261
224	0.2647	0.1237	0.0117	0.8078	-0.2704
255	0.1475	0.1528	0.0187	1.2502	-1.7078

Appendix F. The data set for the concentrations and the ΔE*ab values of 252 samples from the interimage effects model.

	dr	dg	db	del A	del D50	Cc	Cm	Cy	C^c	C^m	C^y
1	0	0	0	0.47	0.46	4.025	3.163	5.080	4.025	3.163	5.008
2	32	0	0	0.84	0.96	3.244	3.108	5.145	3.226	3.150	5.029
3	64	0	0	1.84	2.24	1.940	3.009	5.244	1.913	3.172	5.050
4	96	0	0	2.19	2.62	1.364	2.965	5.291	1.340	3.166	5.064
5	128	0	0	2.25	2.67	0.923	2.997	5.367	0.892	3.177	5.069
6	160	0	0	2.16	2.61	0.613	2.991	5.397	0.574	3.172	5.078
7	192	0	0	1.97	2.45	0.388	2.963	5.377	0.341	3.165	5.084
8	224	0	0	1.85	2.27	0.161	2.975	5.400	0.116	3.143	5.095
9	255	0	0	1.94	2.15	0.035	3.003	5.340	0.026	3.102	5.109
10	0	32	32	4.45	4.78	4.084	2.520	3.520	4.091	2.260	3.421
11	32	32	32	2.76	2.81	3.270	2.429	3.509	3.326	2.300	3.426
12	64	32	32	2.73	2.65	2.010	2.411	3.628	2.017	2.402	3.423
13	96	32	32	3.65	3.66	1.459	2.448	3.738	1.446	2.425	3.429
14	128	32	32	2.93	2.97	0.985	2.433	3.654	0.983	2.439	3.434
15	160	32	32	3.16	3.29	0.656	2.429	3.683	0.647	2.446	3.439
16	192	32	32	4.54	4.61	0.418	2.493	3.833	0.405	2.437	3.447
17	224	32	32	4.34	4.28	0.156	2.470	3.758	0.168	2.409	3.460
18	255	32	32	4.95	4.69	0.014	2.484	3.724	0.057	2.346	3.480
19	0	64	64	8.63	9.17	4.193	1.649	2.440	4.260	1.353	2.345
20	32	64	64	5.54	6.11	3.606	1.569	2.377	3.604	1.386	2.349
21	64	64	64	2.66	2.41	2.230	1.549	2.455	2.250	1.487	2.348
22	96	64	64	6.60	6.14	1.633	1.642	2.659	1.668	1.518	2.351
23	128	64	64	5.08	4.84	1.118	1.645	2.592	1.136	1.548	2.354
24	160	64	64	5.15	4.95	0.732	1.632	2.604	0.746	1.567	2.356
25	192	64	64	6.53	6.39	0.471	1.715	2.705	0.473	1.572	2.360
26	224	64	64	6.40	6.28	0.166	1.724	2.644	0.192	1.567	2.368
27	255	64	64	5.94	5.92	-0.010	1.711	2.640	0.010	1.539	2.380
28	0	96	96	9.65	11.31	4.184	1.169	1.750	4.226	0.949	1.837
29	32	96	96	7.23	8.53	3.595	1.103	1.705	3.621	0.973	1.842
30	64	96	96	1.96	2.22	2.313	1.101	1.820	2.305	1.061	1.844
31	96	96	96	2.20	2.25	1.722	1.143	1.885	1.735	1.090	1.848
32	128	96	96	0.78	0.78	1.171	1.134	1.845	1.190	1.125	1.849
33	160	96	96	0.62	0.58	0.781	1.149	1.870	0.785	1.148	1.851
34	192	96	96	3.18	3.18	0.500	1.234	1.972	0.501	1.159	1.853
35	224	96	96	3.08	3.16	0.196	1.240	1.954	0.205	1.164	1.858
36	255	96	96	3.03	3.15	-0.018	1.231	1.950	-0.006	1.155	1.865
37	0	128	128	10.21	11.98	4.116	0.830	1.217	4.212	0.640	1.295
38	32	128	128	7.02	8.18	3.544	0.786	1.253	3.534	0.660	1.303
39	64	128	128	2.85	3.18	2.301	0.771	1.283	2.269	0.726	1.310
40	96	128	128	2.96	2.73	1.731	0.808	1.415	1.712	0.749	1.315
41	128	128	128	1.32	1.28	1.237	0.808	1.371	1.218	0.781	1.316
42	160	128	128	3.00	2.78	0.847	0.823	1.418	0.852	0.798	1.319
43	192	128	128	7.15	6.55	0.531	0.884	1.483	0.589	0.810	1.321
44	224	128	128	6.92	6.64	0.299	0.924	1.520	0.320	0.817	1.324

45	255	128	128	3.25	3.29	0.225	0.875	1.481	0.153	0.813	1.329
46	0	160	160	10.31	12.22	4.017	0.585	0.854	4.011	0.425	0.928
47	32	160	160	7.96	9.43	3.388	0.535	0.849	3.429	0.428	0.939
48	64	160	160	3.93	4.59	2.222	0.512	0.880	2.262	0.474	0.950
49	96	160	160	3.20	3.42	1.729	0.545	0.968	1.738	0.490	0.956
50	128	160	160	1.68	1.68	1.234	0.556	0.986	1.229	0.524	0.957
51	160	160	160	1.09	1.00	0.845	0.558	0.993	0.841	0.542	0.960
52	192	160	160	3.37	3.12	0.551	0.603	1.041	0.560	0.557	0.961
53	224	160	160	4.52	4.30	0.263	0.634	1.081	0.267	0.568	0.964
54	255	160	160	4.60	4.29	0.011	0.616	1.037	0.049	0.573	0.967
55	0	196	196	7.29	8.69	3.780	0.364	0.552	3.780	0.270	0.611
56	32	196	196	6.03	7.15	3.185	0.338	0.561	3.222	0.268	0.624
57	64	196	196	3.55	4.05	2.172	0.318	0.566	2.180	0.298	0.636
58	96	196	196	2.70	3.06	1.700	0.336	0.614	1.696	0.308	0.644
59	128	196	196	1.41	1.24	1.226	0.332	0.615	1.215	0.338	0.645
60	160	196	196	1.60	1.39	0.855	0.347	0.618	0.841	0.353	0.649
61	192	196	196	1.46	1.37	0.563	0.377	0.692	0.561	0.366	0.651
62	224	196	196	2.09	2.14	0.275	0.410	0.688	0.270	0.374	0.654
63	255	196	196	2.58	2.68	0.021	0.405	0.662	0.046	0.377	0.658
64	0	224	224	4.14	4.68	3.424	0.167	0.268	3.416	0.107	0.264
65	32	224	224	3.12	3.65	2.868	0.139	0.255	2.894	0.103	0.276
66	64	224	224	1.37	1.30	2.047	0.115	0.257	2.042	0.121	0.289
67	96	224	224	0.62	0.59	1.616	0.117	0.287	1.618	0.126	0.296
68	128	224	224	1.84	1.88	1.179	0.124	0.283	1.180	0.150	0.298
69	160	224	224	3.07	3.25	0.829	0.122	0.291	0.824	0.163	0.302
70	192	224	224	2.14	2.42	0.556	0.152	0.321	0.546	0.174	0.305
71	224	224	224	1.06	1.05	0.250	0.173	0.321	0.258	0.178	0.309
72	255	224	224	0.69	0.68	0.014	0.180	0.313	0.024	0.176	0.315
73	0	255	255	4.59	4.55	2.912	-0.004	0.022	2.937	-0.028	-0.079
74	32	255	255	3.74	3.81	2.487	-0.016	0.024	2.463	-0.037	-0.066
75	64	255	255	3.19	3.14	1.856	-0.027	0.018	1.856	-0.042	-0.052
76	96	255	255	2.82	2.97	1.504	-0.046	0.009	1.508	-0.046	-0.044
77	128	255	255	3.38	3.79	1.125	-0.044	0.006	1.126	-0.028	-0.041
78	160	255	255	3.24	3.56	0.792	-0.032	0.009	0.794	-0.018	-0.037
79	192	255	255	3.17	3.57	0.523	-0.029	0.003	0.519	-0.009	-0.034
80	224	255	255	1.92	2.17	0.239	-0.024	-0.014	0.234	-0.008	-0.028
81	255	255	255	0.75	0.75	0.000	-0.003	-0.004	-0.013	-0.013	-0.021
82	0	0	0	0.79	0.84	4.105	3.143	5.063	4.025	3.163	5.008
83	0	32	0	0.70	0.75	4.169	2.195	5.172	4.134	2.204	5.053
84	0	64	0	2.90	2.70	4.137	1.270	5.222	4.332	1.256	5.075
85	0	96	0	2.32	2.17	4.079	0.881	5.226	4.315	0.848	5.328
86	0	128	0	3.57	3.32	3.979	0.600	5.233	4.307	0.561	5.269
87	0	160	0	2.50	2.32	3.856	0.394	5.230	4.114	0.359	5.379
88	0	192	0	2.90	2.69	3.653	0.244	5.288	3.885	0.218	5.310
89	0	224	0	3.69	3.39	3.238	0.098	5.100	3.526	0.059	5.252
90	0	255	0	4.90	4.49	2.754	-0.027	5.026	3.046	-0.047	5.086
91	32	0	32	4.24	4.50	3.560	3.122	3.575	3.191	3.153	3.341
92	32	32	32	3.09	3.14	3.566	2.272	3.548	3.326	2.300	3.426
93	32	64	32	1.92	1.66	3.514	1.351	3.554	3.635	1.345	3.523

94	32	96	32	2.17	2.05	3.482	0.939	3.696	3.669	0.924	3.778
95	32	128	32	2.52	2.40	3.365	0.635	3.622	3.591	0.619	3.751
96	32	160	32	3.38	3.35	3.224	0.428	3.663	3.495	0.394	3.863
97	32	192	32	2.45	2.23	3.122	0.252	3.793	3.292	0.242	3.818
98	32	224	32	2.10	2.02	2.805	0.095	3.627	2.970	0.082	3.781
99	32	255	32	1.83	1.72	2.477	-0.022	3.700	2.538	-0.033	3.653
100	64	0	64	9.50	10.00	2.395	3.079	2.500	1.858	3.144	2.132
101	64	32	64	7.42	7.63	2.369	2.406	2.422	1.984	2.449	2.206
102	64	64	64	3.07	3.55	2.360	1.463	2.499	2.250	1.487	2.348
103	64	96	64	3.56	3.95	2.467	1.025	2.645	2.320	1.050	2.482
104	64	128	64	2.10	2.06	2.395	0.688	2.581	2.298	0.702	2.536
105	64	160	64	0.80	0.85	2.300	0.434	2.612	2.301	0.447	2.615
106	64	192	64	2.00	2.16	2.313	0.262	2.738	2.225	0.272	2.628
107	64	224	64	1.51	1.46	2.172	0.097	2.701	2.094	0.102	2.642
108	64	255	64	1.06	1.08	1.922	-0.037	2.691	1.911	-0.042	2.619
109	96	0	96	9.77	8.68	1.673	3.065	1.778	1.281	3.105	1.663
110	96	32	96	6.50	6.03	1.658	2.446	1.750	1.402	2.473	1.663
111	96	64	96	0.63	0.66	1.662	1.533	1.774	1.654	1.528	1.742
112	96	96	96	1.04	1.04	1.753	1.071	1.840	1.735	1.090	1.848
113	96	128	96	1.25	1.27	1.721	0.727	1.842	1.727	0.730	1.898
114	96	160	96	2.68	3.03	1.701	0.481	1.870	1.763	0.466	1.973
115	96	192	96	0.29	0.26	1.719	0.281	1.982	1.727	0.282	1.981
116	96	224	96	0.06	0.07	1.657	0.107	1.990	1.655	0.107	1.987
117	96	255	96	2.18	2.05	1.525	-0.040	2.024	1.549	-0.046	1.956
118	128	0	128	9.31	10.12	1.162	3.077	1.305	0.818	3.123	0.997
119	128	32	128	7.77	8.95	1.188	2.453	1.300	0.924	2.492	1.035
120	128	64	128	4.03	4.79	1.188	1.556	1.297	1.108	1.571	1.148
121	128	96	128	3.88	4.53	1.272	1.136	1.395	1.175	1.143	1.254
122	128	128	128	1.79	2.06	1.261	0.777	1.379	1.218	0.781	1.316
123	128	160	128	0.21	0.19	1.244	0.517	1.389	1.239	0.518	1.390
124	128	192	128	2.33	2.63	1.280	0.316	1.479	1.232	0.328	1.409
125	128	224	128	2.73	2.99	1.278	0.136	1.509	1.204	0.146	1.427
126	128	255	128	3.39	3.80	1.206	-0.030	1.526	1.153	-0.016	1.415
127	160	0	160	8.56	8.93	0.773	3.060	0.904	0.496	3.100	0.678
128	160	32	160	6.64	7.73	0.774	2.468	0.890	0.582	2.496	0.678
129	160	64	160	4.54	5.43	0.792	1.582	0.905	0.708	1.595	0.757
130	160	96	160	4.32	5.09	0.855	1.167	0.959	0.759	1.174	0.826
131	160	128	160	1.42	1.61	0.864	0.805	0.943	0.842	0.804	0.895
132	160	160	160	0.86	0.86	0.867	0.543	0.975	0.841	0.542	0.960
133	160	192	160	2.20	2.45	0.902	0.343	1.043	0.848	0.347	0.983
134	160	224	160	2.77	2.97	0.902	0.149	1.056	0.838	0.162	1.004
135	160	255	160	3.12	3.50	0.869	-0.020	1.073	0.813	-0.005	1.001
136	196	0	196	6.30	6.33	0.443	3.048	0.587	0.261	3.079	0.451
137	196	32	196	4.33	5.14	0.443	2.457	0.551	0.338	2.470	0.417
138	196	64	196	3.23	3.70	0.458	1.587	0.540	0.430	1.597	0.449
139	196	96	196	2.41	2.78	0.499	1.188	0.589	0.469	1.188	0.518
140	196	128	196	3.77	3.22	0.505	0.841	0.591	0.571	0.822	0.572
141	196	160	196	1.90	2.22	0.527	0.577	0.602	0.553	0.564	0.638
142	196	192	196	0.80	0.68	0.545	0.366	0.652	0.561	0.366	0.651

143	196	224	196	1.73	1.88	0.585	0.168	0.686	0.553	0.177	0.661
144	196	255	196	2.78	3.13	0.552	-0.002	0.703	0.530	0.007	0.639
145	224	0	224	5.67	4.69	0.154	3.018	0.275	0.037	3.025	0.264
146	224	32	224	2.45	2.83	0.159	2.397	0.247	0.101	2.407	0.183
147	224	64	224	2.81	3.21	0.166	1.572	0.224	0.145	1.577	0.152
148	224	96	224	1.98	2.24	0.184	1.190	0.246	0.167	1.188	0.194
149	224	128	224	5.28	4.52	0.193	0.829	0.231	0.296	0.829	0.239
150	224	160	224	1.99	2.24	0.213	0.579	0.259	0.252	0.577	0.298
151	224	192	224	2.00	2.14	0.228	0.384	0.282	0.263	0.374	0.305
152	224	224	224	1.04	0.96	0.248	0.187	0.317	0.258	0.178	0.309
153	224	255	224	3.87	4.38	0.259	-0.015	0.342	0.239	0.004	0.278
154	255	0	255	6.32	6.21	-0.031	2.946	0.038	-0.048	2.940	0.172
155	255	32	255	1.71	2.02	-0.037	2.284	0.000	-0.001	2.278	0.043
156	255	64	255	1.66	1.61	-0.041	1.518	-0.040	-0.036	1.518	-0.069
157	255	96	255	0.53	0.64	-0.046	1.155	-0.066	-0.048	1.164	-0.072
158	255	128	255	9.47	8.10	-0.044	0.836	-0.050	0.124	0.821	-0.038
159	255	160	255	2.96	3.37	-0.025	0.587	-0.044	0.028	0.583	0.009
160	255	192	255	4.56	5.09	-0.048	0.383	-0.061	0.033	0.375	0.012
161	255	224	255	3.04	3.53	-0.026	0.172	-0.044	0.019	0.168	0.015
162	255	255	255	0.75	0.75	0.000	-0.003	-0.004	-0.013	-0.013	-0.021
163	0	0	0	0.96	0.86	4.097	3.177	4.966	4.025	3.163	5.008
164	0	0	32	1.99	1.67	4.212	3.284	3.308	3.990	3.166	3.320
165	0	0	64	2.44	2.80	4.201	3.309	2.036	3.970	3.135	2.091
166	0	0	96	1.70	1.90	4.149	3.284	1.630	3.966	3.102	1.608
167	0	0	128	2.83	3.26	4.235	3.281	0.877	3.951	3.109	0.936
168	0	0	160	3.05	3.42	4.224	3.281	0.550	3.947	3.092	0.609
169	0	0	192	2.71	2.98	4.192	3.216	0.319	3.945	3.077	0.375
170	0	0	224	2.36	2.48	4.219	3.173	0.134	3.946	3.045	0.177
171	0	0	255	1.73	1.80	4.158	3.040	0.032	3.951	3.001	0.072
172	32	32	0	1.78	1.92	3.436	2.344	5.067	3.369	2.244	5.057
173	32	32	32	3.76	3.53	3.536	2.428	3.351	3.326	2.300	3.426
174	32	32	64	3.88	3.67	3.558	2.488	2.156	3.293	2.348	2.208
175	32	32	96	5.36	5.78	3.571	2.511	1.539	3.281	2.348	1.660
176	32	32	128	3.29	3.41	3.570	2.477	0.992	3.268	2.354	1.026
177	32	32	160	3.30	3.50	3.579	2.462	0.626	3.261	2.350	0.665
178	32	32	192	3.13	3.38	3.593	2.466	0.374	3.258	2.333	0.396
179	32	32	224	2.50	2.45	3.572	2.359	0.121	3.259	2.297	0.149
180	32	32	255	1.50	0.82	3.567	2.237	-0.007	3.267	2.232	-0.011
181	64	64	0	3.12	2.95	2.205	1.365	5.114	2.323	1.391	5.077
182	64	64	32	1.16	1.10	2.230	1.450	3.509	2.282	1.446	3.522
183	64	64	64	0.89	0.91	2.234	1.510	2.357	2.250	1.487	2.348
184	64	64	96	4.00	3.92	2.302	1.533	1.630	2.236	1.497	1.739
185	64	64	128	1.64	1.42	2.295	1.540	1.137	2.222	1.511	1.142
186	64	64	160	1.32	0.93	2.285	1.528	0.748	2.213	1.515	0.748
187	64	64	192	3.18	3.35	2.310	1.565	0.399	2.207	1.512	0.437
188	64	64	224	1.52	1.07	2.298	1.515	0.130	2.203	1.498	0.132
189	64	64	255	2.82	3.34	2.283	1.439	-0.055	2.204	1.466	-0.101
190	96	96	0	4.96	4.66	1.664	0.973	5.348	1.823	0.990	5.339
191	96	96	32	2.79	2.60	1.695	1.026	3.795	1.783	1.041	3.783

192	96	96	64	1.93	1.74	1.680	1.068	2.475	1.750	1.079	2.485
193	96	96	96	2.61	2.86	1.759	1.143	1.819	1.735	1.090	1.848
194	96	96	128	0.98	1.13	1.716	1.129	1.246	1.720	1.108	1.252
195	96	96	160	0.72	0.81	1.687	1.107	0.795	1.709	1.116	0.823
196	96	96	192	3.09	3.21	1.784	1.178	0.500	1.703	1.118	0.512
197	96	96	224	2.33	2.42	1.766	1.159	0.179	1.697	1.114	0.184
198	96	96	255	1.67	2.03	1.693	1.078	-0.069	1.693	1.100	-0.090
199	128	128	0	5.20	5.11	1.202	0.644	5.322	1.313	0.701	5.291
200	128	128	32	4.53	4.43	1.177	0.687	3.773	1.275	0.740	3.764
201	128	128	64	2.47	2.28	1.182	0.737	2.537	1.247	0.756	2.542
202	128	128	96	1.83	1.90	1.264	0.797	1.908	1.233	0.763	1.899
203	128	128	128	1.06	1.02	1.205	0.758	1.277	1.218	0.781	1.316
204	128	128	160	0.66	0.62	1.208	0.774	0.880	1.208	0.787	0.893
205	128	128	192	2.43	2.11	1.271	0.820	0.571	1.200	0.793	0.568
206	128	128	224	2.27	2.05	1.250	0.817	0.223	1.193	0.793	0.230
207	128	128	255	1.56	1.22	1.242	0.803	-0.045	1.188	0.789	-0.050
208	160	160	0	3.70	3.63	0.874	0.440	5.409	0.944	0.477	5.411
209	160	160	32	2.06	1.98	0.868	0.494	3.900	0.907	0.508	3.884
210	160	160	64	1.12	1.06	0.857	0.519	2.629	0.880	0.515	2.625
211	160	160	96	2.59	2.80	0.884	0.556	1.963	0.866	0.518	1.977
212	160	160	128	1.79	1.88	0.876	0.567	1.404	0.851	0.536	1.393
213	160	160	160	0.96	0.94	0.864	0.557	0.971	0.841	0.542	0.960
214	160	160	192	3.70	3.72	0.889	0.594	0.622	0.834	0.549	0.636
215	160	160	224	4.84	4.76	0.904	0.603	0.270	0.826	0.551	0.293
216	160	160	255	3.19	2.92	0.879	0.576	-0.016	0.820	0.552	0.001
217	196	196	0	5.88	5.90	0.579	0.255	5.360	0.666	0.314	5.349
218	196	196	32	5.60	5.43	0.536	0.297	3.855	0.631	0.340	3.845
219	196	196	64	4.82	4.51	0.526	0.331	2.690	0.606	0.340	2.642
220	196	196	96	1.79	1.64	0.557	0.341	1.988	0.593	0.340	1.988
221	196	196	128	2.74	2.45	0.530	0.354	1.429	0.578	0.356	1.415
222	196	196	160	2.50	2.25	0.535	0.356	1.014	0.569	0.360	0.985
223	196	196	192	0.83	0.95	0.544	0.367	0.629	0.561	0.366	0.651
224	196	196	224	1.02	1.04	0.541	0.376	0.300	0.554	0.366	0.301
225	196	196	255	0.84	0.98	0.532	0.364	-0.013	0.548	0.364	0.005
226	224	224	0	7.04	6.82	0.262	0.085	5.307	0.368	0.130	5.297
227	224	224	32	5.05	4.90	0.258	0.123	3.824	0.333	0.157	3.814
228	224	224	64	4.30	3.97	0.230	0.145	2.641	0.309	0.159	2.662
229	224	224	96	4.41	4.20	0.247	0.151	2.072	0.296	0.160	2.000
230	224	224	128	3.29	3.19	0.239	0.150	1.451	0.282	0.174	1.438
231	224	224	160	3.14	3.17	0.244	0.152	1.036	0.273	0.177	1.012
232	224	224	192	2.28	2.19	0.235	0.164	0.673	0.265	0.181	0.666
233	224	224	224	0.36	0.37	0.250	0.174	0.299	0.258	0.178	0.309
234	224	224	255	1.29	1.28	0.221	0.163	-0.014	0.253	0.170	0.009
235	255	255	0	3.46	3.44	0.053	-0.059	5.135	0.096	-0.032	5.143
236	255	255	32	3.17	3.29	0.035	-0.037	3.722	0.062	-0.009	3.698
237	255	255	64	2.11	1.98	0.010	-0.021	2.650	0.041	-0.013	2.650
238	255	255	96	3.08	2.89	-0.013	-0.023	1.997	0.028	-0.013	1.978
239	255	255	128	3.17	3.17	-0.019	-0.027	1.442	0.014	-0.002	1.435
240	255	255	160	2.04	2.12	-0.014	-0.024	1.005	0.006	0.000	1.017

241	255	255	192	3.42	3.65	-0.020	-0.028	0.668	-0.003	0.003	0.651
242	255	255	224	1.93	1.95	-0.025	-0.016	0.294	-0.009	-0.002	0.284
243	255	255	255	0.23	0.22	-0.017	-0.015	-0.022	-0.013	-0.013	-0.021
244	0	0	0	0.75	0.76	4.127	3.188	5.126	4.025	3.163	5.008
245	32	32	32	2.51	2.32	3.571	2.415	3.551	3.326	2.300	3.426
246	64	64	64	1.45	1.54	2.247	1.471	2.406	2.250	1.487	2.348
247	96	96	96	1.68	1.57	1.660	1.078	1.807	1.735	1.090	1.848
248	128	128	128	1.52	1.47	1.168	0.751	1.280	1.218	0.781	1.316
249	160	160	160	1.79	1.83	0.788	0.514	0.892	0.841	0.542	0.960
250	192	192	192	1.49	1.48	0.518	0.352	0.612	0.561	0.366	0.651
251	224	224	224	1.00	1.07	0.236	0.169	0.279	0.258	0.178	0.309
252	255	255	255	0.98	0.97	0.005	0.000	0.000	-0.013	-0.013	-0.021

Appendix G. Computer Codes for Thesis

```
/*==========================================================
   utils.c:
   --------
      Utility functions/procedures.

   gmprod, tri, and invert:
      Written by Dr. Roy S. Berns in Fortran - March, 1993
      Translated & Modified by Helen Hae-Kyung Shin in C - January, 1994

   stripnl, and dsort:
      Written by Helen Hae-Kyung Shin - January, 1994

   spline, and splint:
      Taken from "Numerical Recipes in C," pages 115-6

   dspline, and dsplint:
      spline and splint - Taken from "Numerical Recipes in C," pages 115-6
      Modified by Helen Hae-Kyung Shin - January, 1994
==========================================================*/
#include <stdio.h>
#include <math.h>
#include "nrutil.h"

/*----------------------------------------------------------
   gmprod:
----------------------------------------------------------*/
void gmprod(double **a, double **b, double **r, int n, int m, int l)
{
   int i, j, k;

   for (i = 1; i <= n; i++)
      for (j = 1; j <= l; j++)
      {
         r[i][j] = 0.;
         for (k = 1; k <= m; k++)
            r[i][j] += a[i][k] * b[k][j];
      }
}

/*----------------------------------------------------------
   tri:
----------------------------------------------------------*/
void tri(int nw, double **phi, double **conc, double **te,
         double **tsvd, double **tea, double **tsva)
{
   int i, j;
   double  **dmix, **tmix;
```

```
    dmix = dmatrix(1,35,1,1);
    tmix = dmatrix(1,35,1,1);

    gmprod(phi, conc, dmix, nw, 3, 1);

    for (j = 1; j <= nw; j++)
       tmix[j][1] = pow(10.,-dmix[j][1]);

    gmprod(te, tmix, tsvd, 3, nw, 1);
    gmprod(tea, tmix, tsva, 3, nw, 1);

    free_dmatrix(dmix,1,35,1,1);
    free_dmatrix(tmix,1,35,1,1);
 }

 /*-------------------------------------------------------
    invert:
 -------------------------------------------------------*/
 void invert(double **P)
 {
    double  **wrk;
    int k, me, na;
    int i,j;

    wrk = dmatrix(1,3,1,1);

    for (me = 1; me <= 3; me++)
    {
       wrk[3][1] = (double)1. / (double)P[1][1]
            for (k = 2; k <= 3; k++
         wrk[k-1][1] = (double)P[1][k] / (double)P[1][1];

       for (k = 1; k <= 2; k++)
       {
          P[k][3] = -P[k+1][1] * wrk[3][1];
          for (na = 1; na <= 2; na++)
             P[k][na] = P[k+1][na+1] - P[k+1][1] * wrk[na][1];
       }
       for (k = 1; k <= 3; k++)
          P[3][k] = wrk[k][1];
    }
    free_dmatrix(wrk,1,3,1,1);
 }

 /*-------------------------------------------------------
    stripnl:
 -------------------------------------------------------*/
 void    stripnl(char *str)
 {
    int i;

    i = strlen(str);
```

```
    str[i-1] = '\0';
}

/*-------------------------------------------------------------
    dsort:
    ------
    Sorts an array a[ ] into ascending numerical order, by
    straight insertion, while making the corresponding
    rearrangement of the array b[ ]
-------------------------------------------------------------*/
void dsort(int n, double a[ ], double b[ ])
{
    int i,j;
    double aa, bb;

    for(j = 2;j <= n; j++)  /* pick out each element in turn */
    {
        aa = a[j];
        bb = b[j];
        i = j -1;
        while (i > 0 && a[i] > aa) /* look for the place to insert it */
        {
            a[i+1] = a[i];
            b[i+1] = b[i];
            i--;
        }
        a[i+1] = aa;            /* insert it */
        b[i+1] = bb;
    }
}

/*-------------------------------------------------------------
    spline
    ------
    Given arrays x[1..n] and y[1..n] containing a tabulated
    function, i.e., yi = f(xi), with x1 < x2 < ... < XN, and
    given values yp1 and ypn for the first derivative of the
    interpolating function at points 1 and n,respectively,
    this routine returns an array y2[1..n] that contains the
    second derivatives of the interpolating function at the
    tabulated points xi. If yp1 and/or ypn are equal to 1 x
    10**30 or larger, the routine is signaled to set the
    corresponding boundary condition for a natural spline,
    with zero second derivative on that boundary.
-------------------------------------------------------------*/
void spline(float x[ ], float y[ ], int n, float yp1, float ypn, float y2[ ])
{
    int i,k;
    float p, qn, sig, un, *u;

    u=vector(1,n-1);
    if (yp1 > 0.99e30)  /* The lower boundary condition is set */
```

```
    y2[1]=u[1]=0.0; /* either to be "natural" or else to have a */
  else {            /* specified first derivative. */
    y2[1] = -0.5;
    u[1]=(3.0/(x[2]-x[1]))*((y[2]-y[1])/(x[2]-x[1])-yp1);
  }

  /* This is the decomposition loop of the tridiagonal algorithm. y2 and u are used for temporary storage of
the decomposed factors. */
  for (i=2; i<=n-1; i++){
    sig=(x[i]-x[i-1])/(x[i+1]-x[i-1]);
    p = sig*y2[i-1] + 2.0;
    y2[i] =(sig -1.0)/p;
    u[i] =(y[i+1]-y[i])/(x[i+1]-x[i]) - (y[i]-y[i-1])/(x[i]-x[i-1]);
    u[i] =(6.0*u[i]/(x[i+1]-x[i-1])-sig*u[i-1])/p;
    printf("u[%d] = %f\n", i, u[i]);
  }

  /* The upper boundary condition is set either to be "natural" or else to have a specified first derivative. */
  if (ypn > 0.99e30)
    qn = un = 0.0;
  else {
    qn = 0.5;
    un = (3.0/(x[n]-x[n-1]))*(ypn-(y[n]-y[n-1])/(x[n]-x[n-1]));
  }
  y2[n] = (un-qn*u[n-1])/(qn*y2[n-1]+1.0);

  /* This is the backsubstitution loop of the tridiagonal algorithm.*/
  for (k=n-1; k>=1; k--) {
    y2[k]=y2[k]*y2[k+1]+u[k];
    printf("y2[%d] = %f\n",k, y2[k]);
  }
  free_vector(u,1,n-1);
}

/*-------------------------------------------------------------
  dspline - spline (see above) with double precision
  arithmetic
-------------------------------------------------------------*/
void dspline(double x[ ],double y[ ],int n,double yp1,double ypn,double y2[ ])
{
  int i,k;
  double p, qn, sig, un, *u;

  u=dvector(1,n-1);
  if (yp1 > 0.99e30)  /* The lower boundary condition is set */
    y2[1]=u[1]=0.0; /* either to be "natural" or else to have a */
  else {            /* specified first derivative. */
    y2[1] = -0.5;
    u[1]=(3.0/(x[2]-x[1]))*((y[2]-y[1])/(x[2]-x[1])-yp1);
  }
```

```
   /* This is the decomposition loop of the tridiagonal algorithm. y2 and u are used for temporary storage of
the decomposed factors. */
   for (i=2; i<=n-1; i++) {
      sig=(x[i]-x[i-1])/(x[i+1]-x[i-1]);
      p = sig*y2[i-1] + 2.0;
      y2[i] =(sig -1.0)/p;
      u[i] =(y[i+1]-y[i])/(x[i+1]-x[i]) - (y[i]-y[i-1])/(x[i]-x[i-1]);
      u[i] =(6.0*u[i]/(x[i+1]-x[i-1])-sig*u[i-1])/p;
      printf("u[%d] = %lf\n", i, u[i]);
   }

   /* The upper boundary condition is set either to be "natural" or else to have a specified first derivative. */
   if (ypn > 0.99e30)
      qn = un = 0.0;
   else {
      qn = 0.5;
      un = (3.0/(x[n]-x[n-1]))*(ypn-(y[n]-y[n-1])/(x[n]-x[n-1]));
   }
   y2[n] = (un-qn*u[n-1])/(qn*y2[n-1]+1.0);

   /* This is the backsubstitution loop of the tridiagonal algorithm.*/
   for(k=n-1; k>=1; k--){
      y2[k]=y2[k]*y2[k+1]+u[k];
      printf("y2[%d] = %lf\n",k, y2[k]);
   }
   free_dvector(u,1,n-1);
}

/*-------------------------------------------------------------
   splint:
   -------
   Given the array xa[1..n] and ya[1..n], which tabulate a
   function (with the xai's in order), and given the array
   y2a[1..n], which is the output from spline, and given a
   value of x, this routine returns a cubic-spline
   interpolated value y.
-------------------------------------------------------------*/
void splint(float xa[ ],float ya[ ],float y2a[ ],int n,float x,float *y)
{
   int klo, khi, k;
   float h, b,a;

   /* We will find the right place in the table by means of
      bisection.This is optimal if sequential calls to this
      routine are at random values of x. If sequential calls
      are in order, and closely spaced, one would do better
      to store previous values of klo and khi and test if
      they remain appropriate on the next call. */
   klo =1;
   khi =n;
   while (khi-klo >1) {
      k = (khi+klo) >> 1;
```

```
    if (xa[k] > x) khi = k;
    else klo = k;
  }
  /* klo and khi now bracket the input value of x. */
  h = xa[khi] - xa[klo];
  /* The xa's must be distinct. */
  if(h == 0.0) nrerror("Bad xa input to routine splint");
  a = (xa[khi]-x)/h;
  /* Cubic spline polynomial is now evaluated*/
  b = (x-xa[klo])/h;
  *y=a*ya[klo]+b*ya[khi]+((a*a*a-a)*y2a[klo]+(b*b*b-b)*y2a[khi])*(h*h)/6.0;
}

/*-------------------------------------------------------------
  dsplint - splint (see above) with double precision
  arithmetic.
-------------------------------------------------------------*/
void dsplint(double xa[ ],double ya[ ],double y2a[ ],int n,double x,double *y)
{
  int klo, khi, k;
  double h, b,a;

  /* We will find the right place in the table by means of
    bisection.This is optimal if sequential calls to this
    routine are at random values of x. If sequential calls
    are in order, and closely spaced,one would do better
    to store previous values of klo and khi and test if
    they remain appropriate on the next call. */
  klo =1;
  khi =n;
  while (khi-klo >1) {
    k = (khi+klo) >> 1;
    if (xa[k] > x) khi = k;
    else klo = k;
  }
  /* klo and khi now bracket the input value of x. */
  h = xa[khi] - xa[klo];
  /* The xa's must be distinct. */
  if(h == 0.0) nrerror("Bad xa input to routine splint");
  a = (xa[khi]-x)/h;
  /* Cubic spline polynomial is now evaluated*/
  b = (x-xa[klo])/h;
  *y=a*ya[klo]+b*ya[khi]+((a*a*a-a)*y2a[klo]+(b*b*b-b)*y2a[khi])*(h*h)/6.0;
}
```

```
/*============================================================
  utils.h:
  --------
    Utility functions/procedures.

  gmprod, tri, and invert:
    Written by Dr. Roy S. Berns in Fortran - March, 1993
    Translated & Modified by Helen Hae-Kyung Shin in C -January, 1994

  stripnl, and dsort:
    Written by Helen Hae-Kyung Shin - January, 1994

  spline, and splint:
    Taken from "Numerical Recipes in C," pages 115-6

  dspline, and dsplint:
    spline and splint - Taken from "Numerical Recipes in C," pages 115-6
    Modified by Helen Hae-Kyung Shin - January, 1994
============================================================*/
#ifndef _UTILS_H_
#define _UTILS_H_

#if defined(__STDC__) || defined(ANSI) || defined(NRANSI) /* ANSI */

void gmprod(double **a, double **b, double **r, int n, int m,  int l);
void tri(int nw, double **phi, double **conc, double **te,
         double **tsvd, double **tea, double **tsva);
void invert(double **P);
void stripnl(char *str);
void dsort(int n, double a[ ], double b[ ]);
void spline(float x[ ], float y[ ], int n, float yp1, float ypn, float y2[ ]);
void dspline(double x[ ],double y[ ],int n,double yp1,double ypn,double y2[ ]);
void splint(float xa[ ],float ya[ ],float y2a[ ],int n,float x,float *y);
void dsplint(double xa[ ],double ya[ ],double y2a[ ],int n,double x,double *y);

#else /* ANSI */
/* traditional - K&R */

void gmprod( );
void tri( );
void invert( );
void stripnl( );
void dsort( );
void spline( );
void dspline( );
void splint( );
void dsplint( );

#endif /* ANSI */

#endif /* _UTILS_H_ */
```

```
/*==========================================================
  calc_routines.c:
  ----------------
        Program to calculate CIELAB values

  Written By:
        Helen Hae-Kyung Shin - January, 1994
==========================================================*/
#include <stdio.h>
#include <math.h>
#include <stdlib.h>
#include <string.h>
#include "nrutil.h"
#include "utils.h"

double calc_l(double **m, double d)
{
  return 116.*pow(m[2][1]/d, .333);
}

double calc_a(double **m, double d1, double d2)
{
  return 500.*(pow(m[1][1]/d1,.333)-pow(m[2][1]/d2,.333));
}

double calc_b(double **m, double d1, double d2)
{
  return 200.*(pow(m[2][1]/d1,.333)-pow(m[3][1]/d2,.333));
}

/*==========================================================
  calc_routines.h:

  Written By:
        Helen Hae-Kyung Shin - January, 1994
==========================================================*/
#ifndef _CALC_ROUTINES_H_
#define _CALC_ROUTINES_H_

#include <stdio.h>
#include <math.h>
#include <stdlib.h>
#include <string.h>
#include "nrutil.h"
#include "utils.h"

double calc_l(double **m, double d);
double calc_a(double **m, double d1, double d2);
double calc_b(double **m, double d1, double d2);
#endif
```

```
/*============================================================
   tristimulus_31.c:
   -----------------
      Program to predict tristimulus values of photographic
      film with the idea of determining the c, m, y
      concentrations in the film.

   Written By:
   -----------
      Fortran : Dr. Roy S. Bems - March, 1993

   Translated & Modified By:
   -------------------------
      C : Helen Hae-Kyung Shin - January, 1994

   Important Parameters:
   ---------------------
      Number of wavelengths : 31 (400-700nm, 10 nm
      intervals)
      Maximum number of images to match : 300
    ============================================================*/
#include <stdio.h>
#include <math.h>
#include <stdlib.h>
#include <string.h>
#include "nrutil.h"
#include "utils.h"
#include "calc_routines.h"

int main()
{
   double  **P, **T, **Z;
   double  **tmeas, *tin, **din, *nm;
   double  **d, **ted, **tedphi, **phi, **te;
   double  **conc, **tedf, **tstd, **tsvstd;
   double  **deltat, **deltaconc;
   double  **tea, **tsva, **dstd, **tsvd, **teigenvec;
   double  **tsvastd, **deigenvec, *wave;
   double  ldmix, lamix, ldstd, lastd;
   char    *names[300];
   char    error_text[100];
   int     ncol = 60;
   int     nw  = 31;
   int     i, j, jj, j1, j2;
   double  deamax, dedmax;
   int     iter, icount;
   double  s1;
   double  sum, adstd, bdstd, aastd, bastd, deavga, deavg,
           aamix, bamix, admix, bdmix, ded, dea, sumde, sumdea;
   char    buffer[500];
   FILE    *fp1, *fp13, *fp2, *fp3, *fp7;
```

```
/* allocate spaces for vectors */
T = dmatrix(1,3,1,1);
Z = dmatrix(1,3,1,1);
tin = dvector(1,69);
nm = dvector(1,69);
conc = dmatrix(1,3,1,1);
tedf = dmatrix(1,3,1,1);
tstd = dmatrix(1,3,1,1);
tsvstd = dmatrix(1,3,1,1);
deltat = dmatrix(1,3,1,1);
deltaconc = dmatrix(1,3,1,1);
tsva = dmatrix(1,3,1,1);
dstd = dmatrix(1,nw,1,1);
tstd = dmatrix(1,nw,1,1);
tsvd = dmatrix(1,3,1,1);
tsvastd = dmatrix(1,3,1,1);
wave = dvector(1,nw);

/* allocate spaces for matrices */
P = dmatrix(1,3,1,3);
tmeas = dmatrix(1,300,1,nw);
din = dmatrix(1,20,1,69);
d = dmatrix(1,nw,1,nw);
ted = dmatrix(1,3,1,nw);
tedphi = dmatrix(1,3,1,3);
phi = dmatrix(1,nw,1,3);
te = dmatrix(1,3,1,nw);
tea = dmatrix(1,3,1,nw);
teigenvec = dmatrix(1,3,1,nw);
deigenvec = dmatrix(1,3,1,nw);

fp13 = fopen("2_28_3.dat", "r");
fp1 = fopen("cold_2_28.dat", "r");
fp2 = fopen("d50_2deg_10nm_31.dat", "r");
fp3 = fopen("names2.dat", "r");
fp7 = fopen("ia_2deg_10nm_31.dat", "r");

for (j = 1; j <= nw; j++)
{
   fscanf(fp2, "%lf", &(wave[j]));
   for (i = 1; i <= 3; i++)
      fscanf(fp2, "%lf", &(te[i][j]));
}

for (j = 1; j <= nw; j++)
{
   fscanf(fp7, "%lf", &(wave[j]));
   for (i = 1; i <= 3; i++)
      fscanf(fp7, "%lf", &(tea[i][j]));
}

fgets(buffer, 500, fp13);
```

```
fgets(buffer, 500, fp13);
for (j = 1; j <= nw; j++)
{
   fscanf(fp13, "%lf", &(nm[j]));
   for (i = 1; i <= 3; i++)
      fscanf(fp13, "%lf", &(din[i][j]));
}

jj = 1;
for (j = 1; j <= nw; j+=1)
{
   for (i = 1; i <= 3; i++)
      deigenvec[i][jj] = din[i][j];
   jj += 1;
}

for (i = 1; i <= 3; i++)
   for (j = 1; j <= nw; j++)
      teigenvec[i][j] = pow(10,-deigenvec[i][j]);

for (i = 1; i <= 3; i++)
   for (j = 1; j <= nw; j++)
      phi[j][i] = deigenvec[i][j];

deamax = 0.; dedmax = 0.;
sumde = 0.; sumdea = 0.;

fgets(buffer, 500, fp1);
for (i = 1; i <= ncol; i++)
{
   for (j = 1; j <= nw; j++)
      fscanf(fp1, "%lf", &(tin[j]));

   names[i] = (char *)malloc(40);
   fgets(names[i], 40, fp3);

   for (j = 1; j <= nw; j+=1)
      tmeas[i][j] = tin[j];
   for (j = 1; j <= nw; j++)
   {
      dstd[j][1] = -log10(tmeas[i][j]);
      tstd[j][1] = tmeas[i][j];
   }

   gmprod(te, tstd, tsvstd, 3, nw, 1);
   gmprod(tea, tstd, tsvastd, 3, nw, 1);

   for (j1 = 1; j1 <= nw; j1++)
      for (j2 = 1; j2 <= nw; j2++)
         d[j1][j2] = 0.;

   for (j = 1; j <= nw; j++)
```

```
    d[j][j] = - 2.3026 * tstd[j][1];

  gmprod(tea, d, ted, 3, nw, nw);
  gmprod(ted, phi, tedphi, 3, nw, 3);
  invert(tedphi);
  gmprod(ted, dstd, tedf, 3, nw, 1);
  gmprod(tedphi, tedf, conc, 3, 3, 1);

  iter = 1;

  while (1)
  {
    tri(nw, phi, conc, te, tsvd, tea, tsva);

    for (j = 1; j <= 3; j++)
      deltat[j][1] = tsvastd[j][1] - tsva[j][1];

    sum =
      fabs(deltat[1][1]+deltat[2][1]+deltat[3][1]);
    if (sum < .0001) break;

    gmprod(tedphi, deltat, deltaconc, 3, 3, 1);

    for (j = 1; j <= 3; j++)
      conc[j][1] += deltaconc[j][1];

    iter++;
  }

  tri(nw, phi, conc, te, tsvd, tea, tsva);

  ldstd = calc_l(tsvstd, 100.);
  adstd = calc_a(tsvstd, 96.42, 100.);
  bdstd = calc_b(tsvstd, 100., 82.49);

  lastd = calc_l(tsvastd, 100.);
  aastd = calc_a(tsvastd, 109.85, 100.);
  bastd = calc_b(tsvastd, 100., 35.58);

  ldmix = calc_l(tsvd, 100.);
  admix = calc_a(tsvd, 96.42, 100.);
  bdmix = calc_b(tsvd, 100., 82.49);

  lamix = calc_l(tsva, 100.);
  aamix = calc_a(tsva, 109.85, 100.);
  bamix = calc_b(tsva, 100., 35.58);

  ded = sqrt(pow(fabs(ldmix-ldstd), 2.) + pow(fabs(admix-adstd), 2.)
    + pow(fabs(bdmix-bdstd), 2.));
  dea = sqrt(pow(fabs(lamix-lastd), 2.) + pow(fabs(aamix-aastd), 2.)
    + pow(fabs(bamix-bastd), 2.));
```

```
    sumde += ded; sumdea += dea; icount++;

    if (ded > dedmax) dedmax = ded;
    if (dea > deamax) deamax = dea;

    stripnl(names[i]);
    printf("%s  %lf %lf %lf %lf %lf\n",
       names[i], dea, ded, conc[1][1], conc[2][1], conc[3][1]);

}

deavg = sumde / (double)icount;
deavga = sumdea / (double)icount;

printf("average de daylight %lf\n", deavg);
printf("max de daylight %lf\n", dedmax);
printf("average de ill a %lf\n", deavga);
printf("max de ill a %lf\n", deamax);
printf("icount %d\n", icount);

/* free spaces allocated for vectors and matrices */
free_dmatrix(T,1,3,1,1);
free_dmatrix(Z,1,3,1,1);
free_dvector(tin,1,69);
free_dvector(nm,1,69);
free_dmatrix(conc,1,3,1,1);
free_dmatrix(tedf,1,3,1,1);
free_dmatrix(tstd,1,3,1,1);
free_dmatrix(tsvstd,1,3,1,1);
free_dmatrix(deltat,1,3,1,1);
free_dmatrix(deltaconc,1,3,1,1);
free_dmatrix(tsva,1,3,1,1);
free_dmatrix(dstd,1,nw,1,1);
free_dmatrix(tstd,1,nw,1,1);
free_dmatrix(tsvd,1,3,1,1);
free_dmatrix(tsvastd,1,3,1,1);
free_dvector(wave,1,nw);
free_dmatrix(P,1,3,1,3);
free_dmatrix(tmeas,1,300,1,nw);
free_dmatrix(din,1,20,1,69);
free_dmatrix(d,1,nw,1,nw);
free_dmatrix(ted,1,3,1,nw);
free_dmatrix(tedphi,1,3,1,3);
free_dmatrix(phi,1,nw,1,3);
free_dmatrix(te,1,3,1,nw);
free_dmatrix(tea,1,3,1,nw);
free_dmatrix(teigenvec,1,3,1,nw);
free_dmatrix(deigenvec,1,3,1,nw);
```

```
/*=============================================================
   Dhat_Chat_xyz.c:
   ----------------
      Program to calculate tristimulus values from
      predicted density values using the interimage effects
      model and cmy concentrations using the Tristimulus
      matching algorithm and calculate color difference
      value between them.


   Written By:
   -------------------------
      Helen Hae-Kyung Shin - March, 1994
=============================================================*/
#include <stdio.h>
#include <math.h>
#include <stdlib.h>
#include <string.h>
#include "nrutil.h"
#include "utils.h"
#include "calc_routines.h"

int main()
{
   double  **P, **T, **Z;
   double  **tmeas, *tin, **din, *nm;
   double  **phi, **te;
   double  **conc, **conc2, **tstd, **tsvstd;
   double  **deltat, **deltaconc;
   double  **tea, **tsva, **dstd, **tsvd, **teigenvec;
   double  **tsvastd, **deigenvec, *wave;
   double  ldmix, lamix, ldstd, lastd;
   char    *names[300];
   char    error_text[100];
   int     ncol = 252;
   int     nw  = 31;
   int     i, j, jj, j1, j2;
   double  deamax, dedmax;
   int iter, icount;
   double s1;
   double  sum, adstd, bdstd, aastd, bastd, deavga, deavg,
         aamix, bamix, admix, bdmix, ded, dea, sumde, sumdea;
   char    buffer[500];
   FILE    *fp1, *fp13, *fp2, *fp3, *fp7, *fp10, *fp11;

   /* allocate spaces for vectors */
   T = dmatrix(1,3,1,1);
   Z = dmatrix(1,3,1,1);
   tin = dvector(1,69);
   nm = dvector(1,69);
   conc = dmatrix(1,3,1,1);
   conc2 = dmatrix(1,3,1,1);
```

```
tstd = dmatrix(1,3,1,1);
tsvstd = dmatrix(1,3,1,1);
deltat = dmatrix(1,3,1,1);
deltaconc = dmatrix(1,3,1,1);
tsva = dmatrix(1,3,1,1);
dstd = dmatrix(1,nw,1,1);
tstd = dmatrix(1,nw,1,1);
tsvd = dmatrix(1,3,1,1);
tsvastd = dmatrix(1,3,1,1);
wave = dvector(1,nw);

/* allocate spaces for matrices */
P = dmatrix(1,3,1,3);
tmeas = dmatrix(1,300,1,nw);
din = dmatrix(1,20,1,69);
phi = dmatrix(1,nw,1,3);
te = dmatrix(1,3,1,nw);
tea = dmatrix(1,3,1,nw);
teigenvec = dmatrix(1,3,1,nw);
deigenvec = dmatrix(1,3,1,nw);

fp13 = fopen("2_28_4.dat", "r");
fp2 = fopen("d50_2deg_10nm_31.dat", "r");
fp3 = fopen("names2.dat", "r");
fp7 = fopen("ia_2deg_10nm_31.dat", "r");
fp10 = fopen("Dhat1_Chat_60.dat", "r");
fp11 = fopen("D_C_60.dat", "r");

for (j = 1; j <= nw; j++)
{
   fscanf(fp2, "%lf", &(wave[j]));
   for (i = 1; i <= 3; i++)
      fscanf(fp2, "%lf", &(te[i][j]));
}

for (j = 1; j <= nw; j++)
{
   fscanf(fp7, "%lf", &(wave[j]));
   for (i = 1; i <= 3; i++)
      fscanf(fp7, "%lf", &(tea[i][j]));
}

fgets(buffer, 500, fp13);
fgets(buffer, 500, fp13);
for (j = 1; j <= nw; j++)
{
   fscanf(fp13, "%lf", &(nm[j]));
   for (i = 1; i <= 3; i++)
      fscanf(fp13, "%lf", &(din[i][j]));
}

jj = 1;
```

```
for (j = 1; j <= nw; j+=1)
{
   for (i = 1; i <= 3; i++)
      deigenvec[i][jj] = din[i][j];
   jj += 1;
}

for (i = 1; i <= 3; i++)
   for (j = 1; j <= nw; j++)
      teigenvec[i][j] = pow(10,-deigenvec[i][j]);

for (i = 1; i <= 3; i++)
   for (j = 1; j <= nw; j++)
      phi[j][i] = deigenvec[i][j];

deamax = 0.; dedmax = 0.;
sumde = 0.; sumdea = 0.;
fgets(buffer, 500, fp10);
fgets(buffer, 500, fp11);
for (i = 1; i <= ncol; i++)
{
   for (j = 1; j <= 3; j++)
      fscanf(fp10, "%lf", &(conc[j][1]));

   tri(nw, phi, conc, te, tsvd, tea, tsva);

   for (j = 1; j <= 3; j++)
      fscanf(fp11, "%lf", &(conc2[j][1]));

   tri(nw, phi, conc2, te, tsvstd, tea, tsvastd);

   ldstd = calc_l(tsvstd, 100.);
   adstd = calc_a(tsvstd, 96.42, 100.);
   bdstd = calc_b(tsvstd, 100., 82.49);

   lastd = calc_l(tsvastd, 100.);
   aastd = calc_a(tsvastd, 109.85, 100.);
   bastd = calc_b(tsvastd, 100., 35.58);

   ldmix = calc_l(tsvd, 100.);
   admix = calc_a(tsvd, 96.42, 100.);
   bdmix = calc_b(tsvd, 100., 82.49);

   lamix = calc_l(tsva, 100.);
   aamix = calc_a(tsva, 109.85, 100.);
   bamix = calc_b(tsva, 100., 35.58);

   ded = sqrt(pow(fabs(ldmix-ldstd), 2.) + pow(fabs(admix-adstd), 2.)
      + pow(fabs(bdmix-bdstd), 2.));
   dea = sqrt(pow(fabs(lamix-lastd), 2.) + pow(fabs(aamix-aastd), 2.)
      + pow(fabs(bamix-bastd), 2.));
```

```
    sumde += ded; sumdea += dea;
    icount += 1;

    if (ded > dedmax) dedmax = ded;
    if (dea > deamax) deamax = dea;

    printf("%d  %lf %lf \n",
          icount, dea, ded);
}
deavg = sumde / (double)icount;
deavga = sumdea /( double)icount;

printf("average de daylight %lf\n", deavg);
printf("max de daylight %lf\n", dedmax);
printf("average de ill a %lf\n", deavga);
printf("max de ill a %lf\n", deamax);
printf("icount %d\n", icount);

/* free spaces allocated for vectors and matrices */
free_dmatrix(T,1,3,1,1);
free_dmatrix(Z,1,3,1,1);
free_dvector(tin,1,69);
free_dvector(nm,1,69);
free_dmatrix(conc,1,3,1,1);
free_dmatrix(conc2,1,3,1,1);
free_dmatrix(tstd,1,3,1,1);
free_dmatrix(tsvstd,1,3,1,1);
free_dmatrix(deltat,1,3,1,1);
free_dmatrix(deltaconc,1,3,1,1);
free_dmatrix(tsva,1,3,1,1);
free_dmatrix(dstd,1,35,1,1);
free_dmatrix(tstd,1,35,1,1);
free_dmatrix(tsvd,1,3,1,1);
free_dmatrix(tsvastd,1,3,1,1);
free_dvector(wave,1,35);
free_dmatrix(P,1,3,1,3);
free_dmatrix(tmeas,1,300,1,35);
free_dmatrix(din,1,20,1,69);
free_dmatrix(phi,1,35,1,3);
free_dmatrix(te,1,3,1,35);
free_dmatrix(tea,1,3,1,35);
free_dmatrix(teigenvec,1,3,1,35);
free_dmatrix(deigenvec,1,3,1,35);
```

```
/*============================================================
   dspline_main2.c:
   ----------------
        Program to interpolate data points using dspline, dsplint and dsort functions with double precision.
        Generate 1-D LUT for vectors and scalars from the analysis of interimage effects.

   Written By:
        Helen Hae-Kyung Shin - January, 1994

============================================================*/
#include <stdio.h>
#include <math.h>
#include <stdlib.h>
#include "nrutil.h"
#include "utils.h"

int main()
{
   double  *X, *Y, *y2;
   double  yp1, ypn;
   double  *Xi, *y;
   int     j, n=9, m=256;
   FILE    *fp1, *fp2, *fp3;

   /* allocate spaces for dvector */
   X = dvector(1,n);
   Y = dvector(1,n);
   y2 = dvector(1,n);
   Xi = dvector(1,m);
   y = dvector(1,m);

   /* open files for *X, *Y, *Y2 */
   fp1 = fopen("dc_ii4_spline.dat", "r");
   fp2 = fopen("DR_S2_ii4.dat", "r");
   fp3 = fopen("spline_Xi.lut", "r");

   for (j = 1; j <= n; j++)
   {
      fscanf(fp1, "%lf", &(X[j]));
      fscanf(fp2, "%lf", &(Y[j]));
   }

   dsort(n, X, Y);
   for ( j = 1; j <= m; j++)
   {
      fscanf(fp3, "%lf", &(Xi[j]));
   }

   yp1 = 1.0e30;
   ypn = 1.0e30;

   dspline(X, Y, n, yp1, ypn, y2);
```

```
    for ( j = 1; j <= m; j++)
    {
       dsplint(X, Y, y2, n, Xi[j], &(y[j]));
       printf("%lf\n", y[j]);
    }
}
```

```
/*==========================================================================
   interimage_model2.c:
   --------------------
      This program models the interimage effect between each layer of color film
(ektachrome plus 100) using cubic spline interpolation algorithms.

   Written By:
   -----------
      C : Helen Hae-Kyung Shin - April, 1994
==========================================================================*/
#include <stdio.h>
#include <math.h>
#include <stdlib.h>
#include <string.h>
#include "nrutil.h"
#include "utils.h"

int main()
{
   double  *DhatR, *DhatG, *DhatB;
   double  *Dhatr, *Dhatg, *Dhatb;
   double  *V0_R, *V1_R, *V2_R, *V0_G, *V1_G, *V2_G, *V0_B, *V1_B,
         *V2_B;
   double  *S1_R, *S2_R, *S1_G, *S2_G, *S1_B, *S2_B;

   char    error_text[100];

   int     i, j;
   int     r, g, b;

   FILE    *fp1, *fp2, *fp3, *fp4, *fp5, *fp6, *fp7, *fp8, *fp9;
   FILE    *fp10, *fp11, *fp12, *fp13, *fp14, *fp15, *fp16;
   FILE    *fpR, *fpr;

   char    buffer[500];

   DhatR = dvector(0,255);
   DhatG = dvector(0,255);
   DhatB = dvector(0,255);
   Dhatr = dvector(0,255);
   Dhatg = dvector(0,255);
   Dhatb = dvector(0,255);
   V0_R = dvector(0,255);
   V1_R = dvector(0,255);
   V2_R = dvector(0,255);
   V0_G = dvector(0,255);
   V1_G = dvector(0,255);
   V2_G = dvector(0,255);
   V0_B = dvector(0,255);
   V1_B = dvector(0,255);
   V2_B = dvector(0,255);
   S1_R = dvector(0,255);
```

```
   S2_R = dvector(0,255);
   S1_G = dvector(0,255);
   S2_G = dvector(0,255);
   S1_B = dvector(0,255);
   S2_B = dvector(0,255);

/*
   open files (read the LUT for each vectors and scalars
   using the cubic spline interpolation method).
*/

   fp1 = fopen("DRmean_lut", "r");
   for (i = 0; i <= 255; i++)
   {
      fscanf(fp1, "%lf", &(V0_R[i]));
   }
   fclose(fp1);


   fp2 = fopen("DGmean_lut", "r");
   for (i = 0; i <= 255; i++)
   {
      fscanf(fp2, "%lf", &(V0_G[i]));
   }
   fclose(fp2);


   fp3 = fopen("DBmean_lut", "r");
   for (i = 0; i <= 255; i++)
   {
      fscanf(fp3, "%lf", &(V0_B[i]));
   }
   fclose(fp3);

   fp4 = fopen("DR_V1_lut", "r");
   for (i = 0; i <= 255; i++)
   {
      fscanf(fp4, "%lf", &(V1_R[i]));
   }
   fclose(fp4);

   fp5 = fopen("DR_V2_lut", "r");
   for (i = 0; i <= 255; i++)
   {
      fscanf(fp5, "%lf", &(V2_R[i]));
   }
   fclose(fp5);

   fp6 = fopen("DG_V1_lut", "r");
   for (i = 0; i <= 255; i++)
   {
      fscanf(fp6, "%lf", &(V1_G[i]));
```

```
}
fclose(fp6);

fp7 = fopen("DG_V2_lut", "r");
for (i = 0; i <= 255; i++)
{
   fscanf(fp7, "%lf", &(V2_G[i]));
}
fclose(fp7);


fp8 = fopen("DB_V1_lut", "r");
for (i = 0; i <= 255; i++)
{
   fscanf(fp8, "%lf", &(V1_B[i]));
}
fclose(fp8);

fp9 = fopen("DB_V2_lut", "r");
for (i = 0; i <= 255; i++)
{
   fscanf(fp9, "%lf", &(V2_B[i]));
}
fclose(fp9);

fp10 = fopen("DR_S1_lut", "r");
for (i = 0; i <= 255; i++)
{
   fscanf(fp10, "%lf", &(S1_R[i]));
}
fclose(fp10);

fp11 = fopen("DR_S2_lut", "r");
for (i = 0; i <= 255; i++)
{
   fscanf(fp11, "%lf", &(S2_R[i]));
}
fclose(fp11);

fp12 = fopen("DG_S1_lut", "r");
for (i = 0; i <= 255; i++)
{
   fscanf(fp12, "%lf", &(S1_G[i]));
}
fclose(fp12);

fp13 = fopen("DG_S2_lut", "r");
for (i = 0; i <= 255; i++)
{
   fscanf(fp13, "%lf", &(S2_G[i]));
}
fclose(fp13);
```

```
   fp14 = fopen("DB_S1_lut", "r");
   for (i = 0; i <= 255; i++)
   {
      fscanf(fp14, "%lf", &(S1_B[i]));
   }
   fclose(fp14);

   fp15 = fopen("DB_S2_lut", "r");
   for (i = 0; i <= 255; i++)
   {
      fscanf(fp15, "%lf", &(S2_B[i]));
   }
   fclose(fp15);
/* array for predicted density using 2 vectors */

   fpR = fopen("DhatC_density.out", "w");

/* array for predicted density using 1 vectors */

   fpr = fopen("Dhatc_density.out", "w");

/* Interimage Model for density of color film */


   fp16 = fopen("digital_count.txt", "r");

   for (i=0; i<252; i++)
   {
      fscanf(fp16, "%d %d %d\n", &r, &g, &b);

/* Using one adjacent scalars */
      DhatR[i] = V0_R[r] - S1_R[g]*V1_R[r] - S2_R[g]*V2_R[r];
      DhatG[i] = V0_G[g] - S1_G[r]*V1_G[g] - S2_G[r]*V2_G[g];
      DhatB[i] = V0_B[b] - S1_B[g]*V1_B[b] - S2_B[g]*V2_B[b];


/* average two scalars effect */
      Dhatr[i] = V0_R[r] - ((S1_R[g]+S1_R[b])/2.0)*V1_R[r]
               - ((S2_R[g]+S2_R[b])/2.0)*V2_R[r];
      Dhatg[i] = V0_G[g] - ((S1_G[r]+S1_G[b])/2.0)*V1_G[g]
               - ((S2_G[r]+S2_G[b])/2.0)*V2_G[g];
      Dhatb[i] = V0_B[b] - ((S1_B[r]+S1_B[g])/2.0)*V1_B[b]
               - ((S2_B[r]+S2_B[g])/2.0)*V2_B[b];

      fprintf(fpR, "%lf %lf %lf\n", DhatR[i], DhatG[i], DhatB[i]);
      fprintf(fpr, "%lf %lf %lf\n", Dhatr[i], Dhatg[i], Dhatb[i]);
   }


/* free the memory space for vectors and matrixes */
   free_dvector(DhatR,0,255);
```

```
free_dvector(DhatG,0,255);
free_dvector(DhatB,0,255);
free_dvector(Dhatr,0,255);
free_dvector(Dhatg,0,255);
free_dvector(Dhatb,0,255);
free_dvector(V0_R,0,255);
free_dvector(V1_R,0,255);
free_dvector(V2_R,0,255);
free_dvector(V0_G,0,255);
free_dvector(V1_G,0,255);
free_dvector(V2_G,0,255);
free_dvector(V0_B,0,255);
free_dvector(V1_B,0,255);
free_dvector(V2_B,0,255);
free_dvector(S1_R,0,255);
free_dvector(S2_R,0,255);
free_dvector(S1_G,0,255);
free_dvector(S2_G,0,255);
free_dvector(S1_B,0,255);
free_dvector(S2_B,0,255);
```